

UNCLASSIFIED



Australian Government

Department of Defence
Science and Technology

Bistatic Radar Concept Demonstrator (BiRCD) System Development and Verification

Timothy Chiknaikin

National Security and ISR Division
Defence Science and Technology Group

DST-Group-TN-1856

ABSTRACT

In this document we describe the development and verification of an experimental bistatic radar system. Project objectives are defined followed by the capture and definition of system requirements. A software defined radio (SDR) based hardware platform is outlined, along with a non-real-time radar controller with offline processing of radar data. Analysis of experimental data from a field trial provides validation of system performance. The conclusion considers project outcomes and insights, and discusses possible future work. Technical details and analysis are left to the appendixes.

RELEASE LIMITATION

Approved for public release

UNCLASSIFIED

UNCLASSIFIED

Produced by

*National Security and ISR Division
DST Edinburgh
PO Box 1500
Edinburgh SA 5111*

Telephone: 1300 333 362

*© Commonwealth of Australia 2019
March 2019*

UNCLASSIFIED

UNCLASSIFIED

Bistatic Radar Concept Demonstrator (BiRCD) System Development and Verification

Executive Summary

In this report the development and verification of the Bistatic Radar Concept Demonstrator (BiRCD) system within the Surveillance and Reconnaissance Systems Branch (SRS) is described. The motivation for this project was to develop an experimental bistatic pulse Doppler radar capability where none existed, so as to facilitate research in support of science and technology objectives. The capability is anticipated to stimulate advancements in the detection of targets against the backdrop of clutter, which will contribute to enhanced situational awareness and decision superiority in complex battlefield environments. The project doubles as the author's final year honours project for submission to the University of South Australia.

The developmental process followed is detailed; beginning with broadly defined objectives and culminating with the successful field demonstration of a functional bistatic radar system in May of 2018. The primary drivers of capability and requirements are identified; they include future integration with the second Experimental Phased Array Radar (XPAR-II) and research into bistatic characterisation of sea clutter.

Two bistatic nodes were built which utilise a software defined radio (SDR) based hardware platform with a custom L-band radio frequency (RF) front-end. The RF front-end was designed so as to compliment the SDR hardware and offers improved radar performance. Synchronisation between the nodes is accomplished through use of GPS disciplined oscillators. A user generated script file which is common to all nodes directs the deterministic scheduling of radar operations across all nodes. While all remote nodes have identical hardware and software, a unique identifier is referenced to the script file to direct node specific behaviour. The radar return is captured simultaneously on all nodes where it is stored for offline processing.

The use of SDRs as the hardware platform provides valuable exposure to this innovative technology. While SDRs provide great flexibility, development was less than straightforward; perhaps an indication of an immature product. Insights into their use are provided which may prove useful in informing future projects as to the advantages and disadvantages they afford. SDR hardware driver limitations were encountered as were the limitations of driving the radar from a non-real-time operating system.

A land based field trial was conducted which provided experimental validation of system functionality and performance. The accuracy of the system was compared against returns from a known target source yielding satisfactory results. Aircraft

UNCLASSIFIED

UNCLASSIFIED

detections were confirmed by correlation against ADS-B data, demonstrating valid detections of aircraft up to the maximum unambiguous range of 19kms.

It is demonstrated that all capability requirements and scheduled project objectives have been met or exceeded. The system presently supports multistatic operation, requiring only the construction of additional nodes at reasonable cost. Future integration with XPAR-II will provide additional capabilities including electronic beam scanning and greater transmitter power. Future work may focus on continued development and expanded applications, making use of the flexibility provided by the SDR hardware solution, including instantaneous sample rates of up to 160Msps.

UNCLASSIFIED

Contents

1. INTRODUCTION	1
1.1. Bistatic Radar Overview	1
2. PROJECT CHARTER	2
2.1. Project Background	2
2.2. Project Roles	2
2.3. Project Objectives	3
2.4. Project Approach	3
2.4.1. Project Phases	4
2.4.2. Focus of Effort	4
2.4.3. Schedule Slippage and Implementation of Contingencies	4
3. CAPABILITY NEEDS	6
3.1. Research Interests	6
3.1.1. Sea Clutter Characterisation.....	6
3.2. Capability Needs	9
3.3. System Requirements & Constraints	9
4. ARCHITECTURE DESIGN	10
4.1. BiRCD System Overview	10
4.2. XPAR-II Description	10
4.3. Functional Solution	12
4.3.1. Radar Controller	12
4.3.2. Script File	12
4.3.3. Communication	13
4.3.4. Synchronisation	13
4.3.5. Signal Processing	14
4.4. Functional Diagram	14
5. REMOTE NODE SYSTEM DEVELOPMENT	17
5.1. Hardware Platform Choice	17
5.1.1. Surplus XPAR-II hardware	17
5.1.2. Test and Measurement Equipment	17
5.1.3. Software-defined Radio (SDR).....	17
5.2. Radar Controller Development	18
5.2.1. Context	18
5.2.2. Radar Operations.....	18
5.2.3. Computing Platform	19
5.2.4. USRP Hardware Platform	20
5.2.5. USRP Software Environment.....	21
5.2.6. Software Development	21
5.2.7. Synchronisation	24

5.2.8.	Timing Signals.....	25
5.3.	RF Front-end Development.....	26
5.3.1.	Context	27
5.3.2.	Hardware Selection	27
5.3.3.	Noise Figure	28
5.4.	Remote Node Assembly	29
5.5.	Signal Processing	30
5.5.1.	Implementation.....	30
5.5.2.	Functionality.....	31
5.5.3.	Improve Processing Speed	31
6.	REMOTE NODE INTEGRATION AND VERIFICATION	32
6.1.	Alignment of transmitter and receiver events	32
6.2.	Active Switching	32
6.2.1.	Examination of noise artefacts	34
6.3.	Waveform Optimisation	36
6.4.	Verification of Capability Requirements	37
7.	TEST AND VALIDATION	39
7.1.	Field Trial	39
7.1.1.	Preparation	39
7.1.2.	System Configuration	39
7.1.3.	Supporting Equipment	41
7.1.4.	Deployment.....	41
7.1.5.	Outcome	43
7.2.	Analysis of Trial Data	43
7.2.1.	Bursts Chosen for Examination	43
7.2.2.	Range and Doppler Validation.....	47
7.2.3.	Correlation of ADS-B Data with Observed Target Returns	47
7.2.4.	Examination of Detections and Artefacts.....	50
7.2.5.	Comment on the Availability of ADS-B Message Data.....	51
7.2.6.	SNR of distant targets	52
8.	CONCLUSION	53
8.1.	Project Outcomes.....	53
8.2.	Project Costs	54
8.3.	SDR Insights	54
8.4.	Future work	55
9.	REFERENCE.....	56
APPENDIX A	SYSTEMS ANALYSIS.....	57
A.1.	Remote Node Noise Factor	57
A.2.	Verification of System SNR.....	58
A.3.	Minimal measuring range	64

A.4. Timing Diagram	65
APPENDIX B DATA ANALYSIS.....	67
B.1. Apparent Range of Radar Target Generator	67
B.2. Apparent Range and Doppler Calculation for ADS-B Targets.....	67
9.1.1. Calculation of Expected Range and Doppler for ADS-B Targets ...	69
APPENDIX C SYSTEM OPERATION	71
C.1. Hardware Configuration	71
C.2. Procedure for Initialisation of Communications via PCI Express	72
C.3. Radar Controller Configuration.....	73
C.4. Running the Radar Controller.....	74
C.5. Receiver Data Files.....	76
APPENDIX D MISCELLANEOUS SYSTEM DETAILS.....	77
D.1. Capability Requirements.....	77
D.2. XPAR-II System Constraints.....	78
D.3. XPAR-II Search Waveforms	79
D.4. System Script File Definition	80
D.5. Modifications Required to the XPAR-II System.....	81
APPENDIX E REMOTE NODE ASSEMBLY SCHEMATICS DIAGRAM.....	83

UNCLASSIFIED

DST-Group-TN-1856

This page is intentionally blank.

UNCLASSIFIED

Glossary

ADC	Analog to digital converter
ADS-B	Automatic dependent surveillance - broadcast
API	Application programming interface
ARPANSA	Australian Radiation Protection and Nuclear Safety Agency
BiRCD	Bistatic Radar Concept Demonstrator
CFAR	Constant false alarm rate
COTS	Commercial off-the-shelf
CN	Capability need
CPI	Coherent processing interval
CPU	Central processing unit
CR	Capability requirement
DAC	Digital to analogue converter
DPG	Doppler processing gain
DSP	Digital signal processing
DST	Defence Science and Technology
FPGA	Field-programmable gate array
FSPL	Free-space path loss
GPS	Global positioning system
GPSDO	Global positioning system disciplined oscillator
GUI	Graphical user interface
IP	Intellectual property
IQ	In-phase and quadrature
ISR	Intelligence surveillance and reconnaissance
LNA	Low noise amplifier
MIDD	Major interface design document
MIMO	Multiple-input, multiple-output
MRS	Microwave Radar Systems (Group)
NLOS	Non-line of sight
NRCS	Normalised radar cross-section
NSID	National Security & Intelligence, Surveillance & Reconnaissance Division

OBJ	Objective
PA	Power amplifier
PAR	Phased array radar
PCR	pulse compression ratio
PDF	Probability density function
PPM	Parts per million
PPS	Pulse per second
PRF	Pulse repetition frequency
PRI	Pulse repetition interval
PRN	Protected Research Network
RCS	Radar cross section
RF	Radio frequency
RNA	Remote Node Assembly
RPM	Revolutions per minute
RTC	Real time clock
RX	Receiver
SDR	Software-defined radio
SES	Scientific Engineering Services (Group)
SNR	Signal to noise ratio
SQM	Square metre
SRS	Surveillance and Reconnaissance Systems (Branch)
STALO	Stable local oscillator
STF	Sensor Trials Facility
S&T	Science & technology
TR	Transmit receive
TX	Transmitter
XPAR-II	Experimental Phased Array Radar 2
UniSA	University of South Australia
USRP	Universal software radio peripheral

1. Introduction

The Bistatic Radar Concept Demonstrator (BiRCD) project was undertaken in order to demonstrate a bistatic pulse Doppler radar capability to the Surveillance and Reconnaissance Systems Branch (SRS). The developed system tests the viability of innovative technology and is experimental in nature.

This report is structured to reflect the rudimentary systems engineering approach applied to the project, as is visible by the major sections. It forms the author's submission to the University of South Australia (UniSA) for his Bachelor of Engineering final year honours project, and has been written for academic assessment against the requirements of the Engineering Internship Research Project (ENGG 4004) course.

1.1. Bistatic Radar Overview

Bistatic radar is a type of radar where the transmitting and receiving antennas are physically separated (Willis, 1991). This is in contrast to monostatic radar (the now traditional form of radar) where the transmitting and receiving antennas are co-located. Given the scope of this report, radar operation in general will not be discussed as such information can be readily sourced elsewhere.

While bistatic radars have been around for just as long as monostatic radars, the complexities inherent in their design have resulted in their development lagging that of monostatic. These additional complexities include synchronisation, antenna alignment, data communications between transmitter and receivers, and increased complexity of calibration and radar algorithms. More specifically, the processing at the bistatic receiver ideally needs the following information:

1. locations of the transmitter and receiver;
2. relative pointing direction of the transmitter's and receiver's directional antennas;
3. instant of transmission of each pulse;
4. transmitted waveform; and
5. relative starting phases of each transmit pulse (Griffiths et al., 2014, Weib, 2004).

In recent years, interest in bistatic radar has increased, owing to several potential advantages along with advancements in available technology (Griffiths et al., 2010). Advantages include:

1. improved detection of covert targets, as targets designed with a minimized monostatic radar cross section (RCS) may nevertheless present a high bistatic RCS;
2. reduction of target scintillation effects, enabling improved performance of tracking radars;
3. improved detection of targets against the backdrop of clutter, as the bistatic RCS differs from that of the monostatic; and
4. a covert receiver, reducing detectability and increasing resilience to electronic countermeasures (Griffiths et al., 2014).

2. Project Charter

2.1. Project Background

The project was first proposed by Dr Joe Fabrizio in support of Surveillance and Reconnaissance Systems (SRS) branch Science & Technology (S&T) objectives and research interests. Access to practical radar infrastructure is indispensable to the SRS Branch in the pursuit of S&T objectives, developing meaningful partnerships, growing staff professionally and, above all, delivering evidence-based advice and enhanced capability to Defence.

More widely, the project supports the science and technology community's interest into the extended set of capabilities and performance that may be afforded by networked and synchronized sensors in terms of countering low observable targets (detection), target localisation and tracking, non-cooperative target recognition (identification), and electronic protection. Such improvements in integrated intelligence surveillance and reconnaissance (ISR) contribute to enhanced situational awareness in complex battlefields and decision superiority.

The project was undertaken by the author in conjunction with other work duties, doubling as his final year honours project.

2.2. Project Roles

This project is a result of collaboration between a number of key stakeholders, outlined in Table 1.

Table 1. Project Roles

Host organisation	Defence Science and Technology (DST)	
Project lead and author	Timothy Chiknaikin	Electronics Technician, MRS Group, NSID
Project sponsor	Dr Joe Fabrizio	Group Leader, MRS Group, NSID
Academic supervisor	Prof. Anthony Finn	Director, Defence & Systems Institute, UniSA
Industry supervisor	Dr Joachim Trinkle	Electronics Engineer, MRS Group, NSID

2.3. Project Objectives

In recognition of the current interest into innovation and optimisation of bistatic radar systems, the objectives of this project are outlined in Table 2.

Table 2. *Project Objectives*

OBJ 1	The BiRCD shall provide SRS branch with a bistatic radar capability, with requirements directed by branch research interests.
OBJ 2	The BiRCD shall be integrated with the existing Experimental Phased Array Radar 2 (XPAR-II) system.
OBJ 3	An effective design shall be demonstrated by the generation of a bistatic range Doppler map.
OBJ 4	The BiRCD shall support future expandability to a multi-node (multistatic) system while maximising hardware reuse.

2.4. Project Approach

A rudimentary systems engineering approach was applied to this project involving: (1) definition of project objectives and exploration of required functionality; (2) risk identification and mitigation strategies, as documented in the preliminary report; and (3) design synthesis and system validation while considering the complete problem. Concessions have been made due to external factors and the scope of the project.

The systems development model used is that of a rudimentary waterfall model, as shown in Table 3. Following each stage is a review process. This simple model was chosen as the scope of the project did not necessitate a more complex model. The structure of this report approximates these stages.

Table 3. *Waterfall model*

Stage 1	User requirements definition
Stage 2	Capability requirements definition
Stage 3	Architecture design
Stage 4	Component development
Stage 5	Integration and verification
Stage 6	Test and validation
Stage 7	Operation and support

2.4.1. Project Phases

As the scope of the project exceeded the requirements of the Engineering Internship Research Project (ENGG 4004) course, project objectives were divided into two phases as outlined in Table 4.

Table 4. *Project phases showing the division of project objectives*

Phase 1	<p>The portion of the project which includes all project components within the scope and directly relevant to the ENGG 4004 course.</p> <ul style="list-style-type: none"> • Phase 1 aimed to meet OBJ 3 and work towards OBJ 1 and OBJ 4. • Decisions made in Phase 1 were guided by the continuation of the project into Phase 2.
Phase 2	<p>The portion of the project that fell outside the scope of ENGG4004, and follows on from Phase 1. Phase 2 aims to deliver additional capability, as required by SRS. At the time of writing, work on Phase 2 had not yet begun.</p> <ul style="list-style-type: none"> • Phase 2 includes system integration and verification with the XPAR-II system. • Phase 2 will meet OBJ 2 and complete OBJ 1 and OBJ 4.

As XPAR-II's availability was anticipated to be limited, a risk mitigation decision was made early on to integrate a portion of its hardware during Phase 1. This decision was later dropped as it was realised to provide little benefit and would have resulted in increased delays. The reasons behind this decision are covered in section 4.3. This contingency was originally identified as such in the preliminary report.

2.4.2. Focus of Effort

As both human resources and the timeframe were constrained, risk was mitigated by making use of existing commercial off-the-shelf (COTS) equipment where possible. Effort was focused largely on systems engineering elements and design synthesis, integration, and validation, rather than detailed and component level design.

2.4.3. Schedule Slippage and Implementation of Contingencies

Part-way through the project, it became apparent that project schedule slippages were soon to impact upon project deliverables. The causes of these slippages were attributed to several factors including:

1. the project lead's other work commitments took priority
2. appropriate host computers were not available until mid-way through the project
3. the software driver for the hardware platform was only lightly documented while support from the supplier was minimal
4. field trial preparation activities were more involved than anticipated.

Due to these reasons, the following contingencies were implemented, as originally identified in the preliminary project report:

1. No integration with XPAR-II until project Phase 2. As the XPAR-II system has a distinct hardware platform and architecture from that of the BiRCD nodes, even partial integration would have resulted in significantly increased development time. To facilitate this, two remote nodes were constructed and used for concept demonstration against project objectives.
2. Basic project work was outsourced to the Scientific Engineering Services (SES) Group, whom assembled the Remote Node Assembly (RNA).

3. Capability Needs

The BiRCD's capability requirements were directed by branch research interests, with the project's primary driver being characterisation of bistatic sea clutter. The capability needs set out in this section are solution independent. Refer to D.1 for a breakdown of the derived system requirements.

3.1. Research Interests

Table 5 lists ongoing research interests within the branch which this project supports, and have been listed in order of pertinence to this project.

Table 5. Project Research Interests listed in order of pertinence

Sea clutter characterisation	To facilitate improvements in detection of targets against the backdrop of sea clutter by gaining an improved understanding of the properties of the sea surface as viewed by radar.
Low-bandwidth radar imaging	To support research into inverse synthetic aperture radar (ISAR), 3D imaging, and interferometry techniques.
Multistatic adaptive constant false alarm rate (CFAR) detection in clutter	To support research into adaptive techniques aimed at improving target detection in clutter. By actively switching between multistatic receivers, the receiver with the lowest clutter return at any given point in time is used for target detection. (Palamà et al., 2016)
Distributed MIMO	To facilitate research into multiple-input, multiple-output (MIMO) techniques. By grouping multiple devices into a virtual antenna array, target detection performance can be improved by exploiting the spatial domain of fading channels.

3.1.1. Sea Clutter Characterisation

Radar clutter is defined as unwanted echoes, typically from the ground, sea, rain or other precipitation, chaff, birds, insects, meteors, and aurora (Institute of Electrical and Electronics Engineers Standards Association, 2008). Bistatic sea clutter refers to radar clutter from the sea, as measured by bistatic radar.

As characterisation of bistatic sea clutter is the project's primary driver of capability, an attempt has been made to gain some insight into this field of research. A brief literature review was conducted to provide context, while a data collection scenario facilitates the requirements analysis process.

3.1.1.1. Overview

The motivation for research into this field is to facilitate improvements in detection of targets by marine radar systems. As marine targets are set against the backdrop of sea clutter, it is first necessary to gain a better understanding of the properties of the sea surface as viewed by radar.

Of specific interest are the characterised radar returns from the sea surface itself, collectively termed the normalised radar cross section (NRCS or σ^0) of the sea for backscatter. Radar echoes from sea clutter are time varying and difficult to predict due to the movement of waves across water. For this reason, the NRCS of sea clutter is mapped to a probability density function (PDF), providing a statistical description of the likely strength of the radar return. The type, median, and standard deviation of the PDF can have important implications on the detectability of marine targets.

While monostatic sea clutter has been well characterised and modelled, few programmes have attempted to characterise bistatic sea clutter due to additional complexities (Griffiths et al., 2010). These complexities will be explored the following sections.

3.1.1.2. Literature Review

One of the earliest papers on bistatic sea clutter by Pidgeon (1966) provided in-plane¹ scattering results in the C and X-bands. Pidgeon's paper appears to be one of the first publicly available on this topic and did not reference any other literature on bistatic sea clutter. This and eight other classic bistatic studies have been comprehensively reviewed by Weiner (2007), of which only four involve sea clutter and only a single study investigated out-of-plane geometries². Significantly, none of the studies provide any statistical analysis of bistatic sea clutter, nor did they measure monostatic and bistatic NRCS returns simultaneously.

A study by Kochanski et al. (1992) provides some preliminary analysis of bistatic NRCS statistics of sea clutter at X-band, with a Lognormal PDF providing the best fit to their measured data. The study did not provide a comparison to monostatic sea clutter, and ignored out-of-plane geometries.

One of the few studies to measure monostatic and bistatic NRCS returns simultaneously was by Clancy and Len (1995) who measured the bistatic NRCS for both land and sea environments at S-band. Rudimentary statistical analyses as well as forward scattering bistatic observations for out-of-plane geometries were detailed.

More recently, a collection of comprehensive studies were conducted using University College London's S-band NetRAD radar (Al-Ashwal et al., 2011, Fioranelli et al., 2016, Palamà et al., 2015). The data sets cover a range of bistatic angles³ and include out-of-plane geometry. The researchers reported that the bistatic NRCS of sea clutter is best represented by K-distribution, with the bistatic

¹ In-plane refers to those bistatic geometries where the azimuthal angle between incident and scattering waves is equal to zero degrees (Simpson, 1993, Willis, 1991).

² Out-of-plane refers to those bistatic geometries where the azimuthal angle between incident and scattering waves is greater than zero degrees (Simpson, 1993, Willis, 1991).

³ Bistatic angle is defined as the angle between the transmitter and receiver with the vertex at the target. (Willis, 1991)

PDF having a lower standard deviation than that of the monostatic. These data sets are believed to be the first published statistical analysis of simultaneous bistatic and monostatic sea clutter.

As identified in this literature review, the current research gap into the characterisation of bistatic sea clutter primarily consists of the need for

1. characterisation over a larger range of bistatic angles, particularly out-of-plane geometries
2. comparison of simultaneous monostatic and bistatic NRCS
3. characterisation over a greater set of frequency bands
4. characterisation over a greater range of sea states and atmospheric conditions.

3.1.1.3. Data Collection Scenario

The collection of data for the characterisation of radar sea clutter requires a quantitative observational study (i.e. measurement of sea clutter). As out-of-plane sea clutter characterisation is of interest, field measurements involve placing the transmitter and receiver at horizontally separated locations along a suitable coast line. Alternatively, out-of-plane forward scattering may be observed by placing the transmit and receive antennas on opposite sides of a suitable strait (e.g. Backstairs Passage, between Fleurieu Peninsula and Dudley Peninsula on the eastern end of Kangaroo Island).

To fully characterise sea clutter, the variables listed in Table 6 need to be observed and/or measured. The study's approach, to capture bistatic and monostatic RCS returns simultaneously, simplifies the preservation of internal validity in the presence of confounding variables.

Table 6. Variables required for a quantitative observational study

Independent variables	<ul style="list-style-type: none"> • Transmitter and receiver location, height, and antenna beam direction. These infer bistatic angle, distance between transmitter and receiver, and patch size (where antenna beams meet and overlap). • Radar configuration information including transmitter frequency, power, polarisation, and waveforms.
Moderating and confounding variables	<ul style="list-style-type: none"> • Sea state • Atmospheric conditions • External interferers (location and types of ships, planes, etc, in radar field of view)
Dependent variables	<ul style="list-style-type: none"> • Bistatic RCS returns • Monostatic RCS returns

3.2. Capability Needs

The project's capability needs along with justifications are outlined in Table 7. These are required to satisfy project objectives with respect to branch research interests.

Table 7. *Capability needs and justifications*

CN 1	Simultaneous monostatic and bistatic radar capability	Facilitates direct comparison between monostatic and bistatic target and clutter returns
CN 2	Synchronization of time and frequency between the nodes	Facilitates bistatic range determination and coherent processing
CN 3	Communication of configuration and status information between the nodes	Facilitates a cooperative bistatic radar configuration
CN 4	Recording of receiver data and node configuration information	Facilitates offline processing and analysis of radar measurements
CN 5	Transportability to and operation from remote measurement sites	Facilitates participation in radar measurement field trials

3.3. System Requirements & Constraints

Refer to D.1 for a breakdown of derived system requirements. Many of the system's constraints originate from the XPAR-II system; refer to D.2.

4. Architecture Design

An important element of the systems engineering process is that of architectural design, which takes the capability requirements and constraints and describes the hardware, software, and network environment.

4.1. BiRCD System Overview

Project capability requirements and constraints (refer Appendix D) necessitated the development of a bistatic pulse Doppler radar, comprising of an L-band transceiver (the remote node) which will ultimately be synchronised with XPAR-II (the primary node). An overview of the system is shown in Figure 1. When scheduled, the node's radar controller will run a pre-defined sequence of radar operations, transmitting waveforms while capturing receiver data for off-line processing.

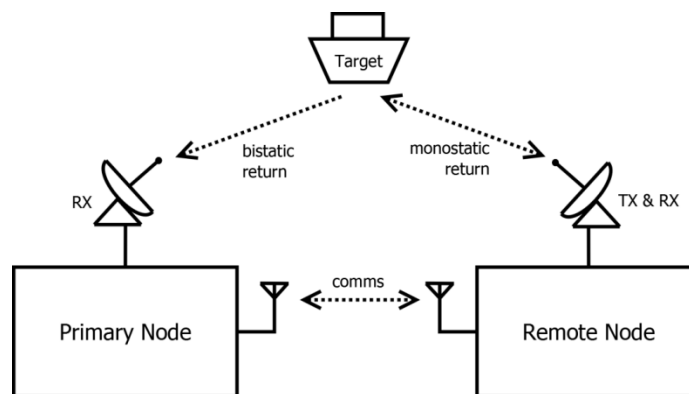


Figure 1. System diagram showing remote node as the illuminator

To clarify the distinction between primary node and remote nodes, the primary node is XPAR-II, while the remote node comprises of portable hardware which was specifically developed for this project. XPAR-II is primary only in the sense that it has the most capable hardware. Each node (including the primary) operates independently yet cooperatively. Whilst there is only one primary node, the system supports multiple remote nodes. BiRCD refers to the system as a whole, including both XPAR-II (primary node) and remote nodes.

4.2. XPAR-II Description

As the BiRCD system is required to integrate with the existing XPAR-II system, a brief description of XPAR-II is provided here to offer context and background information as a prologue to the BiRCD architecture design.

XPAR-II is a L-band phased array radar currently configured as a simple instrumentation radar; that is, the radar will transmit a group of pre-defined radar pulses and capture large amounts of receiver data for offline processing. Appointing XPAR-II as the primary node allows simultaneous capture of multiple bistatic angles without the need to manually move the receiver antenna, as it is

electronically scanned in azimuth and can accomplish different look directions during post processing.⁴

XPAR-II is composed of eight sub-arrays, each being a vertical column of the phased array antenna connected to a Transmit-Receive Module (TR Modules). A functional representation of XPAR-II is shown in Figure 2.

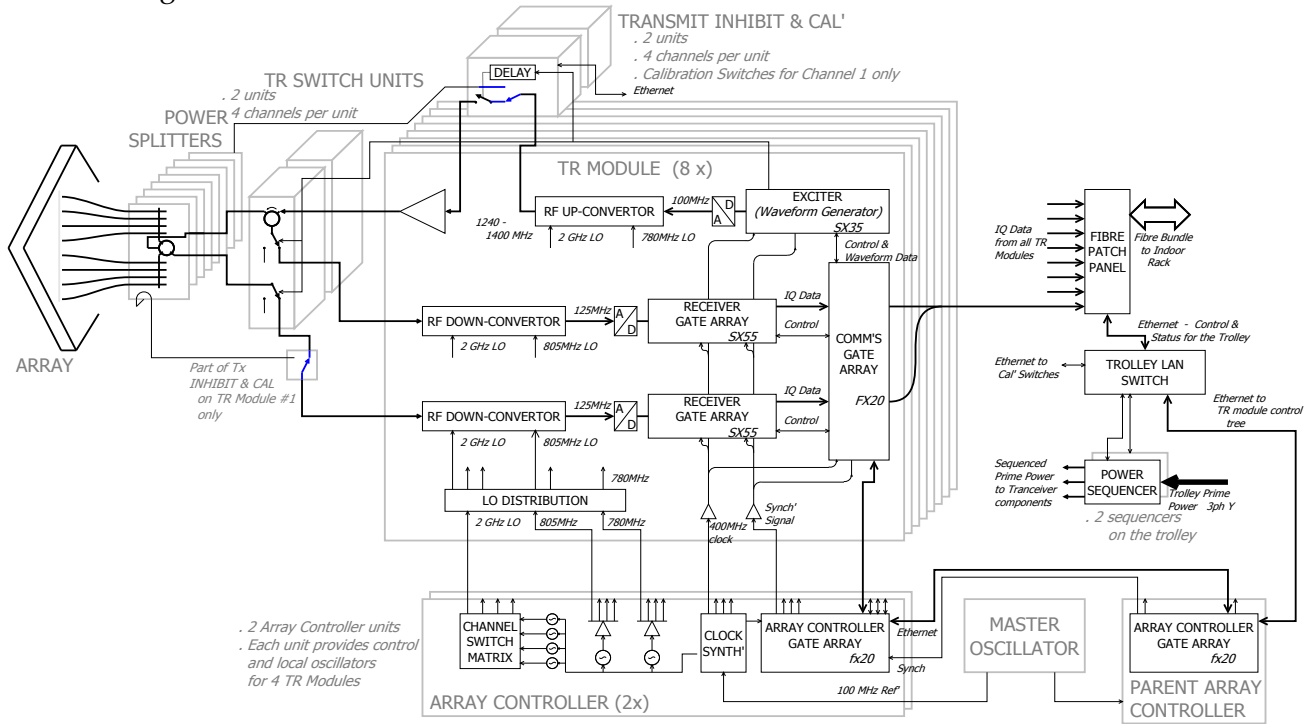


Figure 2. XPAR-II functional block diagram (XPAR II Architectural Design Document, 2009)

An overview of XPAR-II’s characteristics is outlined in Table 8. For further details, refer to Appendix D.2.

Table 8. XPAR-II characteristics overview

Item	Value	Notes
Operating frequency band	1240 - 1400 MHz	In four sub-bands centred at 1260, 1300, 1340 & 1380 MHz
Instantaneous bandwidth	40 MHz	While only 10MHz is currently achievable, 40MHz is expected in the near future.
Transmitter power (at antenna)	560W peak, 5% duty cycle max.	While each TR module can transmit 200W peak, the total system output power once calibrated is 560W peak at the antenna. Higher total output power may be realisable in the future.
Analogue to digital converter (ADC)	12 bits	

⁴ The XPAR-II system records IQ data for each column element as a separate data file. This allows for offline beam forming on receive in arbitrary azimuth directions.

4.3. Functional Solution

The developmental plan, as defined in the preliminary report, outlines the integration of a portion of XPAR-II hardware (system spares, representing one sub-array) for use during development as a representative primary node. However, it became apparent during the architectural design process that this was not the best approach. The initial motivation for this approach was to ensure compatibility between the remote nodes and XPAR-II. This would have required the development of two distinct radar controllers, one operating on the XPAR-II subarray, and another upon the remote node hardware. However, the XPAR-II subarray controller would have become completely redundant upon integration with the full XPAR-II in project Phase 2. It would not have been functionally representative either. A better solution was realised by defining a common interface with which to schedule radar operations. This approach offered several advantages:

1. Commonality with existing XPAR-II functionality, requiring only limited modifications to XPAR-II which reduces integration risk. Refer to Appendix D.5.
2. Facilitated expansion to a multimode system (OBJ 4), as hardware and software are identical across all remote nodes.
3. Simplified communication requirements between nodes.

4.3.1. Radar Controller

The radar controller directs and synchronises radar operations on each node. When commanded, it will run a predefined scheduled sequence of radar operations. Surplus XPAR-II hardware could not be used for the remote node, as doing so would have precluded expandability to a multi-node system (OBJ 4). This was due to limited quantities of existing hardware with no option to have more manufactured. As such, the hardware platform and architecture of the remote node differs from that of the primary node; therefore, BiRCD requires two distinct radar controllers, one for XPAR-II and another for the remote nodes. XPAR-II's radar controller already existed, but will require some minor modifications (refer to Appendix D.5). A radar controller for the remote nodes was developed and ties together all of the required functionality; implementation details were heavily dependent upon the chosen remote node hardware platform.

4.3.2. Script File

A script file which is common to all nodes directs the deterministic and synchronised scheduling of radar operations across all nodes (deterministic in the sense that they can be predicted). Each node's radar controller references the common script file to schedule each node with the appropriate sequence of radar operations. While all remote nodes have identical hardware and software, an identification number unique to each node is referenced to the script file to direct node specific behaviour. Refer to D.4 for the definition of the script file.

4.3.3. Communication

Certain information must be known by each node prior to a cooperative bistatic radar capture. The information requirements are

1. the exact sequence of the radar's transmissions (as defined in the script file), and
2. the timing of the radar's transmissions.

While additional information is required to process captured bistatic radar data (refer to 1.1), it is not required for a cooperative bistatic radar capture itself and can be provided later. An important note here is that if the desired radar operations and capture times are known in advance, these can be preloaded onto each node to achieve a cooperative bistatic radar configuration without any real-time communications whatsoever. The communications prerequisites are therefore related to the level of flexibility required.

As XPAR-II operates on the DST Protected Research Network (PRN), communications have to comply with DST Group policies' restrictions on information transfer which influenced the choice of medium and protocol. Due to the deterministic nature of the functional solution, communication requirements were simplified to that of the initial start time of the radar's scheduled operations and certain configuration parameters such as frequency and script file. Once the nodes have begun to run the scheduled sequence of radar operations, a common schedule and clock base will ensure that all nodes operate synchronously. This removed operational risks such as communications dropouts and processing delays during a run, and simplified DST security implications.

When considered within the context of DST security requirement and schedule slippage, it was decided that communication requirements would be met by human operators. This proved simple to achieve; once a common start time and configuration parameters are communicated between the node's operators (via mobile phone or hand held radio for example), the deterministic nature of the radar operations ensures a cooperative radar configuration. In practice, this simple solution was found to work remarkably well.

4.3.4. Synchronisation

A crucial problem associated with bistatic systems is that of frequency and time synchronisation between transmitter and receiver for coherent signal processing and range measurements (Weib, 2004). In radar, coherence refers to the required consistency in the phase of a signal from one pulse to the next.

Synchronisation of the local references of the nodes could have been achieved by either

1. correlation of the transmitted signal over the baseline (direct-path) to that of the bistatic target return, such as is used by non-cooperative bistatic radars; or
2. use of local clocks that have been synchronized before the start of operations (Willis, 1991).

For this project, the GPS based synchronisation solution was chosen as it delivered suitable accuracy⁵ at low cost and was simple to implement.

4.3.5. Signal Processing

The problem presented was how to process all of the necessary information and the receiver data to form a bistatic range Doppler map. For simplicity, no real-time processing of receiver data is performed.

Radar signal processing techniques are employed to separate targets from clutter on the basis of Doppler content and amplitude characteristics. Specifically, pulse compression and Doppler processing are employed to improve the signal to noise ratio of the target in the captured receiver data. The processed data, when combined with information about the bistatic configuration, is plotted on a range Doppler map.

4.4. Functional Diagram

The primary node is comprised of XPAR-II and ancillary components to achieve communication and synchronisation between the nodes. A representative block diagram illustrating the node's functional components is shown in Figure 3. The functions of the components are described in Table 9.

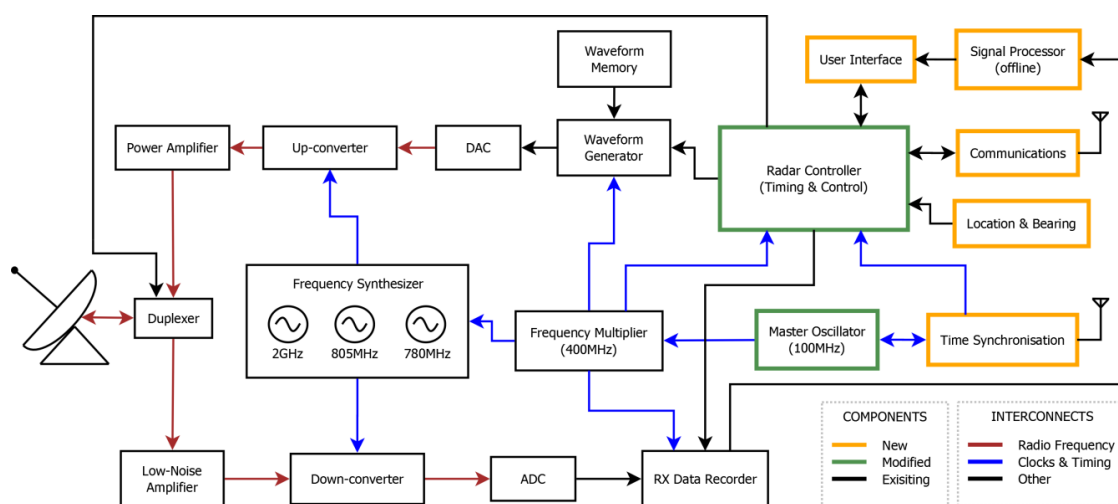


Figure 3. Primary node functional block diagram (showing one of eight transceiver channels)

⁵ Typical GPSDO accuracy of 1 PPS pulse is ± 30 ns to UTC RMS which equates to a range error of less than 18 metres, but is typically lower, dependent on bistatic geometry and tracking accuracy between GPSDO units. In comparison, XPAR-II's 10MHz instantaneous bandwidth results in a nominal range resolution of 15 metres. This error is acceptable as BiRCD is not a tracking radar and does not require fine range accuracy.

The remote nodes functionally comprise of transceiver components, a radar controller, and communication and synchronisation components. The remote node is a completely new design. A representative block diagram illustrating the node's functional components is shown in Figure 4. The functions of the components are described in Table 9.

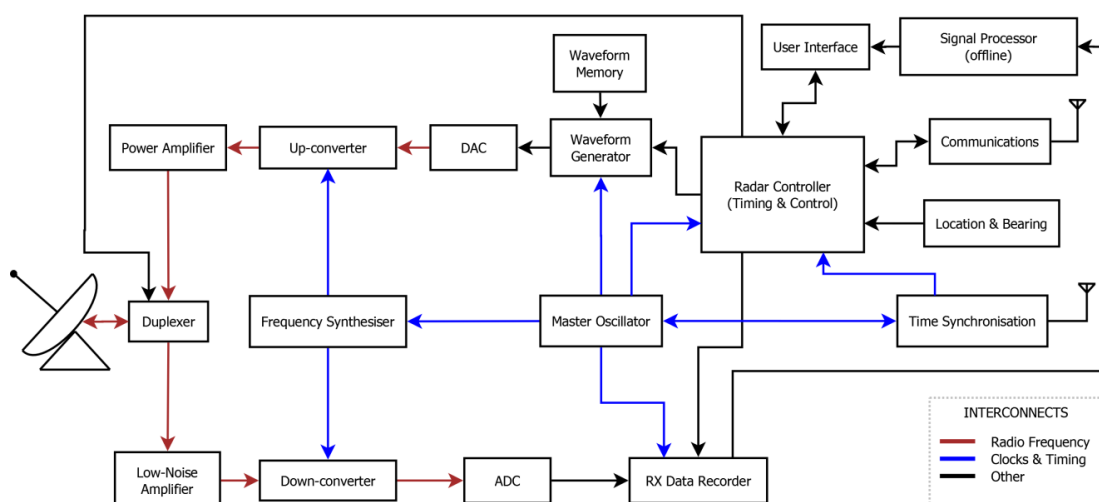


Figure 4. Remote node functional block diagram

Table 9. Description of node functional components

Radar controller	Controls and schedules radar activity. Provides synchronising signals that time and control radar operations.
User interface	Displays and accepts radar status and configuration updates to/from the operator. Allows user to load the script file for execution.
Communications	Provides a data communications link between the nodes. Required for a cooperative bistatic radar configuration.
Location & bearing	Provides node location and antenna bearing information. Required for bistatic target range and position estimates.
Time synchronisation	Provides a synchronised timing reference to each node. The primary and remote nodes require a synchronised common time base to allow bistatic radar operation.
Master oscillator	Provides a low phase noise frequency reference to each node.
Frequency synthesiser	Provides the various basic frequencies to achieve frequency agile capabilities. The generated frequencies are used to shift the frequency of transmitted and received signals.

Waveform memory	Stores the baseband transmitter pulses which comprise of in-phase and quadrature (IQ) data that defines pulses that are to be transmitted.
Waveform generator	Plays the baseband transmitter pulse data when a synchronisation pulse is received from the radar controller. The pulse data are digital and originates from IQ data stored in waveform memory.
DAC	Converts the digital baseband transmitter pulses to an analogue signal.
Up-converter	Converts the baseband transmitter pulses to a high frequency signal for transmission.
Power amplifier	Amplifies the low power transmitting signal.
Duplexer	Alternately switches the antenna between the transmitter and receiver. This allows the use of only one antenna, while protecting the sensitive receiver from the high power transmitting signal.
Antenna	Transfers the transmitter energy to signals in space with the required distribution and efficiency. The reverse occurs on reception.
Low-noise amplifier	Amplifies the very weak backscatter signals while minimising the addition of noise which would reduce the signal to noise ratio of the received signal.
Down-converter	Converts the high frequency received signal to base band (low-frequency). Signal conditioning and sampling is easier at the lower frequency.
ADC	Converts an analogue version of received signals to a digital form which is easier to process and store.
Data recorder	Stores the digital received signals for later offline processing.
Signal processor	Provides offline processing of stored receiver data in regards to Doppler content and amplitude characteristics, separating targets from clutter.

5. Remote Node System Development

In this section, a set of solutions are developed with reference to the architectural design which satisfy the project's capability requirements (refer D.1) and constraints (refer D.2). Given the scope of this report, only high-level implementation details are discussed.

The majority of design decisions involve compromises between performance, cost, and complexity. For example, the power amplifier and antennas were chosen out of those already available to the Branch; they were not necessarily the optimal equipment choices. Considering these compromises, system analysis techniques were employed during development to optimise system performance and to ensure that capability requirements would be satisfied; the details of which have been included in Appendix A.

5.1. Hardware Platform Choice

Several options were investigated as to their suitability as a hardware platform for the remote nodes. A Commercial off-the-shelf (COTS) option was sought, as both human resources and the timeframe were constrained. The major options which were considered are discussed briefly below, with the final choice being a software-define radio (SDR) device.

5.1.1. Surplus XPAR-II hardware

Surplus XPAR-II transceivers were considered as the hardware platform for the remote nodes, as this would have likely simplified integration with XPAR-II (OBJ 2) due to commonality. However, doing so would have precluded future expandability to a multi-node system (OBJ 4). This is due to the existing limited quantities of transceivers and no option to have more manufactured. As such, the hardware platform and architecture of the remote node differs from that of the primary node.

5.1.2. Test and Measurement Equipment

While a readily available COTS option when combined with instrumentation software, high associated purchase costs would have limited expandability to a multi-node system (OBJ 4), and limited customisability may have restricted integration with XPAR-II (OBJ 2) as well as system flexibility and functionality.

5.1.3. Software-defined Radio (SDR)

A SDR is a radio communications device in which some or all of its functionality is software defined. These devices typically consist of a transceiver combined with IQ sampling and control all in one device. As SDRs are configured and driven by software, they are very flexible in application. Such devices offer several advantages to this project including low cost, high flexibility, and scalability. There are a wide variety of SDRs available, ranging from low-cost units aimed at hobbyists to high-performance units aimed towards professional use. They are popular within the open source community as code is often portable for a given SDR architecture.

SDR technology affords future expandability to a multi-node system (OBJ 4), as additional devices could be purchased at reasonable cost. Their flexibility would aid in integration with XPAR-II (OBJ 2) along with furthering secondary research interests (independent of the XPAR-II system and its constraints) such as higher-bandwidth radar imaging or MIMO techniques. Furthermore, there was interest from within the branch into the performance and capabilities offered by this relatively new technology and its suitability for future projects.

For these reasons, SDRs were chosen as the remote node hardware platform. Several options were considered. The Ettus brand of Universal Software Radio Peripheral (USRP) was chosen as a few members of DST had some exposure to USRPs, they appeared to have the greatest open source presence, and appeared to be the most mature of the SDR products available. While one of their more modest models would have sufficed for this particular project, the high-performance X310 USRP along with UBX-160 daughterboards were chosen to better accommodate future changes in project direction.

5.2. Radar Controller Development

5.2.1. Context

The radar controller provides core system functionality which defines the radar's behaviour and to a large extent, its performance. Developed was initially quite daunting, as the project lead had no prior experience with the USRP device, Linux, or radar development in general, and proving to be the most challenging aspect of system development. As the learning curve was great, development was approached progressively; that is, by developing and integrating minor functionality in stages. While this approach has resulted in a more improvised form of radar controller application, it was necessary given the circumstances. To give an indication of the complexity of the final BiRCD radar controller, it comprises of approximately 1,300 physical source lines of code.

This section discusses the development of the radar controller. Refer to Appendix C for an overview of how to configure and run the radar controller, including necessary runtime parameters and files. The full source code can be made available upon request.

5.2.2. Radar Operations

The radar controller is responsible for scheduling each node's transmit and receive events, referred to hereafter as bursts. A burst comprises of a single coherent processing interval (CPI) in which multiple pulses are transmitted and/or receiver data are captured. A CPI denotes a single continuous receiver capture, while a transmit pulse denotes transmission of up-converted in-phase and quadrature (IQ) pulse data (typically a linear frequency modulated chirp). The succession of transmitter pulses within a burst constitutes the waveform. Burst parameters are specified in a script file which includes the burst number, the number of transmit pulse repetitions, the time between each transmit pulse (PRI), and the IQ pulse data file reference. A simplified example of these radar operations is shown in Figure 5 which illustrates the terminology. Each burst comprises multiple transmit pulses spaced by the pulse repetition interval (PRI); the spacing between successive bursts is termed the inter-burst spacing (IBS) in which there are no radar operations, typically on the order of 10-50ms.

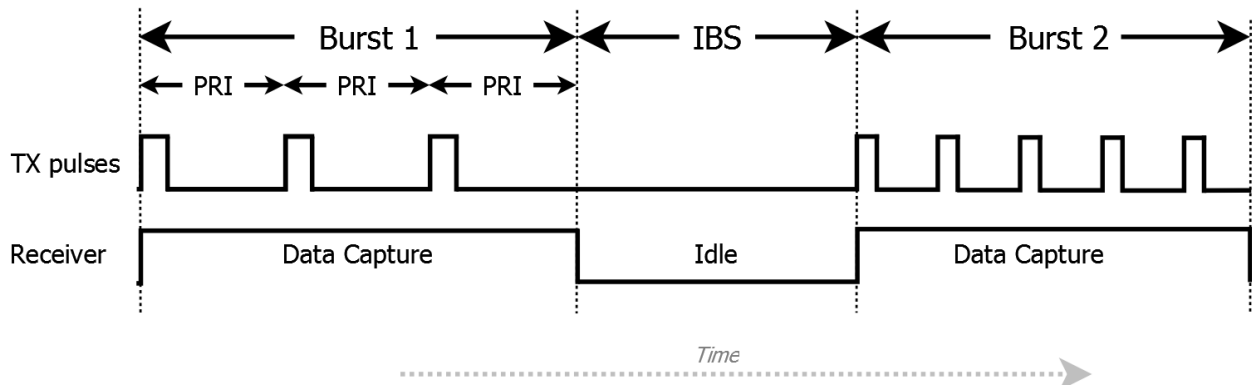


Figure 5. Example of radar operations, showing burst parameters

Burst parameters are tailored according to the intent of the radar operation. Examples of burst types may be short PRI (Doppler unambiguous), medium PRI (range and Doppler ambiguous), long PRI (range unambiguous), long CPI (high coherent processing gain), and passive receive; each representing a compromise between performance and capability. Refer to section 6.3 for details on how the burst parameters were chosen to meet project objectives.

5.2.3. Computing Platform

The platform on which the radar controller operates consists of a host computer which interfaces with the Ettus X310 USRP as shown in Figure 6. Unfortunately, much of the initial development took place on computer hardware which did not satisfy the USRP's recommended requirements, as more suitable computers were not initially available. This slowed development, as additional time was needed to improve performance and solve related interface issues. These computers were eventually replaced by some more capable; the final computing platform specifics are shown in Table 10.

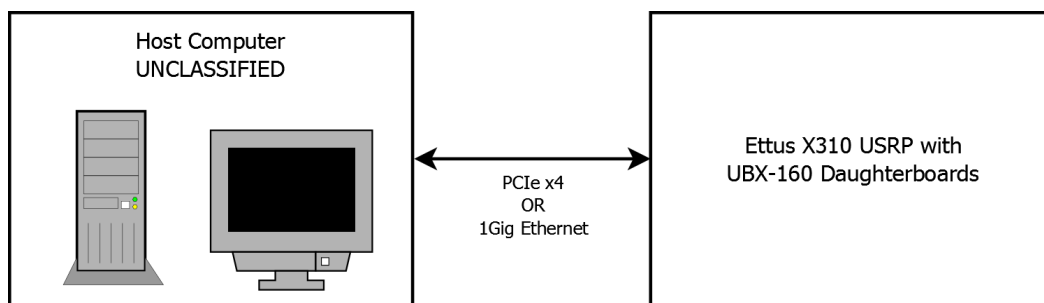


Figure 6. Radar controller computing platform diagram

The two interface options are shown in Table 10. The Ethernet interface was used during initial development as it is plug-and-play and offers sufficient bandwidth; however, its reliability was a continual concern as it proved difficult to eliminate recurrent packet errors. The final system interfaces with the USRP device via a PCIe x4 interface as it proved to be much more reliable.

Table 10. Radar controller computing platform specifics

Host computer	Ubuntu 16.04 x64 operating system Intel i7-6700 CPU 32GB RAM 1TB SSD HDD
Interface	PCI-Express x4, supporting 200Ms/s throughput @ 16-bit OR 1 Gigabit Ethernet, supporting 25Ms/s throughput @ 16-bit
SDR Platform	Ettus X310 USRP fitted with two UBX-160 RF daughterboards, capable of up to 160MHz instantaneous bandwidth over 10MHz to 6GHz.

5.2.4. USRP Hardware Platform

The basis of the remote node’s hardware platform is the Ettus X310 USRP. The USRP is a highly flexible and scalable software-defined radio (SDR) intended for the development of wireless communication systems. Fitted with the UBX-160 daughterboard, the USRP can operate from 10MHz to 6GHz with up to 160MHz of instantaneous bandwidth.

At the core of the USRP is the Xilinx Kintex-7 field-programmable gate array (FPGA) which runs the USRP hardware driver (UHD) firmware written in Verilog. The FPGA provides major connectivity between USRP components including the USRP’s internal RF front-end, host interfaces, and memory. As the USRP is software defined, some of the transceiver’s functional blocks are provided by the FPGA core including digital up/down-conversion, fine-frequency tuning, and other digital signal processing (DSP) functions. The block diagram of the X310 is shown in Figure 7.

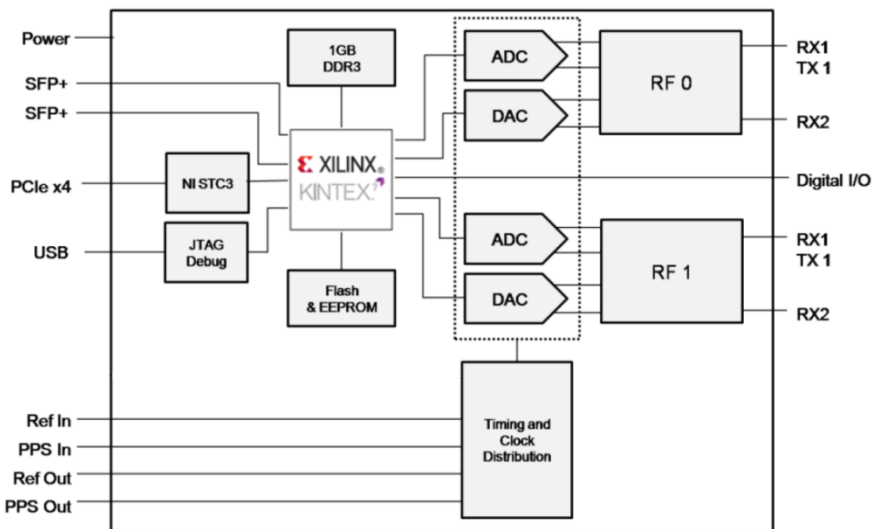


Figure 7. Ettus X310 USRP block diagram (USRP X310, 2017)

The USRP’s internal RF front-end consists of the UBX-160 daughterboard which provides full-duplex transceiver functionality. The block diagram of the UBX-160 is shown in Figure 8.

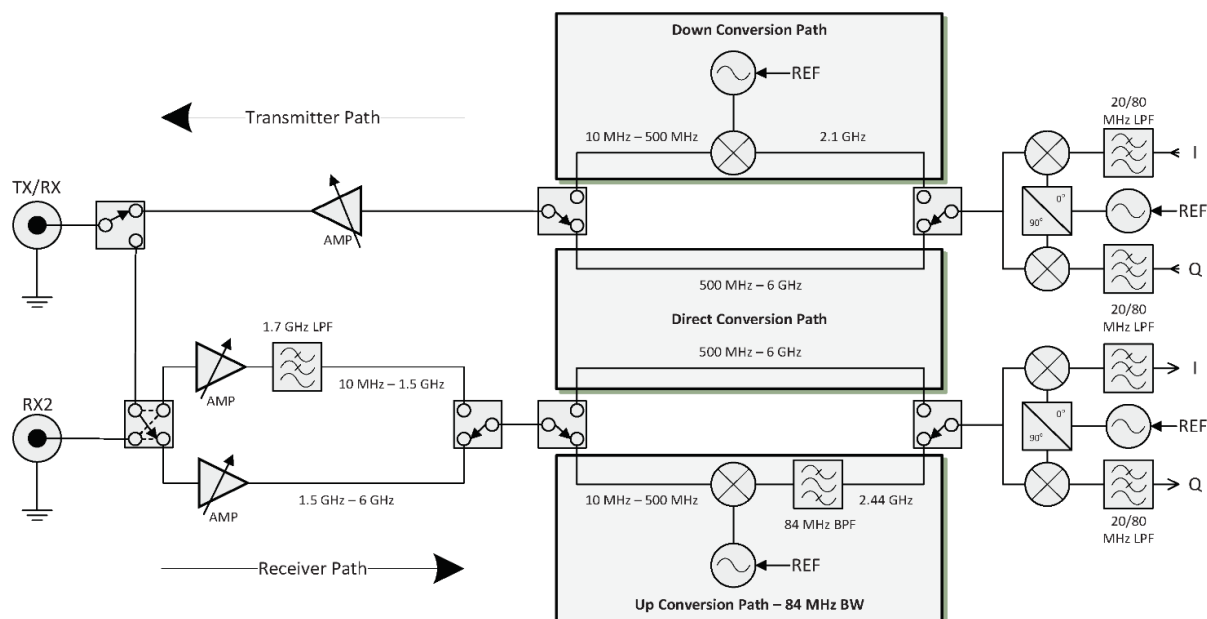


Figure 8. Ettus UBX-160 daughterboard block diagram (USRP X310, 2017)

5.2.5. USRP Software Environment

The majority of USRP hardware driver (UHD) code is open source, along with some of the high-level application frameworks. The USRP software environment is layered and rather complex, comprising principally of the low-level UHD including FPGA firmware and host drivers, mid-level C++ and Python application programming interfaces (API), and several high-level application frameworks.

Several of the high-level application framework options were explored as to their suitability for implementation of the radar controller; specifically GNU Radio, LabVIEW, and Matlab. However, it was found that none of these frameworks support scheduled USRP events; a requirement for cooperative bistatic radar operation. The mid-level Python API was also considered but is still in development and is completely undocumented. The most suitable API with which to implement the radar controller is the UHD C++ API.

5.2.6. Software Development

The radar controller application was developed progressively, a reflection of the project lead's learning curve. During the learning process, it was soon realised that perceived support for the Ettus USRP was exaggerated. In the opinion of the project lead, the most comprehensively supported API (C++) is inadequately documented, requiring many functional and implementation details to be discovered from source and example code. Furthermore, the support provided by Ettus itself was nominal. These factors unfortunately contributed to a much steeper learning curve than anticipated.

Development of the radar controller software was approached as shown in Table 11.

Table 11. Radar controller development steps

Step 1	Verify the hardware and software configuration	The hardware and software configuration was tested and debugged through UHD utility applications and by compiling and running the UHD example code provided.
Step 2	Learn how to program the USRP device	Learning took place primarily through reviewing the available documentation, and by experimenting with the supplied example code while observing changes in functionality.
Step 3	Implement own functionality	Initial radar controller functionality was first explored by making modifications to existing example code. These changes were gradual, slowly morphing the original code to express the required functionality of the radar controller.
Step 4	Integrate major functional blocks	By this stage, the functionality and interface of the USRP were well understood. A radar controller application was created and major functional blocks implemented.
Step 5	Debug and optimise performance	Initial evaluation of the performance and reliability of the radar controller took place on the single available computer. Changes were made to the radar controller software architecture to reduce the number of communications errors and the processing overhead.
Step 6	System test and verification	The radar controller was run on the final hardware and host computers as a complete system. Any remaining functionality necessary for the successful deployment of the BiRCD radar was implemented. The system as a whole was tested and verified on a functionally complete system comprised of two remote nodes.

5.2.6.1. USRP limitations

A complicating factor encountered during development was that the USRP Hardware Driver (UHD) only supports scheduling one receive capture at a time, as the UHD receive function is a blocking call. Consequently, the radar controller must wait until the receiver capture is complete before the subsequent burst may be scheduled. However, as the host computer does not run a real-time operating system, the thread in which the radar controller is running may at times not receive any central processing unit (CPU) time for an extended period; by which time the scheduled start time of the next burst may have already passed. The implications of this observation are significant: the spacing between bursts must be greater than the upper end of this time period or missed bursts must be well tolerated, either of which may markedly reduce radar performance.

This issue was resolved by (1) increasing host computing resources by using more capable desktop computers, (2) implementing the radar controller as a multi-threaded application, and (3) optimising the radar controller so as to require less computing resources. These improvements were sufficient to ensure that burst schedule slippages were seldom encountered during testing. To give an indication as to how frequently these burst schedule slippages occur, 64,000 bursts per

node were executed during the field trial with an inter-burst spacing (IBS) of 20ms, of which remote node 1 (RN1) reported 11 burst errors while remote node 2 (RN2) reported 36 burst errors. No other errors were reported (refer to section 7.1.5). The frequency of errors can be further reduced by increasing the IBS, but at the expense of radar performance as the duty cycle is effectively decreased. In the author's opinion, this UHD architectural limitation has significant implications in regards to the way USRP devices should be used in future radar projects.

5.2.6.2. Software Architecture

The structure of the radar controller application is shown in Figure 9 configured for monostatic operation (both transmitting and receiving). Four threads are depicted: (1) the main thread from where all other threads are launched, responsible for initialisation, logging, and processing; (2) the TX worker thread which configures the USRP for transmitter pulses, returning once scheduled; (3) the RX worker thread which configures the USRP for receiver capture, returning once the entire capture has completed; and (4) the TX helper thread which monitors the interface for any reported transmitter errors. There are as many TX and RX worker threads as there are bursts, but a maximum of four total threads running at any one point in time.

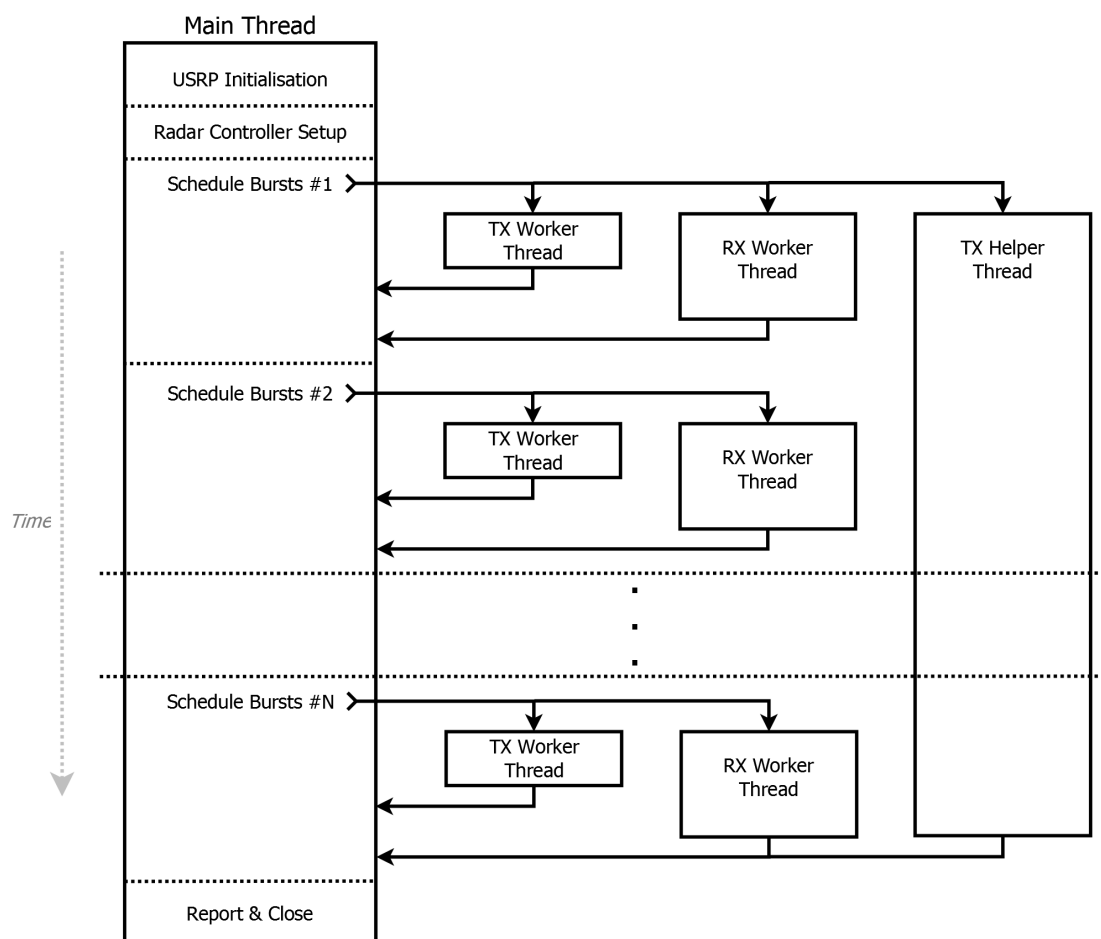


Figure 9. Radar controller application architectural diagram, showing use of multiple processor threads

As the USRP can only be scheduled with one receiver capture at a time, the RX worker thread encapsulates this limitation while allowing other threads to proceed with their tasks. The radar controller will be ready to proceed with the subsequent burst prior to the RX worker thread returning.

5.2.6.3. Error Handling

All USRP related errors are captured and logged. Receiver errors are captured by the RX worker thread and returned to the main thread for logging. Transmitter errors are asynchronously captured by the TX helper thread and returned to the main thread for logging. Burst errors are well handled; if an error is encountered during a burst, the error details are recorded and the radar controller proceeds with the next burst. The most common errors encountered are `ERROR_CODE_LATE_COMMAND` where the requested start time of a burst has already elapsed, and `OUT_OF_SEQUENCE` errors where the interface has either dropped a packet or received data out of order. `OUT_OF_SEQUENCE` errors were somewhat frequent while using the 1Gig Ethernet interface. Since changing to the PCIe interface, they have not been observed. `ERROR_CODE_LATE_COMMAND` errors occur when CPU tasking, which is controlled by the operating system, results in insufficient CPU time allocation. These errors been observed to occur more frequently when both the inter-burst spacing (IBS) is short in duration (e.g. 10ms) and the operating system is heavily tasked by other applications (such as when processing range Doppler maps while the radar controller is running).

5.2.7. Synchronisation

A cooperative bistatic radar configuration is achieved by synchronising each node to a GPS disciplined oscillator (GPSDO), providing time-aligned and phase coherent samples. Coherence refers to having a consistent phase relationship from one pulse to the next, which can be achieved with reasonably stable oscillators.

The GPSDO provides the nodes with common GPS locked reference signals: a 10MHz reference and a pulse-per-second (PPS) signal. The 10MHz reference provides long-term alignment between the coherent oscillators of the various nodes, which enables detection of frequency shift (i.e. Doppler) to measure the rate of change in round trip delay. The PPS provides a common time base for time-alignment of samples and enables radar operations to execute concurrently between nodes. During initialisation, the radar controller instructs the USRP to (1) lock to the GPSDO's 10MHz frequency reference, (2) latch the real time clock (RTC) to the GPSDO's PPS signal, and (3) set the RTC to coordinated universal time (UTC). UTC is provided by the GPSDO which is used to timestamp all radar operations and captured data. The GPSDO also provides the GPS coordinates of the nodes which are logged for use during post-processing of radar data.

While the timing variance between the nodes has yet to be quantified due to insufficient time, the results achieved during the measurement trial demonstrate that the chosen synchronisation solution effectively satisfies project requirements.

5.2.8. Timing Signals

The radar controller provides timing signals to supporting hardware. Timing signals are required by the power amplifier (PA) and the receiver switch. A PA is required as the USRP is only capable of transmitting at low power and therefore would not be able to satisfy performance requirements. The need for active switching of these devices is covered in section 6.2.

The timing requirements must take into account the switching transition times of the PA and receiver switch. For example, the PA should be gated on in advance of the RF input being applied, so as to allow sufficient time to transition states before the transmit pulse commences, and gated off in delay to removal of RF input. Likewise, hot switching of the receiver switch is undesirable as it may reduce the life expectancy of the switch.

5.2.8.1. USRP Cropping of Samples

It has been observed that the USRP itself requires time to transition between states. During early testing of the USRP in loopback, cropping of the leading and trailing portions of captured samples was observed, as shown in Figure 10. The leading cropped samples are attributed to the USRP receiver, as they are still observable when a signal from a signal generator is input into the receiver. The trailing cropped samples are attributed to the transmitter, as they are still observable on the transmitted signal when viewed on a spectrum analyser.

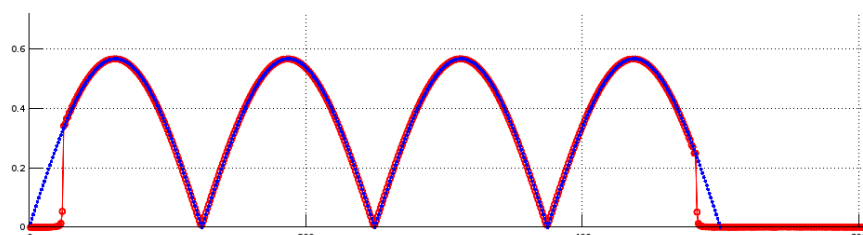


Figure 10. Magnitude response of a transmitted test waveform (blue) shown against the receiver capture in loop-back (red), showing leading and trailing cropping of receiver samples.

To resolve this issue, the leading and trailing portions of the transmitter IQ pulse data samples were padded with zero samples, the result of which is shown in Figure 11. The required number of zero samples is a function of the sample rates of the receiver and transmitter; the higher the sample rate, the more padded samples required, demonstrating that the issue is time related. 260 leading and trailing zero samples were found to be sufficient for sample rates up to and including 100Msps. Such padding has been applied to all of IQ pulse data files.

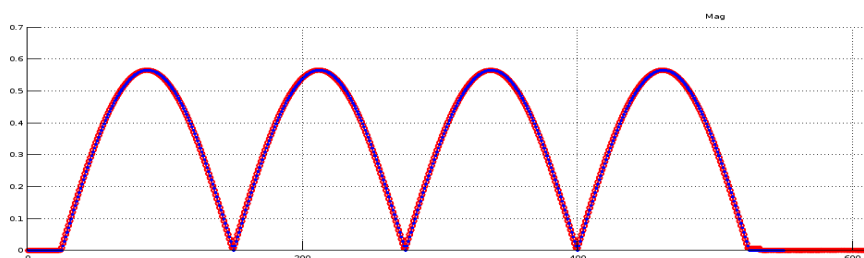


Figure 11. Magnitude responses of a transmitted test waveform (blue) shown against the receiver capture in loop-back (red) where the IQ pulse data are padded with leading and trailing zero samples.

5.2.8.2. Implementation Details

The USRP has a general purpose input output (GPIO) port which has been used to provide timing signals to the power amplifier and the receiver switch. While GPIO events can be manually scheduled using the USRP's real time clock (RTC), UHD provides functionality to automatically trigger the GPIO when the USRP transmits and/or receives, referred to as automatic transmit / receive (ATR).

As previously noted, the transition time requirements of the USRP and supporting hardware must be considered; specifically, the slowest device determines the transition time required. As the transmitter IQ pulse data file is padded either side by 260 zero samples which are processed at 100Msps, the USRP is the slowest device, requiring 2.6 μ s to transition. The padded samples when combined with ATR functionality provide a timed signal from the GPIO which is suitable to switch the power amplifier and the receiver switch. Figure 12 shows the scheduled transmit pulse (which corresponds with the GPIO switching signal) referenced against the actual RF excitation of the transmitter. Due to the padded samples, the power amplifier and receiver switch have an ample 2.6 μ s in which to transition between states. Refer to Appendix A.4 for a full timing diagram of all switched components.

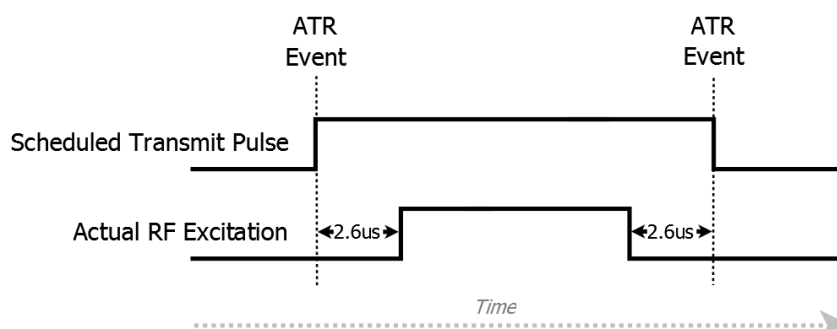


Figure 12. GPIO switching signal referenced against the actual RF excitation of the transmitter

5.3. RF Front-end Development

The term RF front-end generally refers to all circuitry between the antenna up to and including the mixer (Carr, 2001); however for the purposes of this report, the term will be used loosely to refer to all RF circuitry between the antenna and the USRP device, including both transmitter and receiver components. While the USRP contains its own internal RF front-end, external circuitry is required to improve system performance and satisfy capability requirements.

The development of a custom RF front-end focused primarily on (1) improvements to the system noise floor, (2) increased transmitter power, and (3) reduction of out-of-band spurious emissions. Reductions to the system noise floor and greater transmitter power contribute to enhanced target detections, while reduction of out-of-band spurious emissions is necessary for regulatory spectrum compliance. The final form of the RF front-end is shown in Figure 13; refer to Appendix E for the full size diagram. The design decisions involved will be briefly discussed in the following sections.

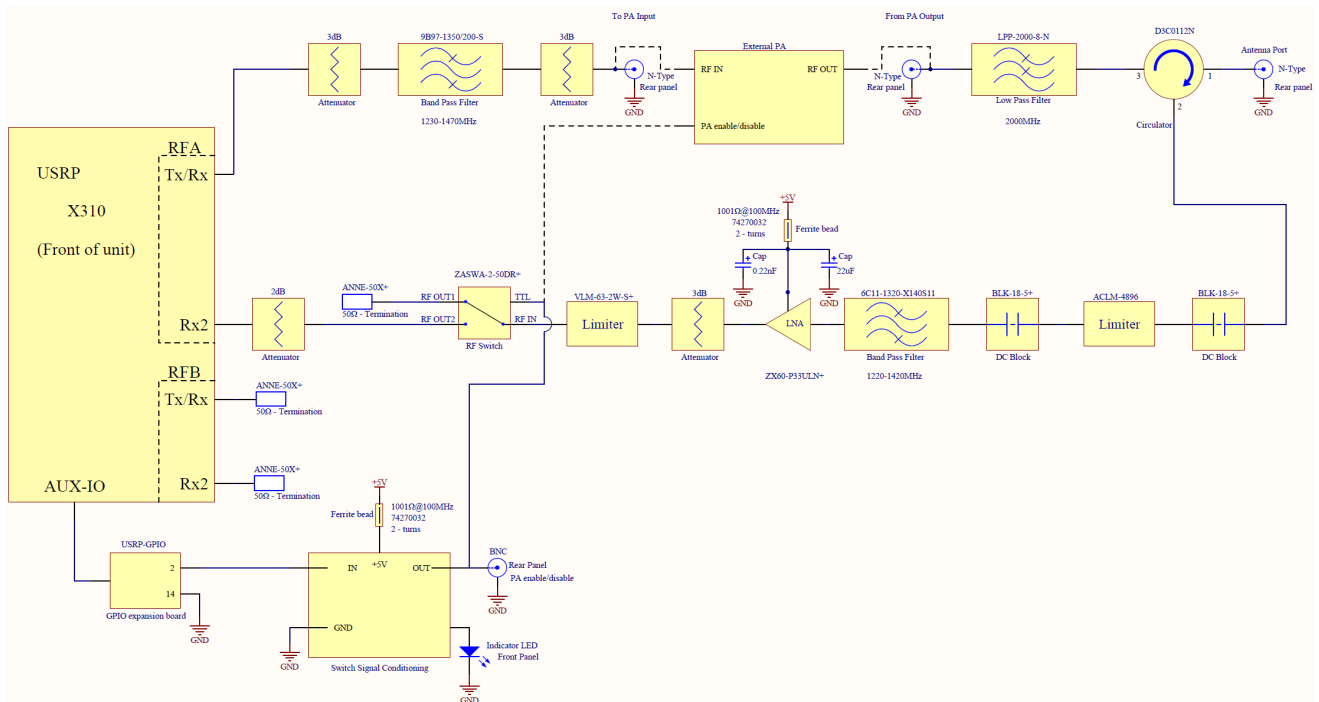


Figure 13. Remote node RF front-end schematic diagram; refer to Appendix E for full size.

5.3.1. Context

It is important to keep in mind that none of the design decisions were made in isolation; that is, the final RF front-end when combined with the rest of the system must meet or exceed the capability requirements set out in Appendix D.1. To ensure this, system analysis techniques were employed and are detailed in Appendix A.

While bistatic sea clutter characterisation is the primary driver of capability for this project, due to limited time and resources, system capability and performance were demonstrated during a land-based field trial. As such, some design decisions reflect this concession.

5.3.2. Hardware Selection

5.3.2.1. Antenna

The choice of antenna was limited to those already available to the branch. A high gain antenna with approximately 3 to 5 degree horizontal beamwidth is desirable to resolve wavefronts for sea clutter characterisation. However, as capability would be demonstrated during a land-based field trial, an antenna with a wider beamwidth was desired so as to offer a larger field of view over which airborne targets can be detected. The PEI 1247X vertically polarised six dipole antenna array was chosen as the most suitable available, with a 41 degree horizontal beamwidth and 18dBi of gain operating over 1260-1360MHz. Being a dipole array, the antenna is more portable than an equivalent L-band dish antenna.

5.3.2.2. Power Amplifier

The choice of power amplifier was limited to those already available to the branch. Requirements include (1) a gated input providing PA enable/disable functionality, so as to provide isolation between the input and output, and to inhibit thermal noise when not transmitting; and (2) a combination of high power and portability. The response time of the gated input is important: PA enable time should be faster than the time delay introduced by zero padding the transmitter samples (refer to section 5.2.8.1), while a fast PA disable time ensures that the radar's minimal minimum range is kept to a minimum (refer to section A.3). Greater transmitter power improves the signal-to-noise ratio (SNR) for a given target return. The Tomco 200W RF L-band amplifier was chosen as the most suitable available, as detailed in Table 12.

Table 12. Tomco 200W power amplifier specifications

Model number	BT00200-Lambda-CW
Peak power	200W for +7dBm drive, but capable of up to ~300W when compressed
Frequency	1.235 GHz- 1.385 GHz
Gain	46dB nominal
PA enable / disable response	430ns / 150ns (measured)

5.3.2.3. Duplexer

A duplexer is required to isolate the transmitter from the receiver, allowing bi-directional communications via a single antenna while protecting sensitive receiver components from the high power transmitted signal. The functionally simplest RF front-end actually does not contain a duplexer, rather separate transmitter and receiver antennas (Quasi-monostatic). However, this approach was not chosen as it requires two antennas per site in addition to extra antenna mounts, impacting on transportability.

Choices for duplexer were either a transmit-receive switch or a circulator. A circulator was chosen as it proved difficult to find an RF switch of the required power rating. However, as circulators offer less isolation than that of a switch, the addition of a limiter to protect sensitive receiver components was necessary.

5.3.3. Noise Figure

The effectiveness with which radar can detect a target echo depends on the ratio of signal power to noise power. This noise originates both from within the system and in the outside environment. Noise figure (NF) is a measure of degradation of the signal-to-noise ratio (SNR) due to components in the RF signal chain. It is a number by which the performance of a system can be specified, lower being better. The noise figure is defined as the ratio of the output noise power of a device to the portion thereof attributable to thermal noise in the input termination at standard noise temperature T_0 (usually 290 K). (Reviews, 2017)

RF front-end components were selected so as to minimise their contribution to receiver noise figure. Furthermore, the PA is disabled when not transmitting so as it remove its otherwise significant contribution to system noise. Refer to section A.1 to view how the receiver noise figure was calculated.

5.4. Remote Node Assembly

The Remote Node Assembly (RNA) is a rack mountable 3U case which houses much of the remote node's hardware. Specifically, the RNA contains the USRP device, RF front-end components, the GPSDO, and supporting components such as power supply and signal conditioning circuitry. Due to time constraints, the RNA was assembled by an apprentice from Scientific Engineering Services Group. Refer to Appendix E for the full schematic diagram of the RNA.



Figure 14. RNA (top-right) and PA (bottom-right) setup during the field trial

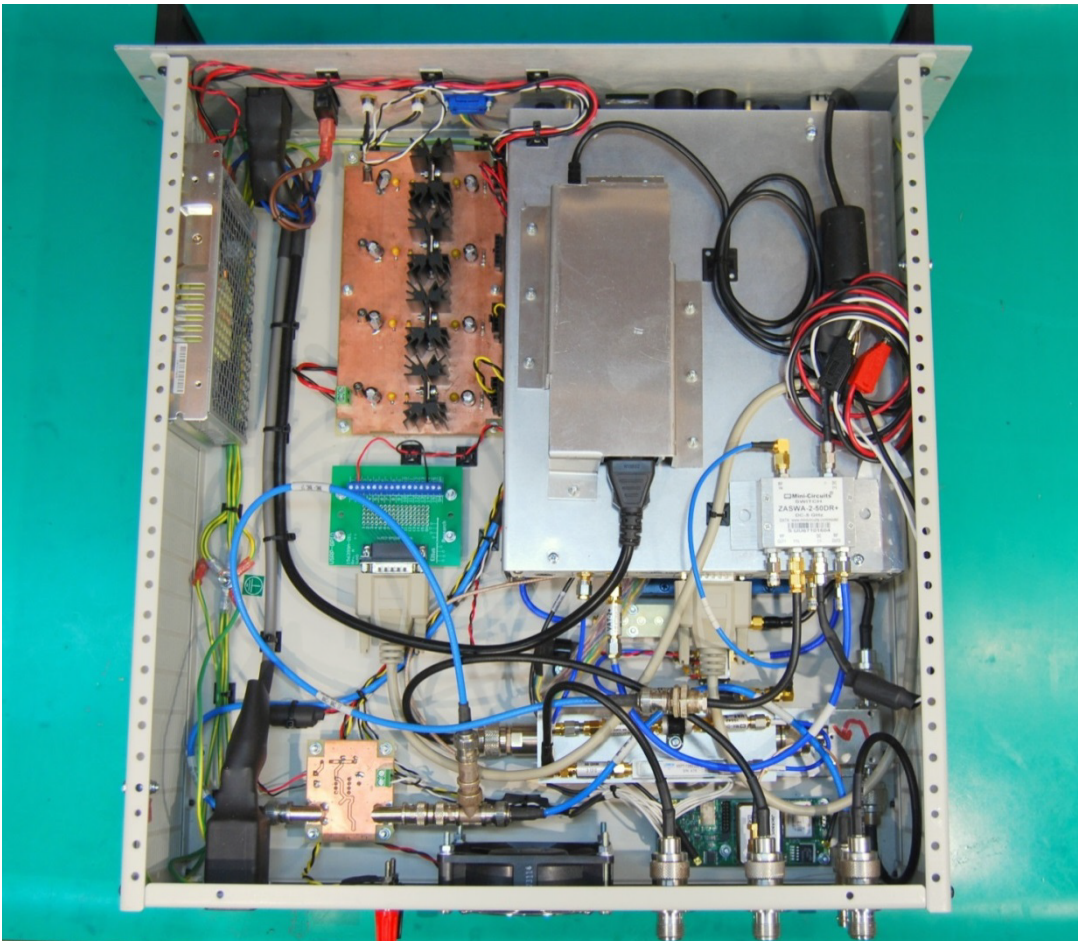


Figure 15. RNA top view, showing internal components

5.5. Signal Processing

Radar signal processing techniques are employed to separate targets from clutter on the basis of Doppler content and amplitude characteristics. Specifically, pulse compression and Doppler processing are employed to improve the signal-to-noise ratio. The receiver data, combined with information about the radar's configuration, is plotted on a range Doppler map.

5.5.1. Implementation

Signal processing is performed on captured receiver data with the end result being a range Doppler map. The principal mathematical operations required are correlation, Fourier transform, complex number manipulation, matrix manipulation, and window and plotting functions. As signal processing is performed offline, the implementation may be completely distinct from that of the radar controller, which is ideal as the requirements solicit a high-level programming language based implementation.

While Matlab appeared the logical choice due to the author's familiarity, the open source GNU Octave was chosen as Matlab would have required the purchase of a unique license for each node. Implementation in Octave proved an excellent choice, as the required mathematical operations are already built-in as it is primarily intended for numerical computations; moreover, its similarity with Matlab simplified learning.

A simple graphical user interface (GUI) was developed which facilitates navigation between bursts and provides plotting functionality. When provided with the receiver data directory and the script file, the GUI will retrieve burst parameters, process the receiver data, and generate a range Doppler plot. The GUI is shown in Figure 16, showing a typical monostatic range Doppler map with several target detections at centre right. Full source code can be made available upon request.

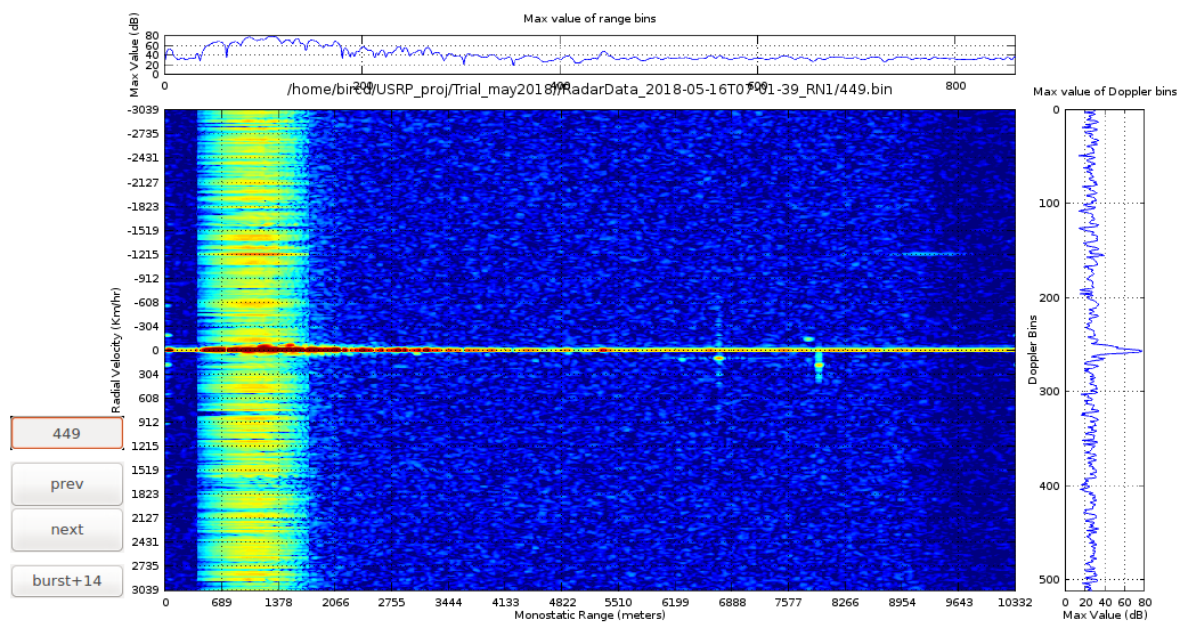


Figure 16. Radar signal processing GUI in Octave. The central display shows a range Doppler map with corresponding maximum value of range (top) and Doppler bins (right). At left are the controls for navigating between bursts.

5.5.2. Functionality

The major functional components of the radar's signal processing are illustrated in Figure 17. The functional description is as follows:

1. The transmitter's IQ pulse samples are windowed in amplitude. Windowing has the effect of suppressing sidelobes in range, at the expense of widening of the main lobe. These sidelobes are an artefact of the finite duration of the transmitted signal. Windowing is important as weak targets may otherwise be obscured by sidelobes of strong targets or clutter.
2. The receiver samples are then cross-correlated with the windowed IQ pulse data. This imparts the pulse compression gain.
3. The pulse compressed receiver samples are collated so that all of the corresponding sample periods align, and each ambiguous range bin is windowed in amplitude. Windowing has the effect of suppressing sidelobes in Doppler, at the expense of widening of the main lobe. These sidelobes are an artefact of the finite number of pulses or PRI.
4. Doppler filtering is accomplished by applying the fast Fourier Transform (FFT) to each of the windowed ambiguous range bins. This separates the spectral content into Doppler bins and imparts the Doppler processing gain (DPG).
5. The magnitude of the Doppler content of each ambiguous range bin is finally plotted on a heat map for visual detection of targets.

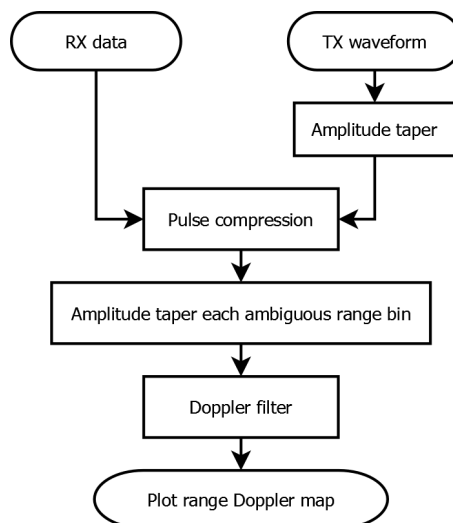


Figure 17. Radar signal processing functional block diagram

5.5.3. Improve Processing Speed

Cross-correlation is a computationally expensive operation. Pulse compression may also be implemented through use of the fast Fourier transform (FFT) in order to improve processing speeds. This makes use of the convolution theorem, which states that convolution in the time domain equals point-wise multiplication in the frequency domain and vice versa; and applies equally to cross-correlation. By performing pulse compression using the FFT, the time required to perform radar signal processing was decreased by approximately 40%.

6. Remote Node Integration and Verification

6.1. Alignment of transmitter and receiver events

Transmit and receive events are scheduled through independent UHD functions. During development, it was discovered that even if both events are scheduled to start at the same time, there will be a discrepancy between the start of the transmitted pulse and the start of recording of receiver samples. This alignment discrepancy was found to be best characterised by number of receiver samples as opposed to time, as it varies depending on sample rate. The alignment doesn't appear to change over time and was similar between the two USRP devices tested, differing by only one or two receiver samples.

The alignment discrepancy may be due to distinct FPGA processes for receiver and transmitter samples. For example, if the receiver samples were buffered in a first-in, first-out (FIFO) data buffer, the samples would be delayed proportionally to the buffer's capacity. Whilst alignment may be stable for a given configuration, it may change if the configuration does. Due to time constraints, this has yet to be fully characterised.

To resolve alignment discrepancies, the radar controller has the input parameter `--rx-samp-delay arg` where the alignment offset can be adjusted. The default offset, which was found to be suitable for both USRP devices, is 31 receiver samples or 2.48us at 12.5Msps.

6.2. Active Switching

All active components generate thermal noise which acts to degrade system performance by reducing the signal-to-noise ratio (SNR). In particular, the power amplifier (PA) is a major contributor to system noise due to its high gain and high power output. By actively switching the PA, so as to be biased off during receive, the PA's contribution to system noise can be largely disregarded.

Figure 18 and Figure 20 show range Doppler maps where the effect of actively switching system components is demonstrated as reductions to the system noise floor. The test setup consists of a single remote node operated in loopback through suitable attenuation. A synthetic target of $\pm 800\text{Hz}$ (plus sidebands) has been introduced into the return signal to provide a reference for comparison.

Figure 18 shows the noise floor comparison both without (left) and with (right) the PA being actively switched. The simplest configuration is without switching. Here all system components are always active and always contributing to system noise. Note the synthetic target is not visible as the SNR is insufficient to distinguish the target return from the noise floor. This is in comparison to the PA being enabled only during transmit pulses, resulting in the elimination of the PA's contribution to system noise during receive. Whilst a more complex configuration, the results is readily visible in Figure 18 (right), where the synthetic target is visible (the band of vertical dashes).

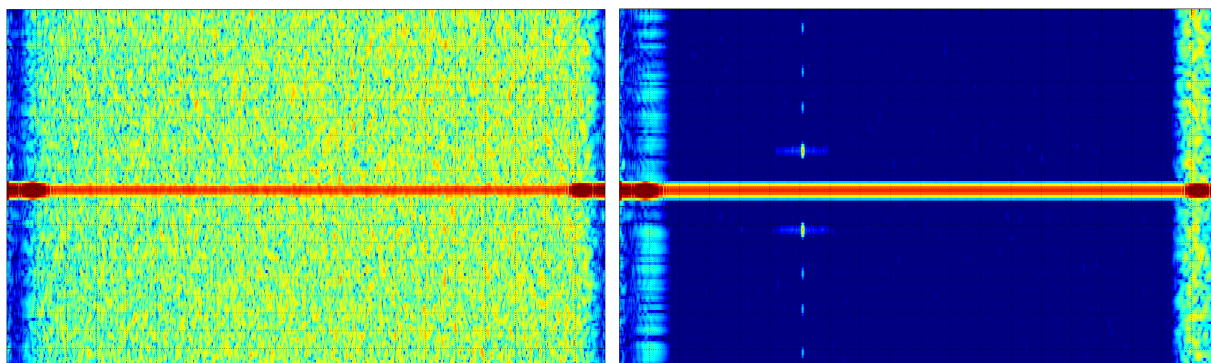


Figure 18. Range Doppler maps without (left) and with (right) active PA switching. Scaling and test setup are identical for each image. X-axis is Range; Y-axis is Doppler centred on 0Hz.

While an improvement, Figure 18 (right) still shows an elevated level about 0Hz Doppler which sticks out from the noise floor (the red central horizontal line). While less of a concern for moving targets which generate a Doppler shift, all returns from stationary objects will be degraded (such as from sea clutter). This artefact was found to be due to RF leakage from the transmitter chain impacting on the performance of the USRP's receiver. The receiver was found to be rather sensitive to the high levels of transmitter leakage, sufficient to impair the receiver's performance even after the transmit event had passed. The impact on the receiver's bias point is shown in Figure 19, where a gradual drift from DC is observed.

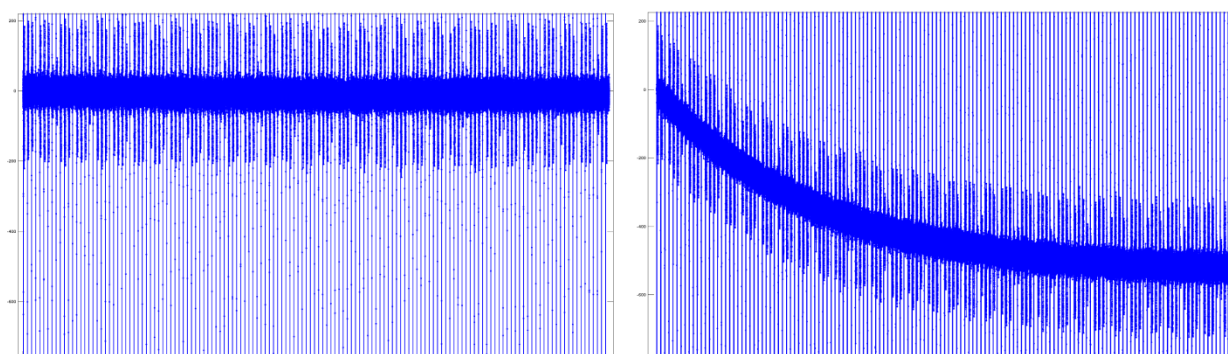


Figure 19. Normal biasing of raw receiver samples (left), and those affected by transmitter leakage (right) for an entire CPI of 19.7ms.

Two contributors to the leakage were found: the primary being direct leakage through the circulator; the secondary being radiated leakage from the USRP into receiver front-end components.

The system front-end employs a circulator design to provide isolation between the transmitter and receiver. As the isolation provided is only 23dB, limiters are employed in the receiver path to prevent receiver damage by high RF levels. To further increase isolation, an RF switch was added before the USRP's receiver, removing the primary contribution to leakage. The secondary contributor to leakage was reduced by the addition of radar absorbing material between the underside of the USRP and the receiver front-end components. The results of these improvements are shown in Figure 20, where the artefact about 0Hz has been reduced by approximately 37dB. While a significant improvement, the artefact is still visible. It was considered that an IQ imbalance may be a contributor. The UHD provides a self-calibration utility to minimise such imbalances, but it did not reduce the level of the artefact.

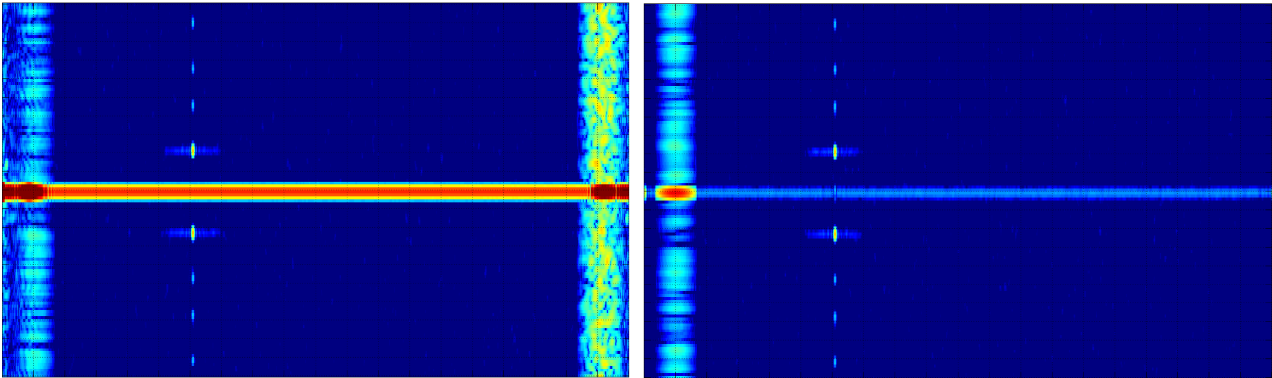


Figure 20. Range Doppler maps without (left) and with (right) active RX switching. Scaling and test setup are identical for each image. X-axis is Range; Y-axis is Doppler centred on 0Hz

6.2.1. Examination of noise artefacts

While the above figures demonstrate a significant improvement in the system noise floor, several noticeable noise artefacts remain. All artefacts are attributable to signals originating in the transmitter and leaking into some stage of the receiver. These artefacts are highlighted in Figure 21, and will be commented on below.

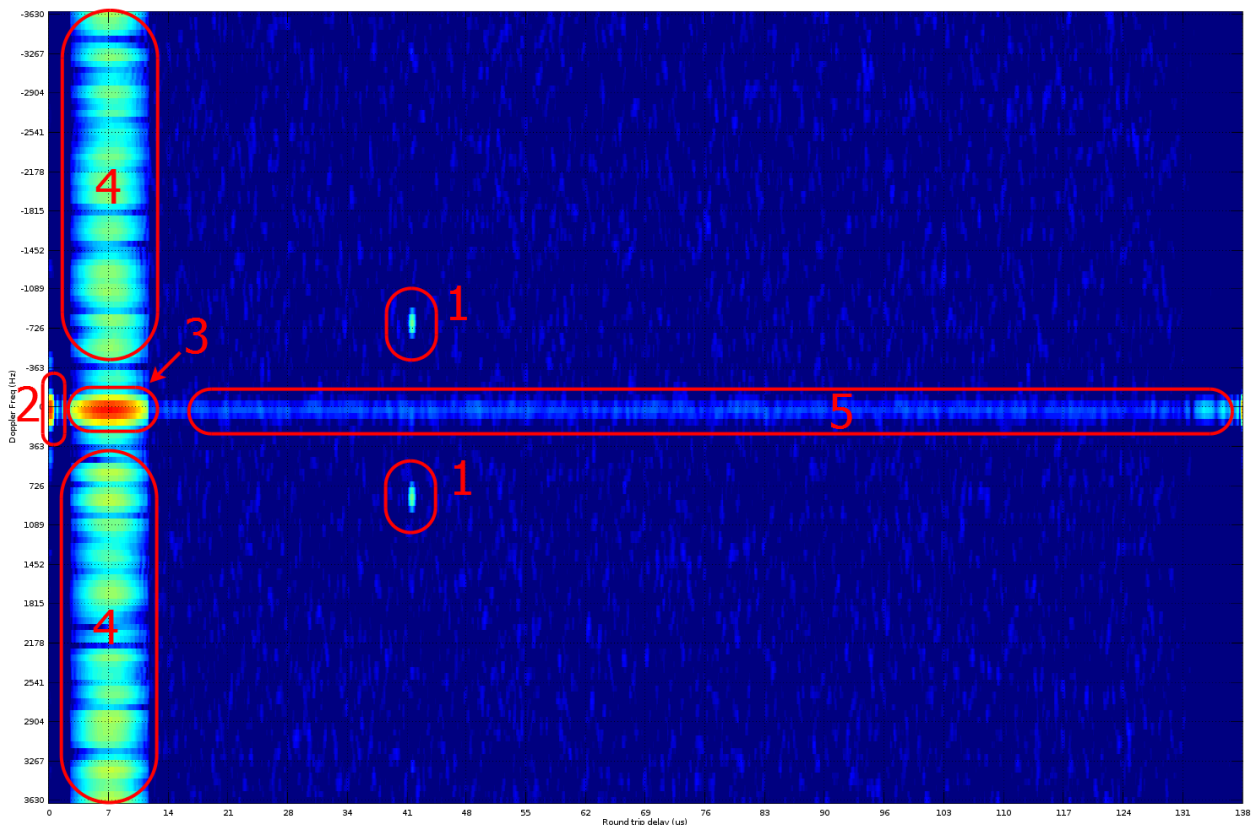


Figure 21. Examination of noise artefacts for a single remote node operated in loopback with an injected synthetic target. X-axis is round-trip delay; Y-axis is Doppler shift centred on 0Hz.

Figure 21 identifies several artefacts which have been labelled for discussion; the label number corresponds with the following list:

1. This is not an artefact but a detection of the returns from the synthetic target which was used for verification purposes. They correspond with the injected $\pm 800\text{Hz}$ signal and $41\mu\text{s}$ delay.
2. This artefact is due to the correlated direct transmitter to receiver leakage corresponding to a target return at 0s delay and 0Hz Doppler.
3. This artefact is associated with transmitter activity, as it is not present on the passive bistatic node or when operating in receive only mode. The origin of the artefact is yet to be determined. The addition of the receiver switch has reduced but not eliminated it. Detection begins at $2.6\mu\text{s}$ and ends at $11.9\mu\text{s}$ delay, which corresponds directly to the transmitted pulses themselves (prior to correlation); in this case $9.27\mu\text{s}$ wide pulses skirted by $2.6\mu\text{s}$ of padded samples. However, this artefact cannot be directly associated with the transmitted pulses as they would have correlated most strongly at 0s delay, as is artefact #2.
4. The vertical band at close range is attributed to the finite instantaneous dynamic range of the receiver. Instantaneous dynamic range is defined as the difference between the smallest signal the receiver can receive and the largest signal that can be present in the receiver bandwidth while the smallest signal is received (Griffiths et al., 2014). It is likely that the signals which resulted in artefact #3 were sufficiently high in amplitude that the noise floor was elevated for that period of time, due to the limited instantaneous dynamic range of receiver.
5. The horizontal band centred about 0Hz Doppler is also attributable to the signals which resulted in artefact #3. The USRP's receiver was found to be rather sensitive to the high levels of transmitter leakage, sufficient to impair the receiver's performance even after the transmit event has passed. It is for this reason that the receiver switch was added.

These artefacts have proven difficult to eradicate; some level of leakage is expected given the high transmitter power levels and highly sensitive receiver. Rather than invest an excessive amount of time and effort to reduce these further, it is worth bearing in mind that:

1. All artefacts detected prior to the completion of the transmit pulse do not impact on system performance, as this is less than the minimum measuring range of the radar (see section A.3). Hence, artefacts labelled #2, #3, and #4 in Figure 21 have no impact on system performance.
2. These artefacts are all attributed to leakage from the transmitter chain into the receiver chain. They are not present when the remote node operates as a passive bistatic receiver when ample isolation is present between the passive node and the radiating node. Ample isolation can be achieved by separating the nodes by a few kilometres or topographical features.
3. The horizontal band of noise (artefact #5) centred about 0Hz Doppler does adversely impact system performance for slow moving or stationary objects such as sea clutter, but does not adversely impact performance for fast moving targets such as aircraft. The degradation to SNR has been observed to be greater for those bursts with a shorter PRI.

SNR about 0Hz Doppler for the burst designated as FM1 (which has the shortest PRI) is approximately 15dB worse.

6.3. Waveform Optimisation

Coherent processing gain can be increased by optimising waveform parameters to better suit operational requirements. For example, Doppler processing gain (DPG) is given by

$$DPG = 10 \log(CPI \cdot PRF) \quad (1)$$

Equation (1) shows that DPG is increase by increasing the CPI and/or the PRF. However, increasing CPI has some disadvantages including

1. increased potential for target smearing across range and Doppler cells (for fast targets), and
2. increased potential for target scintillation effects reducing coherence of returns.

Increasing the PRF (i.e. the transmitted duty cycle) has the disadvantage of reducing the maximum unambiguous range. In order to choose an optimal CPI and PRF, consideration must be given to these trade-offs. This process begins by considering the types of targets which are to be detected; specifically, the targets maximum speed and maximum rate of change of both bearing and speed. In order to realize an increase in DPG, a target's radar return must be captured within one range cell. The length of a range cell is approximately the range resolution, given by

$$Range\ resolution \approx \frac{c_0}{2B} \quad (2)$$

where

c_0 = speed of light

B = bandwidth of modulation

Range resolution should not be confused with range bin rate which is given by

$$range\ bin\ rate = \frac{c_0}{2 * sampleRate} \quad (3)$$

As the sample rate is 12.5Msps while the bandwidth of the FM chirp is 3.87MHz, the system is oversampling by a factor of 3.2.

To illustrate, an aircraft traveling at 100m/s, a CPI longer than $38.8/100 = 0.39s$ will result in the targets return being smeared across range cells with no further increase to SNR. However, for a target traveling at 50m/s, doubling the CPI to 0.78s will increase the SNR by 3dB.

The airborne targets expected during the field trial included slow moving light aircraft and some large passenger aircraft. As XPAR-II's search waveforms accommodate detection of much more agile targets, there is room to increase DPG. A variety of waveforms with different CPIs and PRFs were incorporated into the script file to accommodate a wider variety of targets while providing

maximum coherent processing gain to ensure detection. In addition, a waveform incorporating a different modulation of FM chirp (FM2) was included to aid in determination of targets with unambiguous range. These waveform configurations can be viewed in Table 13.

Table 13. The various waveform configurations chosen for field experimentation

	FM1	FM1_CPI2_DC2	FM1_CPI4_DC2	FM1_CPI8_DC2	FM1_CPI16	FM1_CPI32_DC2	FM2_CPI16
PRI (s)	137.76E-6	68.88E-6	68.88E-6	68.88E-6	137.76E-6	68.88E-6	159.60E-6
Number of pulses	143	572	1144	2288	2288	9152	1952
Active pulse width (s)	9.27E-6	9.27E-6	9.27E-6	9.27E-6	9.27E-6	9.27E-6	11.46E-6
CPI (s)	19.70E-3	39.40E-3	78.80E-3	157.60E-3	315.19E-3	630.39E-3	311.54E-3
Waveform bandwidth (Hz)	3.87E+6	3.87E+6	3.87E+6	3.87E+6	3.87E+6	3.87E+6	3.87E+6
Min. measureing range (m)	1781	1781	1781	1781	1781	1781	2109
Max. unambiguous range (m)	19274	8942	8942	8942	19274	8942	22221
Duty cycle (%)	6.73%	13.46%	13.46%	13.46%	6.73%	13.46%	7.18%
Pulse compression ratio (dB)	15.5	15.5	15.5	15.5	15.5	15.5	16.5
Doppler processing gain (dB)	21.6	27.6	30.6	33.6	33.6	39.6	32.9
Range resolution (m)	38.8	38.8	38.8	38.8	38.8	38.8	38.8
Sample resolution (m)	12.0	12.0	12.0	12.0	12.0	12.0	12.0

6.4. Verification of Capability Requirements

Each of BiRCD's identified capability requirements (as set out in Table 36 in D.1) are considered in Table 14 below for scrutiny against the realised system's capability and performance. To summarise the results, Table 14 provides verification that all of BiRCD's capability requirements have been suitably satisfied; moreover, all requirements listed as desirable have also been satisfied.

Table 14. Verification of capability requirements

CR #	Capability Requirement	CR satisfied?	Comments
1	SNR (after coherent processing) of 10dB minimum or 20dB desirable for a target RCS of -40dB sqm/sqm normalized radar cross section (σ_0) at 10kms range.	YES	Refer to section A.2 - <i>Verification of System SNR</i> and section 7.2.6 - <i>SNR of distant targets</i>
2	Instantaneous bandwidth of 10MHz min. / 40MHz desirable	YES	12.5MHz demonstrated. System capability up to 160MHz.
3	Coherent processing interval (CPI) of 20ms min. / 1s desirable	YES	CPIs of up to 1s duration have been verified
4	RTC sync. accuracy of 100ns	YES	The GPSDO solution is specified to ± 30 ns to UTC, giving a maximum reference error of 60ns between any two nodes. The accuracy with which the USRP RTC runs when locked to the GPSDO clock signals is not specified, but is believed to be negligible in comparison. This has not been fully characterised due to time constraints.
5	Simultaneous monostatic required over one-path	YES	Nodes are capable of monostatic operation. i.e. both transmitting and receiving
6	One-way bistatic operation	YES	Nodes are capable of two-way bistatic operation. i.e. both transmitting and receiving
7	Baseline range of 1km min.	YES	There is theoretically no limit to the baseline range between the nodes
8	Communication of control & configuration data	YES	Achieved through communication of human operators
9	One Remote Node required	YES	Two have been built and tested
10	TX and RX capability required on each node	YES	All nodes are capable of both transmitting and receiving
11	Radar data storage capacity of 1Tb min.	Partial	While each RN has a 1TB HDD, not all of this storage is available for radar data. Additional external storage space is available if required.
12	Location accuracy of ± 15 meters	YES	Location coordinates are provided by the on-board GPS which is typically accurate to within 5m, dependent on conditions.
13	Antenna swaths must overlap	YES	Achievable through manual positioning of antennas
14	Suitable for use at STF and coastal locations (e.g. cliff at Cape Jervis)	YES	Nodes are suitable for transportation and can be operated in most locations

7. Test and Validation

7.1. Field Trial

A field measurement trial was conducted at the Sensor Trials Facility (STF) at the RAAF base Edinburgh to provide real world system validation and demonstration of Phase 1 system performance. The STF location was chosen due to its accessibility and suitability for detections of airborne targets. The trial took place over two days: the 14th of May 2018 was used to verify equipment setup and operation, with aircraft detections taking place on the 16th of May. Several DST staff members provided support to the trial, assisting both with equipment deployment and operation of RN2.

7.1.1. Preparation

Before the trial could take place, the following were required:

1. Defence Spectrum Authority (DSA) approval to transmit,
2. approved safety documentation including a Standard Operating Procedure and risk assessment, and
3. an Electromagnetic Radiation Survey to ensure Australian Radiation Protection and Nuclear Safety Agency (ARPANSA) exposure limits would not be exceeded.

7.1.2. System Configuration

The BiRCD system configuration consisted of two remote nodes (RN) operating in a cooperative bistatic configuration, as shown in Figure 22. Operating parameters are shown in Table 15. RN1 was configured as the monostatic illuminator and RN2 configured as the bistatic receiver. Note that RN2 did not utilise a power amplifier as it operated as a passive receiver.

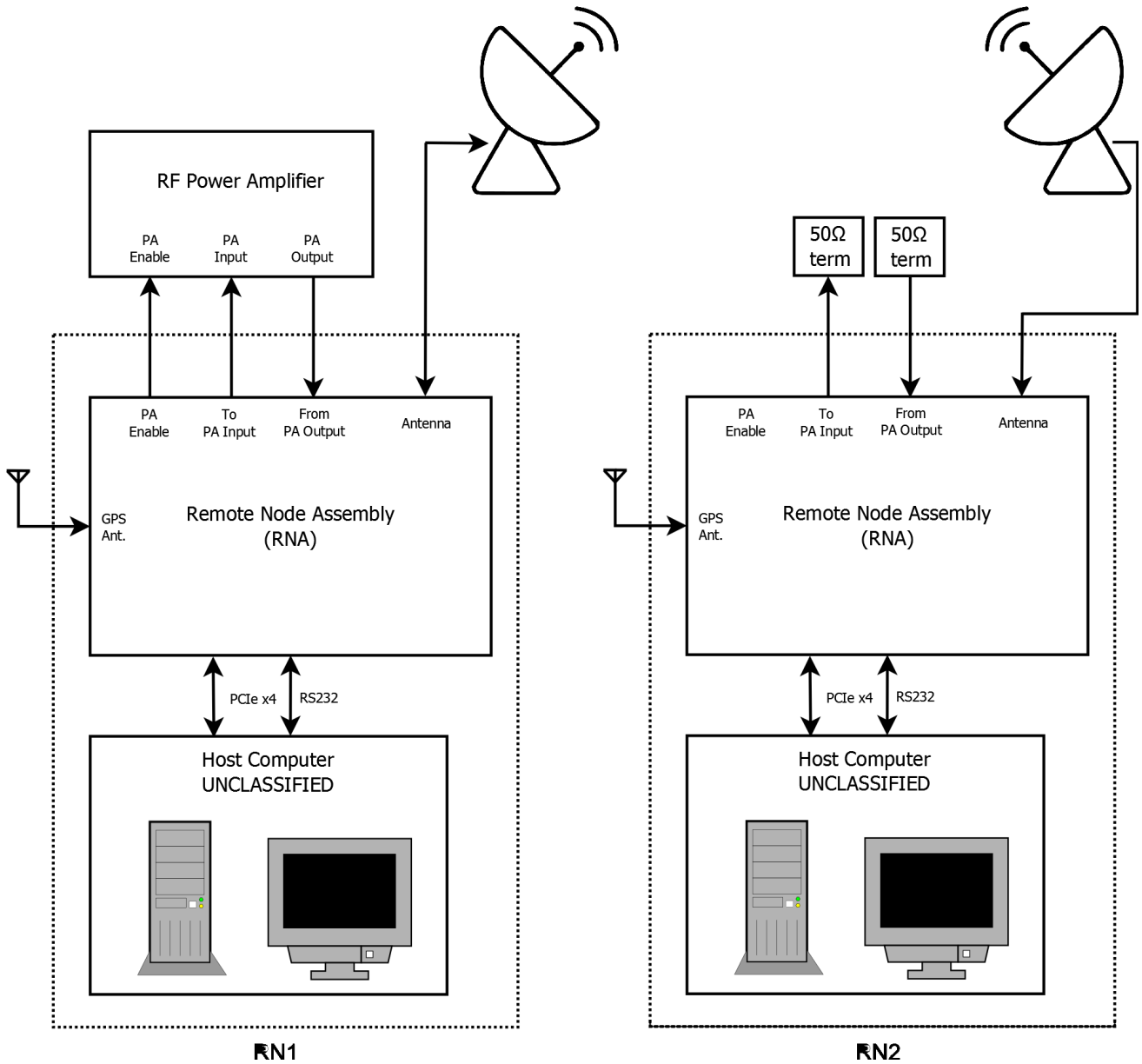


Figure 22. The BiRCD system configuration used during the STF trial

Table 15. Operating parameters

Transmitter frequency	1290MHz
Transmitter power	Approx. 250W at the antenna
Transmitter modulation	Pulsed linear FM chirp of 3.87MHz bandwidth
TX / RX sample rate	100Mpsps / 12.5Mpsps
Waveforms	A mixture of all eight of XPAR-II's search waveforms (Table 38 in Appendix 0) in addition to the custom waveforms identified in Table 13 in section 6.3.

7.1.3. Supporting Equipment

Auxiliary and supporting equipment are identified in Table 16 below.

Table 16. Major auxiliary equipment

Host computer	Ubuntu 16.04 x64 OS Intel i7-6700 CPU 32GB RAM 1TB SSD HDD
Antenna	PEI 1247X vertically polarized six dipole L-band antenna array
Power amplifier	Tomco BT00200-LAMBDA-CW RF power amplifier
Telescopic masts	7.5m and 6m telescopic pump up masts (not deployed to full height)
Generator	Honda EU22i 2200W
Radar target generator	Comprised of a 41.6us delay line, Fluke PM5136 function generator, and Rohde & Schwarz HF907 broadband horn antennas

A radar target generator was deployed in the field to provide range and Doppler validation, configured as shown in Figure 23 with an internal delay of 41.6us and a frequency offset of $\pm 800\text{Hz}$.

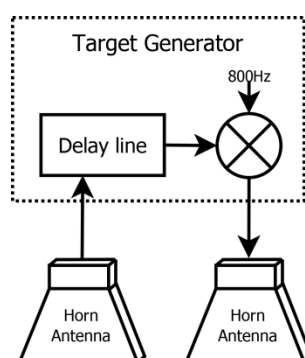


Figure 23. Radar target generator configuration used during the STF trial

7.1.4. Deployment

The deployment locations at the STF site were chosen to provide a suitable orientation for target detection while maximising the baseline distance. Only 589m meters of separation was possible providing a bistatic angle of 6.8 degrees at 5km range. A greater bistatic angle would have been desirable, to further differentiate the monostatic and bistatic returns. The antennas of the remote nodes were oriented due south so as to facilitate detections of light aircraft originating from Parafield Airport and large passenger aircraft on approach to Adelaide Airport.

The coordinates of the deployed equipment are shown in Table 17 in decimal degrees format while Figure 24 shows these locations and the corresponding distances overlaid onto a map. The nodes' coordinates are those reported by the on-board GPS receiver. There was no line-of-sight visibility between the two nodes which were obstructed by earth works. This likely reduced RN1 to RN2 transmitter leakage somewhat due to increased baseline (direct path) isolation.

Table 17. Coordinates of nodes and of radar target generator

	Latitude	Longitude	Antenna orientation	Antenna height (from ground to base)
RN1	-34.722153°	138.624348°	Approx. 180°	6.8m
RN2	-34.720988°	138.618067°	Approx. 180°	Approx. 4.5m
Radar target generator	-34.725583°	138.621489°	Approx. 0°	Approx. 5m

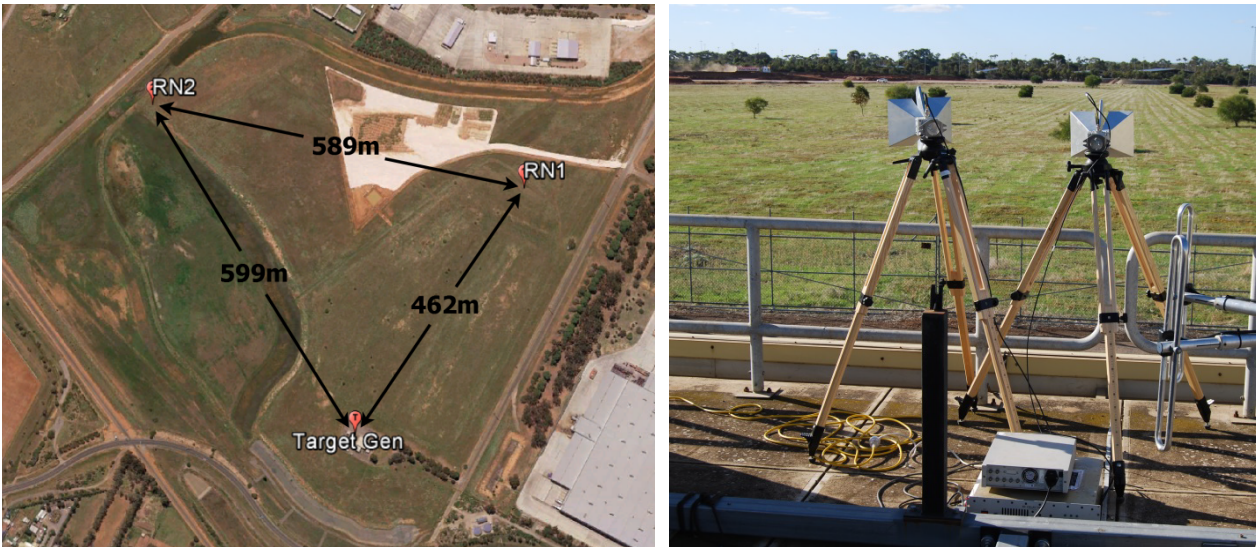


Figure 24. Overview map showing the locations and the respective distances between the sites (left) and radar target generator deployment (right)



Figure 25. Monostatic RN1 deployment (left) and bistatic RN2 deployment (right) showing auxiliary equipment and masts

7.1.5. Outcome

The trial was deemed a success; the BiRCD system functioned as expected and captured valid radar data showing numerous aircraft detections. The synchronisation solution worked without fault, as did the radar controller which recorded a large quantity of receiver data while logging all operations.

In total, three hours of valid bistatic radar data were captured on the 16th May: 327GB of data per node. Whilst additional data were captured prior, they do not represent the full functional bistatic configuration and are therefore of little analysis value. The valid captured radar data comprises approximately 64,000 bursts per node, of which RN1 reported 11 burst errors while RN2 reported 36 burst errors. The radar controller successfully recovered from all burst errors, proceeding with subsequent bursts. All burst errors were reported as `ERROR_CODE_LATE_COMMAND`, which is associated with the operating system allocating CPU time to other tasks (refer to section 5.2.6.3 Error Handling). The error rate can be reduced by increasing the inter-burst spacing (which was set to 20ms in this case).

As the system performed well, the most challenging aspects of the trial related to preparation and staff support. The preparation and approval of documentation involved significant time and effort, and ultimately delayed the trial date by approximately one month; while the limited availability of fellow DST staff members complicated trial organisation and execution.

7.2. Analysis of Trial Data

In this section, the radar data captured during the field trial are used to demonstrate real-world system performance. By choosing two typical bursts (out of 64,000), the following will be examined:

1. Range and Doppler validation by evaluation against the radar target generator return;
2. Correlation of ADS-B data with observed target returns;
3. Examination of detections and artefacts of a range Doppler map, including Doppler spectral characteristics from propeller driven aircraft; and
4. SNR of distant targets.

Note that further analysis was not possible due to time restrictions, but will follow in the later phase of this project.

7.2.1. Bursts Chosen for Examination

From the captured data set `RadarData_2018-05-16T04-28-29`, two bursts have been chosen for analysis in the sections which follow. These bursts, while not target rich, have been chosen as their range Doppler maps show several features which will be examined. These attributes include:

1. the radar target generator return,
2. two or three clear targets,

3. a target return exhibiting Doppler spectral characteristics, and
4. a target return at maximum unambiguous range (~19kms).

As the bursts are spaced less than one second apart, they will be examined as if they occurred at the same point in time, to simplify examination. The bursts and their details are listed in Table 18; their range Doppler plots are shown in Figure 26 and Figure 27.

Table 18. *Bursts chosen for analysis*

RadarData_2018-05-16T04-28-29 script_s14_7840b.csv		
Burst number	Waveform <i>Refer to Table 13</i>	Start of CPI (UTC)
3659	FM1_CPI4_DC2	04:39:06.83
3666	FM1_CPI16	04:39:07.63

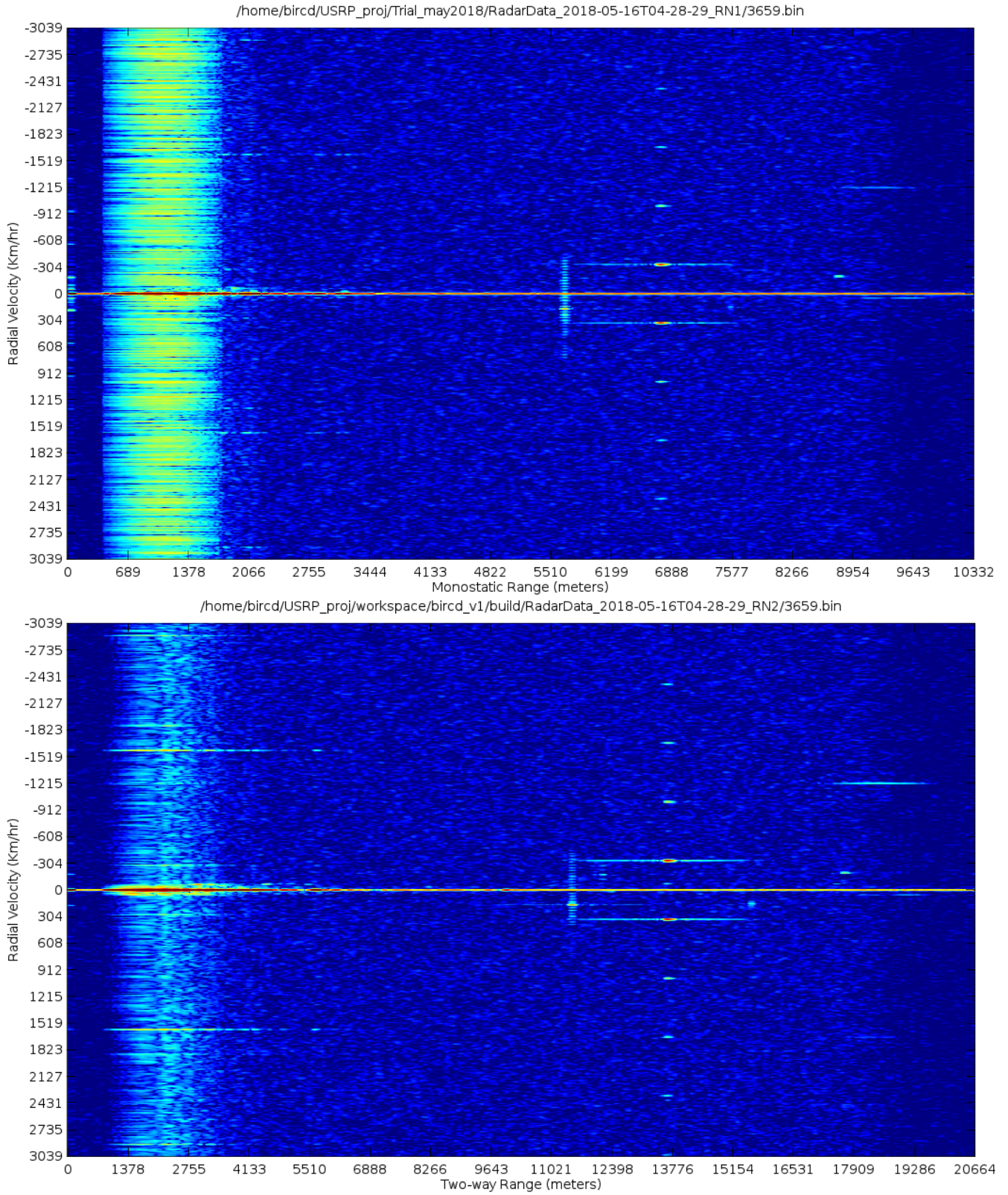


Figure 26. RN1 monostatic return (top) and RN2 bistatic return (bottom) for burst 3659 at 04:39:06.83 UTC. Monostatic range refers to the actual distance to the target whereas two-way range refers to the distance of the total path of travel of the radiated and reflected waves.

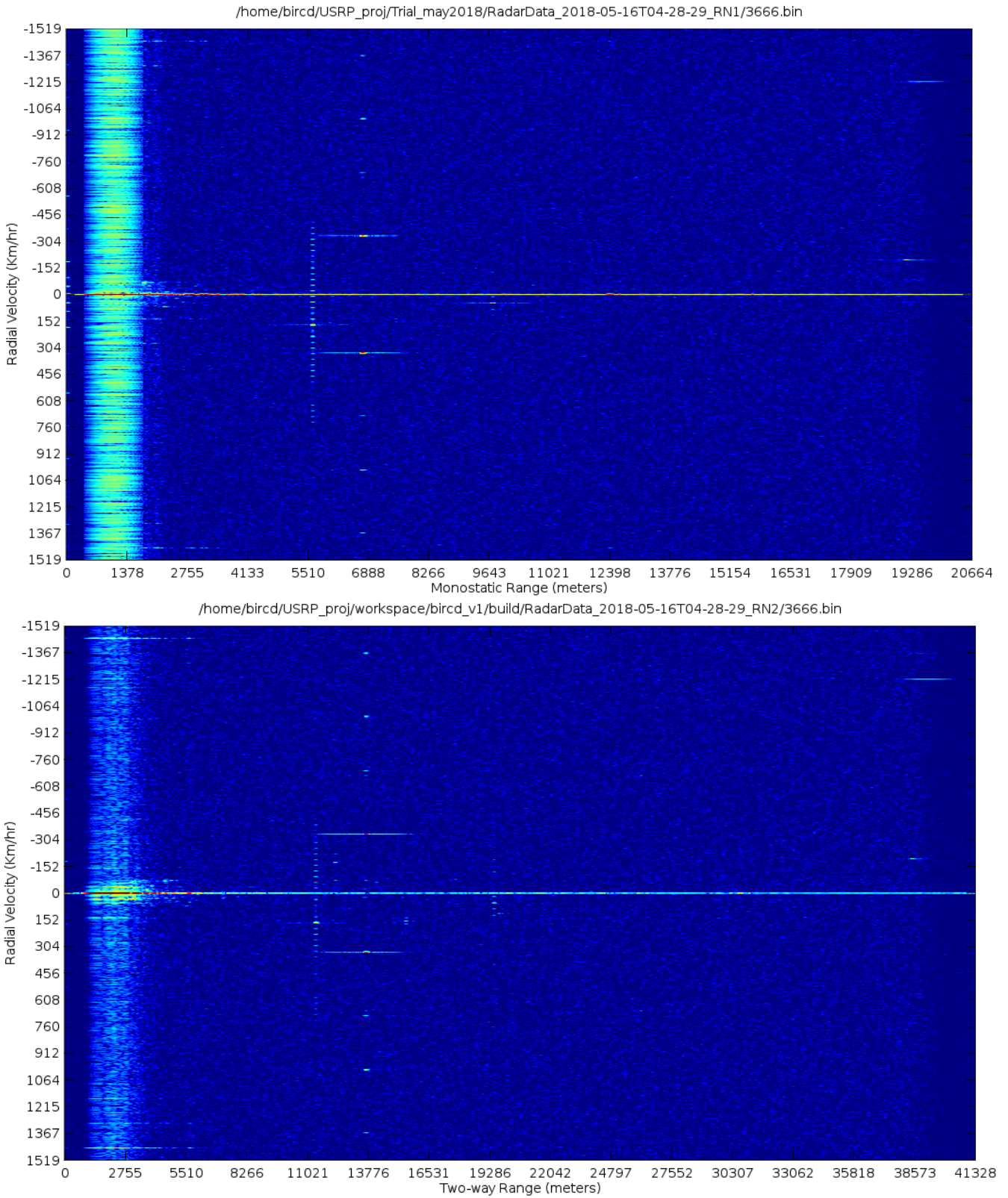


Figure 27. RN1 monostatic return (top) and RN2 bistatic return (bottom) for burst 3666 at 04:39:07.63 UTC. Monostatic range refers to the actual distance to the target whereas two-way range refers to the distance of the total path of travel of the radiated and reflected waves.

7.2.2. Range and Doppler Validation

A radar target generator was used during the trial to provide a target return with a known delay and Doppler shift to assist with system validation. With reference to the respective distances between the sites (Figure 24), the expected range and Doppler frequency have been calculated and compared with that measured. The results are shown in Table 19; the calculation itself is expounded in Appendix B.1. To ease comparison between the monostatic and bistatic case, all ranges are shown as two-way (i.e. the distance of the total path of travel of the radiated and reflected waves).

Table 19. *Expected and measured radar target generator returns of burst 3659*

	Expected two-way range	Measured two-way range	Expected Doppler	Measured Doppler	Two-way range discrepancy	Doppler discrepancy
Monostatic case	13404m	13528m	±800Hz	±808Hz	+124m	+8Hz
Bistatic case	13541m	13670m	±800Hz	±803Hz	+129m	+3Hz

The results show a small Doppler discrepancy which is considered negligible as it is less than the Doppler resolution of 14Hz. As for the range discrepancy, it is noteworthy that the monostatic and bistatic cases are comparable, which suggests a coherent origin that may be correctable by means of an offset or calibration. Several comments can be made:

1. The range discrepancy shown is two-way; hence, the actual distance discrepancy is approximately half of that (~62m). Also bear in mind that the range resolution is 38.8m (refer Table 13).
2. As the discrepancy is comparable between the monostatic and bistatic cases, it is possible that the discrepancy may not originate with the BiRCD system itself, but may result from the target generator; the absolute accuracy of its delay has not been measured.
3. Factors internal to the BiRCD system include the 10m length of antenna cabling and the accuracy of alignment between transmit and receive events.

As the discrepancies between the nodes are comparable, the synchronisation solution is not believed to be a contributor; more accurate results may be obtainable through calibration of the system by making adjustments to the radar controller parameter `--rx-samp-delay` (discussed in section 6.1).

7.2.3. Correlation of ADS-B Data with Observed Target Returns

An ADS-B receiver was used during the trial to record position and velocity data of aircraft in the vicinity, which can be compared with radar detections in order to verify their accuracy. Table 20 shows ADS-B data for three aircraft in the vicinity.

Table 20. ADS-B data for aircraft in the radar's field of view

Callsign	Aircraft type	Latitude	Longitude	Altitude (m)	Heading (deg)	Speed (knot)	Timestamp (last coord. update)
YBX	Diamond DA 42	-34.768143	138.648041	61.0	135	97	04:39:00.437
YNJ	Diamond DA 40	-34.779190	138.669601	122.0	336	87	04:39:05.437
QFA685	Boeing 737-838	-34.893539	138.611694	281.9	231	159	04:39:06.937

Figure 28 shows the locations of these aircraft overlaid onto a map of northern Adelaide. The nodes 3dB antenna beamwidths are also shown. As not all aircraft broadcast ADS-B data, several radar detections do not have corresponding ADS-B data available. Interestingly enough, two of the three aircraft detections which do have ADS-B data are small aircraft flying at low altitude outside of the main beamwidth. This attests to the performance of the radar system.

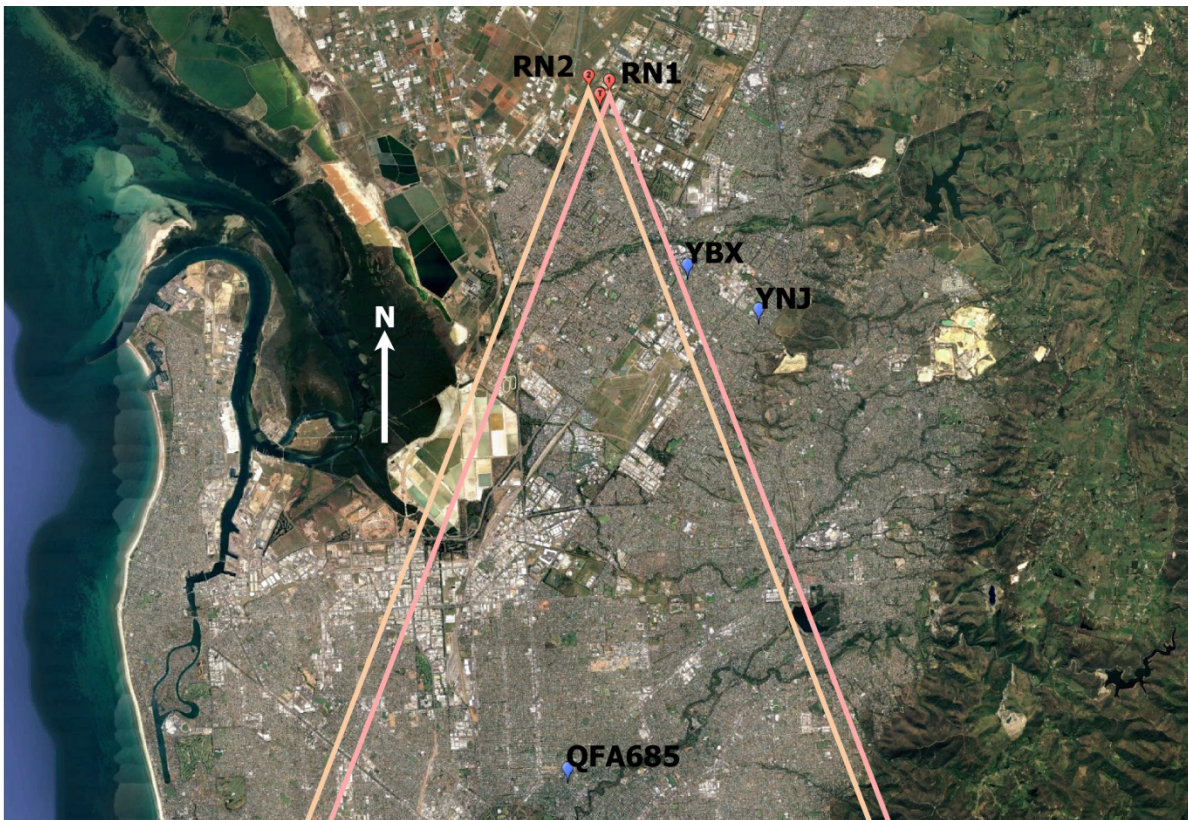


Figure 28. Map of northern Adelaide, showing the 41 degree antenna beamwidths of the remote nodes and ADS-B reported locations of aircraft.

To compare the ADS-B aircraft data with detected radar targets, the range and radial velocity must first be calculated. The calculations have been included in Appendix B.2. The two bursts have been compared together, as they are separated in time by less than one second. The results are presented in Table 21 showing one-way monostatic range, and Table 22 showing two-way bistatic

range. The corresponding aircraft detections are labelled on the range Doppler map in Figure 29 in the following section.

Table 21. Comparison of ADS-B derived range and velocity with corresponding monostatic target detections for bursts 3659 and 3666

Callsign	Expected range	Detected range	Expected radial velocity	Detected radial velocity	One-way range discrepancy	Radial velocity discrepancy
YBX	5851m <i>interpolated</i> ⁷	5900m	-166km/hr	-173km/hr	+49m	-7km/hr
YNJ	7573m	7553m	+159km/hr	+157km/hr	-20m	-2km/hr
QFA685	19098m	19176m	-199km/hr	-198km/hr	+78m	+1km/hr

Table 22. Comparison of ADS-B derived range and velocity with corresponding bistatic target detections for bursts 3659 and 3666

Callsign	Expected bistatic range	Detected bistatic range	Expected radial velocity ⁶	Detected radial velocity	Two-way range discrepancy	Radial velocity discrepancy
YBX	12072m <i>interpolated</i> ⁷	12192m	-169km/hr	-172km/hr	+120m	-3km/hr
YNJ	15579m	15580m	+158km/hr	+161km/hr	+1m	+3km/hr
QFA685	38299m	38460m	-195km/hr	-195km/hr	+161m	0km/hr

The results show negligible velocity and small range discrepancies. Many of the points made in the discussion of discrepancies in section 7.2.2 *Range and Doppler Validation* equally apply here. In addition to those points, the accuracy and availability of the ADS-B data must be considered (section 7.2.5 below). Bear in mind that the bistatic range discrepancy is two-way while the monostatic range discrepancy is one-way.

⁶ The target's velocity component which determines the bistatic Doppler shift is the projected velocity component of the target along the bistatic bisector $\beta/2$. Hence, the bistatic radial velocity is referenced to the bistatic bisector. Refer to Figure 34 in Appendix B.2.

7.2.4. Examination of Detections and Artefacts

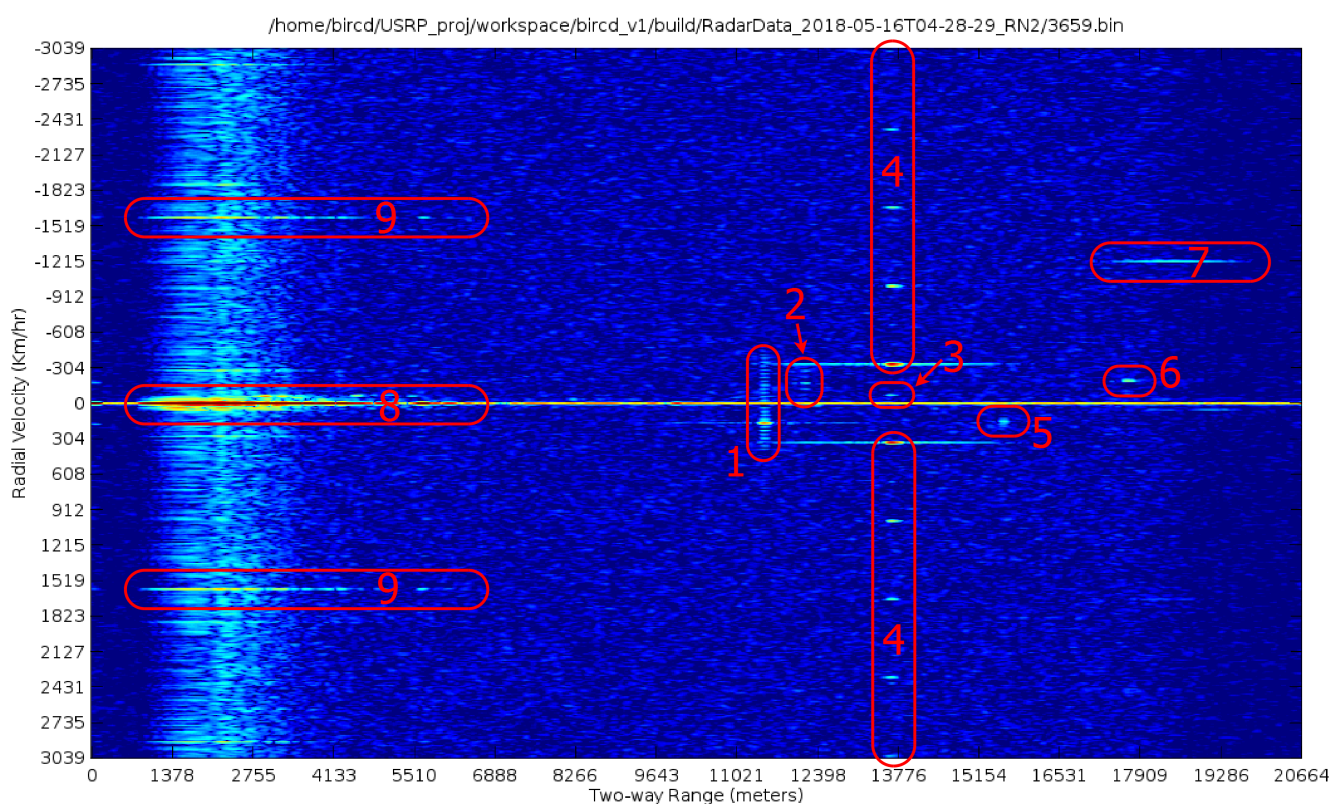


Figure 29. Examination of radar detections for RN2 bistatic burst 3659 at 04:39:06.83 UTC

The bistatic range Doppler map of burst 3659 as examined above has been marked-up in Figure 29. The labelled detections correspond with the following list:

1. This detection at 11480m range and +170km/hr velocity appears to be a small propeller-driven aircraft as it exhibits Doppler spectral characteristics at 78Hz spacing. While there are no corresponding ADS-B data available, it is likely a small trainer or private aircraft originating from Parafield airport. For a three blade aircraft, the 78Hz spacing translates into an engine speed of 1560RPM which is reasonable for such an aircraft.
2. This detection corresponds with ADS-B data for YBX. Doppler spectral characteristics of 120Hz spacing are visible, equating to an engine speed of 2400RPM for the three bladed propellers.
3. This detection at 13650m range and -67km/hr velocity appears to be an aircraft. There are no corresponding ADS-B data available for this detection.
4. These are the returns from the synthetic target which was used for verification purposes. They correspond with an injected ± 800 Hz signal and 41us delay.
5. This detection corresponds with ADS-B data for YNJ.

6. This detection at 17700m range and -193km/hr velocity corresponds with the ambiguous folded return from aircraft QFA685, which is at a distance greater than the maximum unambiguous range for the waveform FM1_CPI4_DC2 (Refer to Table 13). This can be confirmed by adding the detected range to that of the most distant range bin, which totals 38364m range and corresponds with ADS-B data for QFA685.
7. This is not a detection, rather an artefact, as the detection range varies depending on the waveform. It is present for all FM1 and FM3 based waveforms. The Doppler frequency is the same for all FM1 based waveforms, but differs for the FM3 based waveforms. The duration in time of the artefact approximately corresponds with the RF excitation period, and is centred on the ATR switching event at the end of a transmit pulse. This leads to the conclusion that it is likely an artefact related to the active switching of the RF front-end. This artefact is not a concern as it is centred on the maximum unambiguous range which can be seen as the noise floor drop towards the far right end of the figure.
8. The detections here about 0km/hr velocity are the immediate surrounding clutter such as trees, buildings, and hills. Upon closer examination, multiple detections with velocity mostly around 40km/hr and 60km/hr can be seen, corresponding to ground traffic (such as vehicles). These detections are at close range and are more prominent on the bistatic passive node as there is no minimum measuring range.
9. These are images of the detection labelled #8 which look to have mixed with aliased spurs, having the appearance of an attenuated copy. As the detections from #8 are from targets and clutter at close range, the returns are high in amplitude and may drive the receiver into compression, resulting in non-linear performance. However, the exact origin of the artefacts is not known as the Doppler frequency at which they occur varies depending on the waveform.

7.2.5. Comment on the Availability of ADS-B Message Data

Aircraft flown under the visual flight rules (VFR) and below 28500 feet (FL285) are not required to be fitted with an ADS-B transponder, as per Australian aviation rules (*Frequently Asked Questions*, 2014). These are primarily small and recreational aircraft, like many of those based at Parafield Airport. Consequently, not all detected radar targets are verifiable against ADS-B data.

Furthermore, while ADS-B messages are generally broadcast every second or so, each ADS-B message contains only a selected subset of that information shown in Table 20; therefore there will be discrepancies present in the data.⁷

⁷ The ADS-B message for YBX with the nearest timestamp to burst 3659 was received at 04:39:04.837; however this message contained only speed and heading data, not coordinates. The previous message received with coordinates was at 04:39:00.437, some 6.393 seconds prior to burst 3659. On the assumption that the change in speed and heading is negligible in those few seconds, the difference in monostatic range is $\Delta R_M = 6.393 * 49.9 * \cos(158) = -296 \text{ meters}$ and $\Delta R_B = 2 * 6.393 * 49.9 * \cos(160.3) \cos(4.7/2) = -600 \text{ meters}$ for bistatic (refer to Appendix B.2); that is, the radar should detect YBX at a further range than that reported by ADS-B.

A general comment can be made in regards to freely available flight tracking websites which record and display aircraft ADS-B data overlaid onto a map. The historical ADS-B tracks appear to be extrapolated over a subset of the available ADS-B messages, leading to imprecise tracks at best, primarily when an aircraft is changing speed, altitude, or direction. Such historical data was found not to be sufficiently accurate for correlation against radar target returns.

7.2.6. SNR of distant targets

Of interest is the achieved SNR of distant targets. The detection of QFA685, a Boeing 737-838 at 19kms range will be looked at as an example. Figure 30 shows a slice through the range Doppler map for burst 3666, showing the detection of QFA685. The SNR achieved for RN1 and RN2 is 41dB and 37dB respectively with a CPI of 0.315s (waveform FM1_CPI16). For comparison, the aircraft's ambiguous detection in burst 3659 achieved a SNR for RN1 and RN2 of 27dB and 34dB respectively with a shorter CPI of 0.0689s (waveform FM1_CPI4_DC2). Refer to Table 13 in section 6.3 for burst parameters.

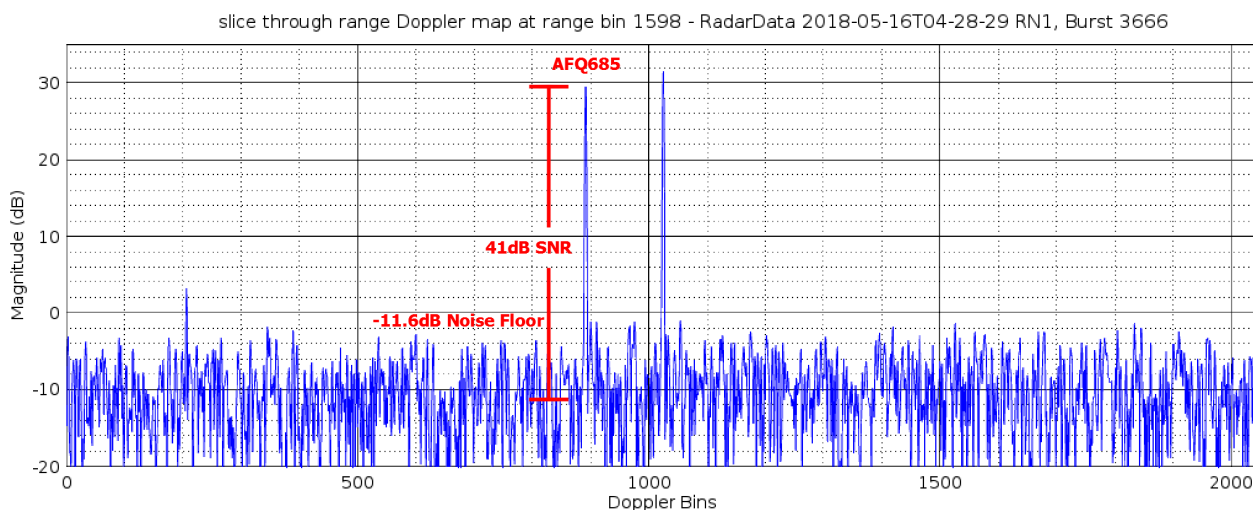


Figure 30. Slice through burst 3666 corresponding to detection of QFA685 (the 2nd strongest return seen at Doppler bin 891)

Capability requirements specify a desirable SNR of 20dB for a target RCS of $-40\text{dB m}^2/\text{m}^2$ normalized radar cross section (σ_0) at 10kms range (CR#1 in Appendix D.1). In our case, this is equivalent to a target RCS of 3m^2 at 10kms range (see Appendix A.2.1). By considering the detection of the Boeing 737, the achieved SNR performance can be compared to capability requirements. By taking the larger RCS (assume 30m^2) and greater range of the Boeing 737 into account, the radar range equation (7) shows that the achieved SNR is approximately 20dB better the desirable capability requirement. This is achieved despite the low gain of the wide-beamwidth antenna.

8. Conclusion

When the search began for a suitable honours project, the majority of project propositions involved the upgrade or redevelopment of a portion of an existing system. While these would have been challenging in their own right, the idea of a bistatic radar project offered a much broader challenge: the opportunity to develop a complete system from scratch. This challenge encompassed all aspects of system analysis and design: requirements analysis refined a loose set of objectives into capability requirements, functional analysis refined the capability requirements into an architecture design, design synthesis turned the architecture design into a functional system, and system validation ensured the original requirements and objectives were satisfied. It was this process which provided the project breadth, while depth was provided by the development and implementation of solutions to satisfy the architecture design.

The project's challenges were not only technical in nature; requiring competence in project management, communication and interpersonal skills, and navigation through process and procedure. The entire project took approximately one year to complete, being interwoven with the project lead's work duties, and provided an excellent opportunity to gain knowledge and experience.

8.1. Project Outcomes

Phase 1 of the project aimed to meet OBJ 3 and work towards OBJ 1 and OBJ 4 (refer to table of objectives in section 2.3, and project phases in section 2.4.1). However, Phase 1 of the project has already met all three of these objectives: specifically,

1. bistatic range Doppler maps have been demonstrated (OBJ 3) during the field trial and have been shown to be accurate (refer to section 7.2);
2. the system provides a bistatic capability which satisfies or exceeds all capability requirements (refer to section 6.4) and is presently available for use (OBJ 1); and
3. the system presently supports multistatic operation (OBJ 4), requiring only the construction of additional remote nodes at reasonable cost.

Arguably, the system has not only met its Phase 1 objectives, but its performance has exceeded expectations.

8.2. Project Costs

Total project expenditure comes in at approximately \$50,000, which comprises all purchases including spare parts; it does not include major auxiliary equipment, which where borrowed, or labour. The approximate cost to build additional Remote Node Assemblies (RNA) is shown in Table 23 below. Note that this is only the RNA cost and does not include major auxiliary equipment (refer to Table 16) of which the power amplifier is the costliest and required only by those Remote Nodes which are required to transmit.

Table 23. *Approximate Remote Node Assembly parts cost per unit; pricing is for two units including shipping.*

Description	Spent (incl. GST)
URSP X310 and Accessories	\$7,719
GPSDO ULN-1100	\$3,341
Circulator D3C0112N	\$539
GPS antenna & misc.	\$526
High-power coaxial limiter	\$1,152
Low-noise amplifier	\$158
Low-power limiter	\$87
Assembly housing and connectors	\$490
Misc. parts for RF front-end	\$357
PCIe cables	\$349
Misc. parts and cables	\$500
TOTAL	\$15,220 per RNA

8.3. SDR Insights

The use of software-defined radios (SDR) as the hardware platform provided valuable exposure to this innovative technology. Insight into the use of SDRs was gained which may prove useful in informing future projects as to the advantages and disadvantages they afford. While they provide great flexibility, development was less than straightforward; perhaps an indication of an immature product. Limitations specific to the SDR employed include:

- cropping of receiver data (refer to section 5.2.8.1);
- timing limitations when driven by a non-real-time operating system (refer to section 0);
- receiver sensitivity to transmitter leakage (refer to section 6.2);
- misalignment of transmitter and receiver events (refer to section 6.1); and
- inadequate documentation of the API, and nominal support (refer to section 5.2.6).

While this project overcame the above limitations, they may present more serious concerns for more demanding applications.

8.4. Future work

There is much room for further system development in support of potential applications. Primary research interests include those listed in section 3.1: sea clutter characterisation, radar imaging, multistatic adaptive CFAR detection, and distributed MIMO. Phase 2 is to follow and involves integration with the full XPAR-II system. Future project work may include:

1. a sea based trial, working towards characterisation of bistatic sea clutter;
2. implementing more advanced signal processing and detection algorithms;
3. higher bandwidth applications, potentially operating fully independent of XPAR-II so as to make use of the up to 160Msps of available instantaneous bandwidth;
4. multistatic operation, potentially using XPAR-II as a 3rd node or constructing additional remote nodes; and
5. development of a real-time scheduler and/or signal processor.

9. Reference

- Al-Ashwal, W. A., et al. (2011) Statistical analysis of simultaneous monostatic and bistatic sea clutter at low grazing angles. *Electronics Letters* **47** (10) 621-622
- Carr, J. (2001) *The Technician's Radio Receiver Handbook: Wireless and Telecommunication Technology*, Elsevier Science
- Clancy, J. and Len, J. (1995) *Bistatic Clutter Measurement Program. Phase 3*. National Technical Information Service
- Fioranelli, F., et al. (2016) Analysis of polarimetric bistatic sea clutter using the NetRAD radar system. *IET Radar, Sonar & Navigation* **10** (8) 1356-1366
- Frequently Asked Questions. Automatic Dependent Surveillance - Broadcast,. (2014) [Accessed; Available from: www.airservicesaustralia.com/wp-content/uploads/FAQ-ADS-B-1-08a-APR14.pdf.
- Friis, H. T. (1944) Noise Figures of Radio Receivers. *Proceedings of the IRE* **32** (7) 419-422
- Griffiths, H., et al. (2014) *Stimson's Introduction to Airborne Radar*. 3rd ed, SciTech Publishing
- Griffiths, H. D., et al. (2010) Measurement and modelling of bistatic radar sea clutter. *IET Radar, Sonar & Navigation* **4** (2) 280-292
- Institute of Electrical and Electronics Engineers Standards Association (2008) *Standard Radar Definitions*. In *IEEE Std 686-2008 (Revision of IEEE Std 686-1997)*: p. 1-41.
- Kochanski, T. P., et al. (1992) *OCEANS 92 Proceedings@m_Mastering the Oceans Through Technology*. Vol. 1:26-29 Oct 1992
- Palamà, R., Greco, M. and Gini, F. (2016) Multistatic adaptive CFAR detection in non-Gaussian clutter. *EURASIP Journal on Advances in Signal Processing* **2016** (1) 107
- Palamà, R., et al. (2015) Statistical analysis of bistatic and monostatic sea clutter. *IEEE Transactions on Aerospace and Electronic Systems* **51** (4) 3036-3054
- Pidgeon, V. (1966) Bistatic cross section of the sea. *IEEE Transactions on Antennas and Propagation* **14** (3) 405-406
- Reviews, C. (2017) *Electronics Principles and Applications*, Cram101
- Simpson, R. A. (1993) Spacecraft studies of planetary surfaces using bistatic radar. *IEEE Transactions on Geoscience and Remote Sensing* **31** (2) 465-482
- USRP X310. Product Details. (2017) [Accessed; Available from: <https://www.ettus.com/product/details/X310-KIT>.
- Weib, M. (2004) *IEEE International Geoscience and Remote Sensing Symposium* Vol. 3
- Weiner, M. (2007) Clutter. In: Willis. N and Griffiths. H (eds.) *Advances in Bistatic Radar*. Raleigh, United States of America, SciTech Publishing 230-319
- Willis, N. J. (1991) Bistatic radar. *Artech House, Boston, London*
- XPAR II Architectural Design Document. (2009). Defence Science and Technology.

Appendix A Systems analysis

A.1. Remote Node Noise Factor

The contributions to noise factor of multiple receiver stages are given by the cascade equation (Friis, 1944)

$$F_{total} = F_1 + \sum_{i=2}^N \left(\frac{F_i - 1}{\prod_{j=1}^{i-1} G_j} \right) \quad (4)$$

where

F_i = noise factor for a given stage

G_i = gain for a given stage (linear format)

Note that noise factor (F) is related to noise figure (NF) and equivalent noise temperature (T_e) by

$$NF = 10 \log(F) = 10 \log \left(\frac{T_e}{T_0} + 1 \right) \quad (5)$$

where $T_0 = 290$ K.

The noise factor of the remote node is calculated in Table 24 below using Equation (4). Several assumptions have been made:

- 1) It is assumed that the transmitter does not contribute to noise figure; that is, the power amplifier is biased off with sufficient receiver isolation. This is not always the case; refer to section 6.2.
- 2) It is assumed that there is no external noise source; that the only noise is that added by the system components. This assumption ignores any external noise captured by the antenna, which is most significant when the antenna is pointed at the ground, as its contribution is not significant in this case.
- 3) Loss and noise figure due to connectors and cable lengths between most components have been estimated and wrapped into that of the corresponding components.

Table 24. Receiver noise calculation

Receiver noise	Antenna	Cables	Circ.	DC block	Limiter	DC block	Filter	LNA	Pad	Limiter	Switch	Pad	URSP RX
Gain (dB)	-0.2	-0.7	-0.4	-0.1	-0.4	-0.2	-0.5	16.9	-3	-0.4	-2	-2.2	
Component NF (dB)	0.2	0.7	0.4	0.1	0.4	0.2	0.5	0.5	3	0.4	2	2.2	4
Cascaded gain (dB)	-0.20	-0.90	-1.30	-1.40	-1.80	-2.00	-2.50	14.40	11.40	11.00	9.00	6.80	6.80
Cascaded gain_lin	0.95	0.81	0.74	0.72	0.66	0.63	0.56	27.54	13.80	12.59	7.94	4.79	4.79
Component F	1.05	1.17	1.10	1.02	1.10	1.05	1.12	1.12	2.00	1.10	1.58	1.66	2.51
Cascaded F	1.05	1.23	1.35	1.38	1.51	1.58	1.78	2.00	2.03	2.04	2.08	2.17	2.48
Cascaded NF (dB)	0.20	0.90	1.30	1.40	1.80	2.00	2.50	3.00	3.08	3.09	3.19	3.36	3.95
Receiver NF	3.95 dB		<i>Referred to the antenna input</i>										

A.2. Verification of System SNR

The parameters for the following calculations are chosen with reference to the project capability requirements set out in Appendix D. Specifically, the primary driving requirement is

CR#1: BiRCD shall achieve a SNR (after coherent processing) of 10dB minimum or 20dB desirable for a target RCS of -40dB sqm/sqm normalized radar cross section (σ_0) at 10kms range.

In order to verify whether the remote nodes satisfy capability requirement #1 (CR#1), the following calculations are required:

- 1) radar cross section of sea clutter,
- 2) signal to noise ratio for the scenario, and
- 3) free-space path loss.

For characterisation of sea clutter, an antenna with a 3 to 5 degree horizontal beamwidth is desirable to resolve wavefronts. However, an antenna with a 41 degree beamwidth has been chosen for the land-based field trial so as to offer a larger field of view over which airborne targets can be detected. To simplify the calculations, a 3 square meter RCS has been assumed for both scenarios as this is both the expected RCS of sea clutter (see Table 25) and of a small aircraft. However, as narrow-beamwidth antennas have higher gain than those with wide-beamwidths, the land-based field trial scenario is disadvantaged by approximately 10dB; that is, the results from the land-based trial would be approximately 10dB better if a narrow-beamwidth antenna was employed.

A.2.1. Radar Cross Section of Sea Clutter

The radar cross section (σ) for the sea is given by

$$\sigma = R \cdot \theta \cdot \Delta r \cdot \sigma_0 \quad (6)$$

Equation parameters are described in Table 25. Using this formula, the RCS of the sea can be calculated for the scenario described by CR#1.

Table 25. Calculation of the RCS of the sea

Input Parameters	
Speed of light (c)	3.00E+08 m/s
Waveform bandwidth (B_w)	3.87E+06 S/s
Normalised radar cross section (σ_0)	1.00E-04 sqm/sqm
Range (R)	10000 m
Antenna beamwidth (θ)	4.5 degrees
RCS (σ) calculation	
Range bin (Δr)	38.8 m
Radar cross section (σ)	3.0 sqm

A.2.2. Signal-to-Noise Ratio

The monostatic radar range equation for SNR from a single pulse (i.e. prior to coherent processing) is given by (Griffiths et al., 2014)

$$SNR_{single_pulse} = 10 \log \left(\frac{P_t G^2 \lambda^2 \sigma}{(4\pi)^3 R^4 k T_0 B_w F} \right) \quad (7)$$

Equation parameters are described in Table 26. The theoretical pulse compression ratio (PCR) gain is given by

$$PCR = 10 \log \left(\frac{\tau_u}{\tau_c} \right) = 10 \log(\tau_u B_w) \quad (8)$$

where

τ_u = uncompressed pulse width

τ_c = compressed pulse width

B_w = matched filter bandwidth or waveform bandwidth

The theoretical Doppler processing gain (DPG) gain is given by

$$DPG = 10 \log(CPI \cdot PRF) \quad (9)$$

The equation for SNR after coherent processing is given by

$$SNR (after coherent processing) = SNR_{single_pulse} + PCR + DPG \quad (10)$$

In a practical system however, windowing functions are employed to suppress sidelobes in both range and Doppler. This has the effect of reducing the signal to noise ratio by approximately 3dB each (depending on the type of window employed).

A.2.2.1 SNR calculation

The SNR calculation is shown in Table 26 describing the scenario outlined by capability requirement #1 (CR#1).

Several assumptions have been made:

1. While waveforms have been defined offering greater coherent processing gain, the standard XPAR-II waveform referred to as FM1 has been used for this calculation.
2. The bandwidth used here is that of the matched filter provided by coherent processing (the waveform bandwidth), which is narrower than the bandwidth of the receiver hardware.
3. High isolation between the transmitter and receiver is assumed, such that noise from the transmitter does not contribute to noise power in the receiver. This has been verified to be true for returns from moving targets (refer to section 6.2.1).

4. A windowing loss of 6dB is assumed, originating from the windowing functions which are employed to suppress sidelobes in both range and Doppler.

Table 26. Monostatic SNR calculation

Input Parameters		
Waveform (XPAR search waveform FM1)		
Waveform bandwidth (B_w)	3.87E+06 Hz	
Coherent processing interval (CPI)	0.01967 s	
Pulse repetition frequency (PRF)	7259 Hz	
Frequency (f)	1.30E+09 Hz	
Uncompressed pulse width (τ_u)	9.27E-06 s	
Transceiver		
Receiver Noise Figure (NF)	3.95 dB	
Antenna gain (G)	63 (linear)	
Transmit power at antenna (P)	300 W	
Target		
Range (R)	10000 m	
RCS (σ)	3 sqm	
Constants		
Speed of light (c_0)	3.00E+08 m/s	
Boltzmann's (k)	1.38E-23 J/K	
Pi (π)	3.14E+00	
Ambient temperature (T_0)	290 K	
Signal to noise ration (monostatic)		
Wavelength (λ)	0.231 m	
Receiver Noise Factor (N)	2.48	
Raw Signal-to-Noise Ratio (SNR)	-6.04 dB	
Pulse Compression Ratio (PCR)	15.55 dB	
Doppler Processing Gain (DPC)	21.55 dB	
Windowing loss	6.00 dB	
SNR after coherent processing	25.06 dB	

A.2.3. Free-Space Path Loss

Free-space path loss (FSPL) refers to the attenuation of a signal in free space between two antennas. The equation for two-way free-space path loss (FSPL) for a monostatic radar is given by (Griffiths et al., 2014)

$$FSPL_{two-way} = 10 \log \left(\frac{(4\pi)^3 R^4}{G^2 \lambda^2 \sigma} \right) \quad (11)$$

Equation parameters are described in Table 27. Using this formula, the FSPL can be calculated for the scenario described by CR#1.

Table 27. Monostatic free-space path loss calculation

Input Parameters	
Frequency (f)	1.30E+09 Hz
Antenna gain (G)	63 (linear)
Range (R)	10000 m
RCS (σ)	3 sqm
Speed of light (c_0)	3.00E+08 m/s
Pi (π)	3.14E+00
Two-way free-space path loss (monostatic)	
Wavelength (λ)	0.231 m
FSPL(two-way)	164.95 dB

A.2.4. SNR Bench Measurement

The conditions of the scenario described by CR#1 have been reproduced on the bench in order to verify system performance against what has been calculated. The nodes were configured in a loop-back configuration with a total path loss of 165 dB (as calculated in Table 27) between transmitter and receiver which included an artificial target of ± 800 Hz Doppler and 41us delay. Figure 31 shows the setup which was used to test the system in a bistatic configuration. The monostatic configuration is similar, where the target generator output is looped back into the receiver of RN1.

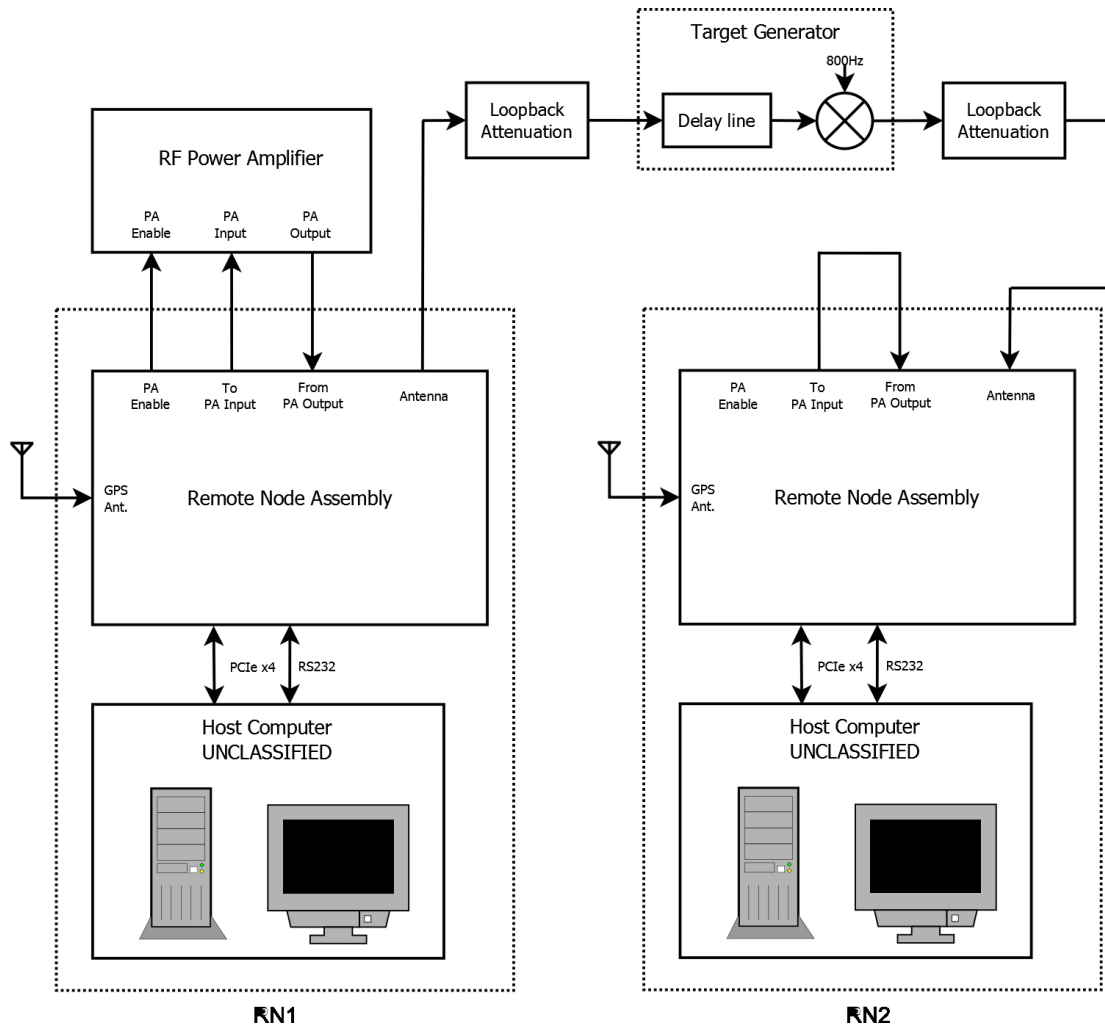


Figure 31. System configuration for bistatic bench test

Range Doppler maps for each configuration were created and the SNR measured by comparing the peak of the target generator return to that of the noise floor. The measured results are shown in Table 28 and compared with the expected SNR from the previous calculations. The expected SNR of the monostatic and bistatic configurations should be similar, as the test setups are very similar.

Table 28. Measured SNR for monostatic and bistatic loopback bench test

	Measured SNR	Expected SNR
Monostatic configuration	35.3 dB	25.1 dB
Bistatic configuration	37.6 dB	25.1 dB

The measured SNR is approximately 10dB better than that calculated. This discrepancy is considered acceptable as both the measurement and calculation are rather complicated and involve several assumptions. Several factors which may have influenced the accuracy of the measurement are:

1. A total path loss of 165dB was verified by measurement; however, the measurement was performed in stages by measuring sections of the loopback attenuation and adding up the total loss. This was done as the combined attenuation is too high to be measured by test equipment.

As the combined total path loss is so high, signal leakage may be a factor which would have the effect of lowering the actual path loss. Leakage, if present, can be observed by taking several SNR measurements for differing total path losses (e.g. a 10dB increase in total path loss should result in a 10dB decrease in SNR). This check was performed with the results shown in Figure 32, which shows only a small variation which is just as likely due to a non-linear receiver or target generator response. Hence, leakage is believed not to be a significant factor.

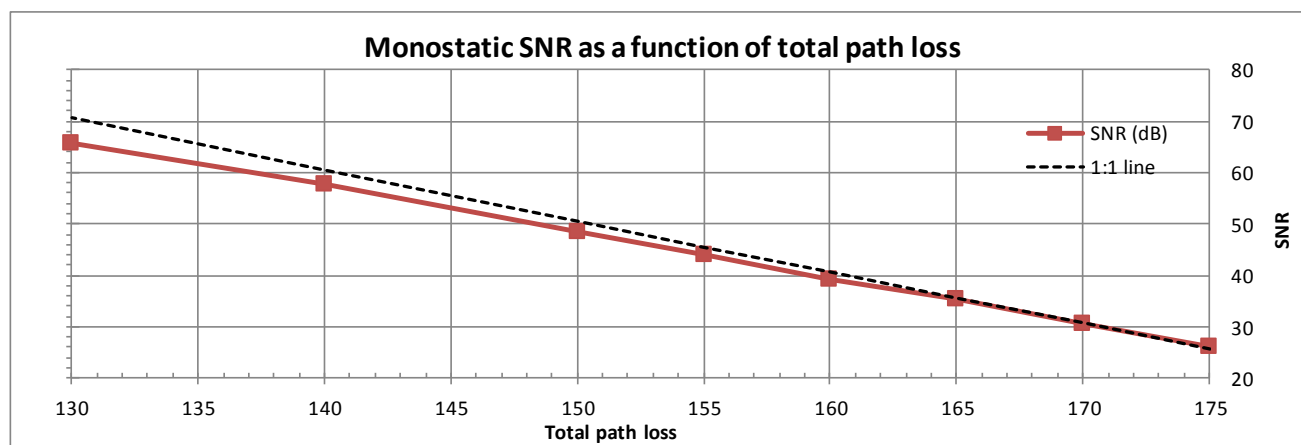


Figure 32. Monostatic SNR as a function of total path loss, showing minimal effect of leaked target return

2. Another source of error may originate from the linearity of the response of the target generator. The target generator gain was measured by test equipment at power levels 100dB or so greater than those present at the input to the target generator during the SNR measurement; note, these levels were low in power and the target generator was not close to saturation. Much of the loop-back attenuation was positioned prior to the target generator (all but ~40dB) to ensure protection from the high power levels from the PA. The target generator contains an 800Hz active source which is fed into a mixer to provide the Doppler frequency offset. It is likely that the mixers response over 100dB of input power levels is not fully linear.

3. The method in which the noise floor is calculated from the receiver samples is imprecise. The method used takes the noise floor to be the mean power of those areas of the range Doppler map that are not affected by noise artefacts (ignores the vertical band covering 0-1700m monostatic range bins and the horizontal band about 0Hz Doppler). The true noise power likely has a conversion factor (likely 3-6dB), as it is a function of the noise variance rather than the median power.
4. In section A.1, the noise factor was calculated on the assumption of no external noise contribution. However, this is not the case for the bench measurement, as the loopback attenuation is at room temperature, while the target generator may be at a higher equivalent noise temperature. This effect serves to make the discrepancy worst.

A.3. Minimal measuring range

In a monostatic configuration, as the same antenna is used for both transmitting and receiving, the radar receiver is effectively blind for the duration of the transmit pulse plus the recovery time of the receiver. This 'blind time' gives the minimal measuring range R_{min} , which is the minimum distance in which targets can be detect. In our case, R_{min} is given by

$$R_{min} = \frac{c_0(\tau_u + t_{dead_time})}{2} \quad (12)$$

where

c_0 = speed of light

τ_u = uncompressed pulse width

t_{dead_time} = switching and recovery time before receiver is available to receiver

Table 29 below shows the minimum measuring range for the XPAR-II search waveforms, while Table 13 in section 6.3 shows the minimum measuring range for the various waveform configurations chosen for field experimentation.

Table 29. Minimum measuring range for the XPAR-II search waveforms

Search waveform ID	FM1	FM2	FM3	FM4	FM5	FM6	FM7	FM8
Pulse width (τ_u) (us)	9.27	11.46	13.59	16.62	19.54	35.1	40.74	46.83
$t_{RX_limiter_recovery}$ (us)	2.6	2.6	2.6	2.6	2.6	2.6	2.6	2.6
R_{min} (m)	1781	2109	2429	2883	3321	5655	6501	7415

t_{dead_time} is the time required from the end of the transmitter pulse before the receiver is able to receive signals effectively. It is equal to the greater of the following:

1. time for 260 zero samples (2.6us at 100Msp/s) of transmitter pulse padding,
2. recovery time of the receiver protection limiter (2us),
3. time for PA to disable (~150ns), and
4. time for receiver switch to switch (~10ns).

In a bistatic configuration, if there is sufficient isolation between the transmitter and receiver sites, then there is no minimum measuring range. In practice however, there is generally some direct path (baseline) leakage between the sites; target detectability at close range is then limited by receiver instantaneous dynamic range for moving targets.

A.4. Timing Diagram

The receiver switch and the PA gated input are both driven by ATR timing signal, as discussed in section 5.2.8.2. The timing signal is further conditioned for suitability for use by the PA and receiver switch (refer to Figure 39 BiRCD - RN PA Enable Conditioner schematic diagram), but this will be overlooked here as the delay is short (150ns) and is not pertinent to this discussion. Figure 33 shows the response of system components leading up to and following a transmit pulse; a high state represents the active state of the device. This timing diagram incorporates each device's transition times and is a useful aid to better understand the system and assist debugging.

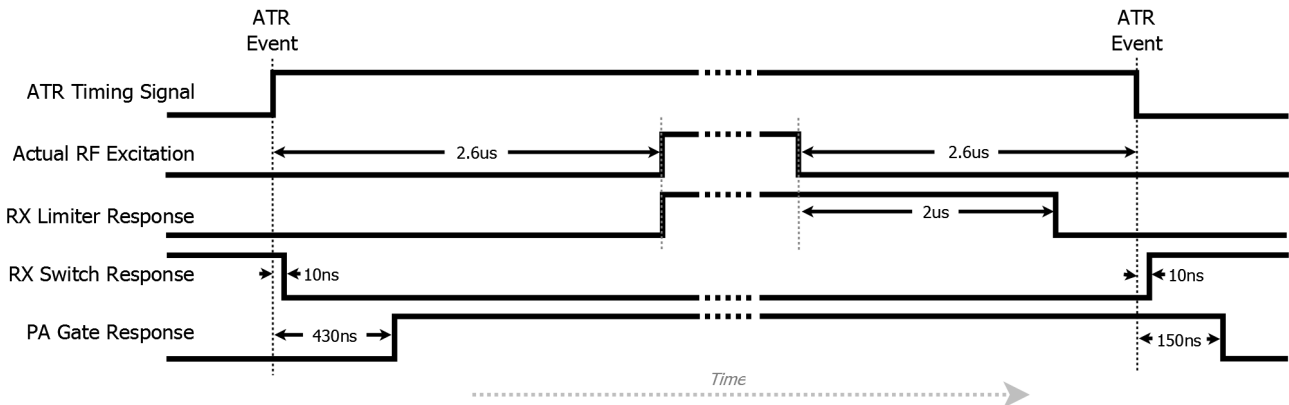


Figure 33. Response of RF front-end components leading up to and following a transmit pulse. Not to scale.

This page is intentionally blank.

Appendix B Data Analysis

B.1. Apparent Range of Radar Target Generator

The monostatic, expected range of the target generator is given by

$$R_M = R_{M_actual} + \frac{c_0 * t_{delay}}{2} \quad (13)$$

where

R_M = apparent one-way monostatic range

R_{M_actual} = actual distance from target generator to monostatic node

c_0 = speed of light

t_{delay} = target generator delay

The bistatic two-way expected range is given by

$$R_B = R_{B_actual} + c_0 * t_{delay} \quad (14)$$

where the actual bistatic range R_{B_actual} is the sum of the distances between the radar target generator and the nodes, as defined in equation (15).

B.2. Apparent Range and Doppler Calculation for ADS-B Targets

B.2.1. Bistatic Range Equation

The bistatic range sum is defined as (Willis, 1991)

$$R_B = R_T + R_R \quad (15)$$

where

R_B = Bistatic range

R_T = Distance from transmitter to target

R_R = Distance from target to receiver

B.2.2. Doppler Shift

A phase shift occurs when radar's electromagnetic waves illuminate a moving target. Note that this phase shift occurs twice, once on the incidence wave and again on the reflected (and already afflicted by a phase-shift) wave.

The monostatic Doppler shift resulting from reflected energy from a target is given by

$$\Delta f_M = \frac{2V}{\lambda} \cos(\alpha) \tag{16}$$

where

- Δf_M = monostatic Doppler shift
- V = target's velocity
- α = angle formed by the target velocity vector with the line of sight from the target to the radar
- λ = wavelength of transmitted signal

With reference to Figure 34, the bistatic Doppler shift resulting from reflected energy from a target is given by (Willis, 1991)

$$\Delta f_B = \frac{2V}{\lambda} \cos(\delta) \cos\left(\frac{\beta}{2}\right) \tag{17}$$

where

- Δf_B = bistatic Doppler shift
- V = target's velocity
- λ = wavelength of transmitted signal
- δ = angle formed by the target velocity vector with the bistatic bisector $\beta/2$
- β = bistatic angle - the angle between the transmitter and receiver with the vertex at the target

The target's velocity component which determines the bistatic Doppler shift is the projected velocity component of the target along the bistatic bisector $\beta/2$. A closing target referenced to the bistatic bisector generates a positive or up Doppler (Willis, 1991).

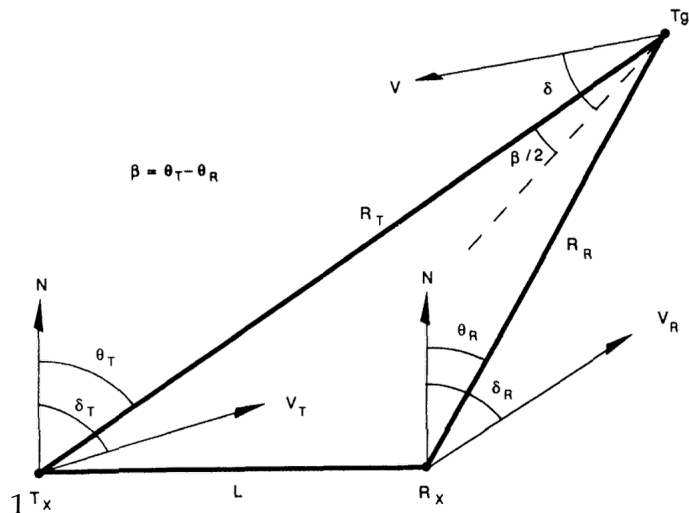


Figure 34. Geometry for bistatic Doppler in the bistatic plane (Willis, 1991)

The Doppler shift resulting from reflected energy from a target may be converted to radial velocity with Equation (18). Note that for the bistatic case, radial velocity is referenced to the bistatic bisector $\beta/2$.

$$V_r = \frac{\Delta f \cdot \lambda}{2} \quad (18)$$

where

V_r = target's radial velocity

Δf = Doppler shift

λ = wavelength of transmitted signal

9.1.1. Calculation of Expected Range and Doppler for ADS-B Targets

The transmitter and receiver look angle (θ_T and θ_R respectively) have been calculated from the coordinates of the aircraft (Table 20) and respective radar nodes (Table 17). RN1 is the transmitter while RN2 is the bistatic receiver. Note that the height of the aircraft has been ignored when calculating range in this case, as it only affects the range by a few meters.

Table 30. Expected monostatic range and Doppler frequency for ADS-B targets

Callsign	Target Speed (m/s)	Target Heading (°)	θ_T (°)	α (°)	R_T (m)	Δf_M (Hz)	V_r (km/hr)
YBX	49.9011	135	157.1	158	5555	-398	-166
YNJ	44.7567	336	146.9	369	7573	380	159
QFA685	81.7967	231	183.5	228	19098	-475	-199

Table 31. Expected bistatic range sum and Doppler frequency for ADS-B targets

Callsign	Target Speed (m/s)	Target Heading (°)	R_T (m)	θ_T (°)	R_R (m)	θ_R (°)	β (°)	δ (°)	R_T+R_R (m)	Δf_B (Hz)	V_r (km/hr)
YBX	49.9011	135	5555	157.1	5917	152.4	4.7	160.25	11472	-404	-169
YNJ	44.7567	336	7573	146.9	8006	144	2.9	370.55	15579	378	158
QFA685	81.7967	231	19098	183.5	19201	181.7	1.8	228.4	38299	-467	-195

This page is intentionally blank.

Appendix C System Operation

This appendix provides a brief overview of how to configure and run the Remote Node in a configuration which will allow verification of system operation.

In order to setup BiRCD, a script file and one or more in-phase and quadrature (IQ) pulse data files are needed. The pulse data files contain baseband IQ samples that define the radar pulses to be transmitted. When scheduled, the appropriate node will transmit those pulses with the parameters specified (the waveform). The radar return is captured simultaneously on all nodes. Receiver data are stored as IQ data in a set of receiver data files for offline processing. All system operations and status are logged.

C.1. Hardware Configuration

The hardware configuration used for system operation and verification is shown in Figure 35. However, if only one node is required to transmit, a simplified configuration is possible as shown in Figure 22 in section 7.1.2.

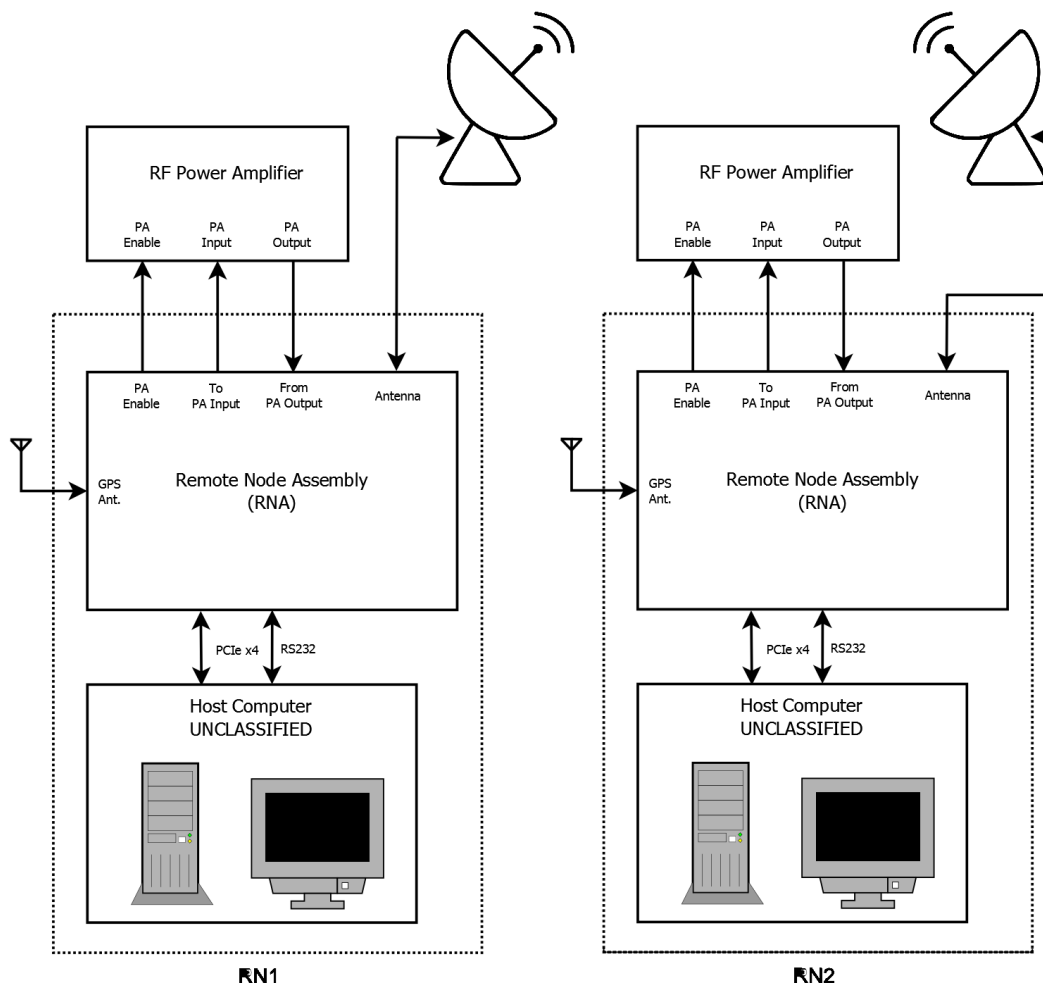


Figure 35. Basic hardware configuration for system operation

C.2. Procedure for Initialisation of Communications via PCI Express

Communications between the host computer and the USRP are via the external PCI Express interface. The USRP device cannot be hot-swapped when connected over PCI Express. Unplugging the PCI Express cable or powering off the device should be done only after disabling the device and powering off the host computer, otherwise the system will become unstable. The procedure is as follows.

Note, communicated via the 1Gb Ethernet connection is also possible but not recommended, due to frequent packet errors. Currently, Ethernet will only work with kernel v4.2.8.

C.2.1. Powering On the Remote Node

1. The host computer and USRP device must both be off. The Remote Node Assembly (RNA) however may remain powered which will keep the GPSDO locked. Ensure the PCIe 4x cable is connected.
2. Power on the USRP device.
3. Power on the host computer. Ensure the kernel version to be loaded is 4.2.x. This should be loaded by default.
4. Once the host computer has booted, run the following command to start the NI USRP RIO driver: `sudo /usr/local/bin/niusrprio_pcie start`
The root password is `Passw0rd`
5. The USRP should now be detectable by the host computer. If correctly configured, running the `uhd_find_devices` command should return the following:

```

bircd@bircd1:~$ uhd_find_devices
linux; GNU C++ version 5.4.0 20160609; Boost_105800; UHD_003.010.002.000-0-unknown

-----
-- UHD Device 0
-----
Device Address:
  type: x300
  resource: RIO0
  product: X310
  fpga: HG
  name:
  serial: 310EEA1

```

C.2.2. Powering Off the Remote Node

1. Run the following commands to stop the NI USRP RIO driver:
`sudo /usr/local/bin/niusrprio_pcie stop`
The root password is `Passw0rd`
2. Shutdown the host computer.
3. After the host computer has shutdown, power of the USRP device.

C.3. Radar Controller Configuration

The BiRCD radar controller application is `bircd_v1.exe`. Running the command `./bircd_v1 - help` will list available argument options, as listed in Table 32 below.

Table 32. Available arguments for BiRCD radar controller application

BiRCD radar controller: Allowed options:	
<code>--help</code>	help message
<code>--tx-args arg</code>	uhd transmit device address args
<code>--rx-args arg</code>	uhd receive device address args
<code>--rx-samp-delay arg (=31)</code>	delay (in number of rx samples) between start of tx playback and start of receiver recording. Used to align TX & RX pulses
<code>--spb arg (=0)</code>	Set max number of IQ data samples for a single <code>uhd::tx_streamer::send()</code> or <code>uhd::rx_streamer::recv()</code> call. 0 (default) will set spb via <code>get_max_num_samps</code> method. A larger spb will result in IQ data fragmentation and reassembly at the UHD driver level rather than at the application level.
<code>--tx-rate arg (=100000000)</code>	rate of transmit outgoing samples
<code>--rx-rate arg (=12500000)</code>	rate of receive incoming samples
<code>--tx-freq arg</code>	transmit RF center frequency in Hz
<code>--rx-freq arg</code>	receive RF center frequency in Hz
<code>--tx-gain arg</code>	gain for the transmit RF chain
<code>--rx-gain arg</code>	gain for the receive RF chain
<code>--tx-ant arg</code>	transmit antenna selection
<code>--rx-ant arg</code>	receive antenna selection
<code>--tx-subdev arg</code>	transmit subdevice specification
<code>--rx-subdev arg</code>	receive subdevice specification
<code>--tx-bw arg</code>	analog transmit filter bandwidth in Hz
<code>--rx-bw arg</code>	analog receive filter bandwidth in Hz
<code>--ref-source arg (=external)</code>	Sets both the 10MHz clock reference & 1PPS time source (internal, external) --> set to external when using GPSDO
<code>--tx-int-n</code>	tune USRP TX with integer-N tuning
<code>--rx-int-n</code>	tune USRP RX with integer-N tuning
<code>--script-file arg</code>	Capture script file in csv format
<code>--ibs arg (=0.050000000000000003)</code>	Inter Burst Spacing - Sets the spacing between bursts (idle time between bursts)
<code>--node-id arg</code>	Remote node ID number (1-8)
<code>--rx-only arg (=0)</code>	Force RX only operation. TX thread will be disabled.
<code>--tx-only arg (=0)</code>	Force TX only operation. RX thread will be disabled.

C.3.1. Script File

In order to run the radar controller, a script file and one or more IQ pulse data files are needed. The script file must be specified, while the pulse data files are specified within the script file. A simple script file is shown in Table 33 below.

Table 33. A simple script file, *script_8b.csv*

	A	B	C	D	E	F	G	H	I	J	K	L	M	N	O	P	Q	R	S	T	U
1	burstid	Npri	PRI_tick	Channel	BeamN	Pls1	Pls2	Pls3	Pls4	Pls5	Pls6	Pls7	Pls8	RN1	RN2	RN3	RN4	RN5	RN6	RN7	RN8
2	1	143	13776	77	5	SchFM1								SchFM1_int16_260pad							
3	2	122	15960	77	5	SchFM2								SchFM2_int16_260pad							
4	3	106	18096	77	5	SchFM3								SchFM3_int16_260pad							
5	4	90	21120	77	5	SchFM4								SchFM4_int16_260pad							
6	5	78	24048	77	5	SchFM5								SchFM5_int16_260pad							
7	6	47	39600	77	5	SchFM6								SchFM6_int16_260pad							
8	7	41	45240	77	5	SchFM7								SchFM7_int16_260pad							
9	8	35	51336	77	5	SchFM8								SchFM8_int16_260pad							

C.3.2. Transmitter IQ Pulse Data Files

IQ pulse data files consist of raw binary IQ samples in `complex<int16_t>` format. Each pulse data file must be padded with 260 leading and trailing zero samples, which provides both the PA and the USRP time required for switching (refer to section 5.2.8.1. USRP Cropping of Samples).

The GNU Octave script `conv_mat_to_bin_int16.m` is useful for converting IQ samples from Matlab format to a suitable format for BiRCD use.

C.4. Running the Radar Controller

The below command shows the arguments for the radar controller in a typical test configuration and includes all key options which must be specified.

```
./bircd_v1 --tx-freq 1300e6 --rx-freq 1300e6 --node-id=2 --script-file=script_8b.csv
```

The operator will be prompted for a scheduled start time, in the format of the number of seconds since 00:00:00 UTC. The current count is displayed for convenience. The radar controller will wait until the scheduled start time, at which point it will begin playing out the scheduled radar operations as defined in the script file. The terminal output for a typical run is shown in Table 34.

Table 34. Radar controller terminal output for a simple script file

```

./bircd_v1 --tx-freq 1300e6 --rx-freq 1300e6 --tx-gain 17 --rx-gain 32 --node-id=1 --script-file=script_8b.csv
***** USRP INITIALISATION *****
Creating the transmit usrp device with: ...
X300 initialization sequence...
Connecting to niusrpriorpc at localhost:5444...
Using LVBITX bitfile /usr/local/share/uhd/images/usrp_x310_fpga_HG.lvbitx...
Setup basic communication...
Loading values from EEPROM...
Setup RF frontend clocking...
Radio 1x clock:200
Detecting internal GPSDO... No GPSDO found
[DMA FIFO] Running BIST for FIFO 0... pass (Throughput: 1304.4MB/s)
[DMA FIFO] Running BIST for FIFO 1... pass (Throughput: 1304.5MB/s)
[RFNoC Radio] Performing register loopback test... pass
Performing timer loopback test... pass
Performing timer loopback test... pass

Creating the receive usrp device with: ...
Setting TX Rate: 100.000000 Msps...
Actual TX Rate: 100.000000 Msps
Setting RX Rate: 12.500000 Msps...
Actual RX Rate: 12.500000 Msps
Setting TX Freq: 1300.000000 MHz...
Actual TX Freq: 1300.000000 MHz
Setting TX Gain: 17.000000 dB...
Actual TX Gain: 17.000000 dB
Setting RX Freq: 1300.000000 MHz...
Actual RX Freq: 1300.000000 MHz
Setting RX Gain: 32.000000 dB...
Actual RX Gain: 32.000000 dB
Max samples per buffer (spb): 1019
Checking TX: TXLO: locked ...
Checking RX: RXLO: locked ...
Checking TX: Ref: locked ...
Checking RX: Ref: locked ...

Setting USRP GPIO's ATR functionality

***** RADAR CONTROLLER SETUP *****
Initialising RS232 port...
Creating RN_logFile: RadarData_workDir/0_EventsLog...
Querying ULN-1100 GPSDO...
-- GPSDO->PTIME?
-- DATE :2018,4,11
-- TIME :6:49:03
-- TINTerval :-1.636E-07
-- LEAPSECOND :18
-- GPSDO->GPS?
-- ANTENNA DELAY:2.5e-08
-- PULSE SAWTOOTH:5.8
-- TRACKED SATS :13
-- VISIBLE SATS :16
-- ACTUAL POSITION:
-- S,3443.7417
-- E,13838.8193
-- 32.00 m
-- 0.00 Knots
-- 0.00 Degrees
-- GPS Receiver Status: 3D Fix
-- JAMMING LEVEL:6
-- FIRMWARE VERSION: 7.03

Loading burst data from capture script csv file: script_8b.csv...
-- scriptData matrix dimentions: 8 rows (bursts) X 21 columns

Querying ULN-1100 GPSDO for UTC...
Using external time source...
Attempting to detect the external UTC 1PPS reference and set USRP RTC to UTC...
  1) catch time transition at pps edge
  2) set times next pps (synchronously)
-- Success!

Querying ULN-1100 GPSDO for UTC...
-- Current GPS UTC (hh,mm,ss): 6,49,5

```

```

-- Current GPS UTC (nSeconds): 24545
-- Current URSP time (nSeconds): 24545.1

>> Enter scheduled radar operations UTC start time (in nSeconds):
-- UTC scheduled start time: 2018-04-11T06-49-10

***** SCHEDULE BURSTS *****

bId  nPulses  PRI(us)  nRxSamps  burstStartTime  burstlength  RN1 TX waveform  timeTillB
1     143     137.76  246246    24550.000000    0.019700  SchFM1_int16_260pad.bin  3.616913
2     122     159.60  243390    24550.069700    0.019471  SchFM2_int16_260pad.bin  0.049744
3     106     180.96  239772    24550.139171    0.019182  SchFM3_int16_260pad.bin  0.049880
4     90      211.20  237600    24550.208353    0.019008  SchFM4_int16_260pad.bin  0.049875
5     78      240.48  234468    24550.277361    0.018757  SchFM5_int16_260pad.bin  0.049839
6     47      396.00  232650    24550.346118    0.018612  SchFM6_int16_260pad.bin  0.049851
7     41      452.40  231855    24550.414730    0.018548  SchFM7_int16_260pad.bin  0.049867
8     35      513.36  224595    24550.483278    0.017968  SchFM8_int16_260pad.bin  0.049787

***** SUMMARY OF OPERATIONS *****
UTC scheduled start time: 2018-04-11T06-49-10
UTC scheduled stop time: 2018-04-11T06-49-10
-- Runtime of scheduled radar operations (sec): 0.501246

Number of reported bursts with RX errors: 0
Reported bursts with RX errors:

Number of reported bursts with TX errors: 0
Reported bursts with TX errors:

```

All radar controller output is stored in a folder unique to each run, named with the UTC scheduled start time and node ID. All terminal output is recorded in a similarly names System Log file within the folder. Any errors encountered are logged and reported in summary at the end of each run.

C.5. Receiver Data Files

Receiver IQ data samples are stored in the same format as the IQ pulse data file. The GNU Octave application `rangeDopplerGUI_v2.m` can be used to process these files and form range Doppler maps; terminal output is shown in Table 35 while the GUI is shown in *Figure 16* of section 5.5.1.

Table 35. Terminal output from the `rangeDopplerGUI_v2.m` script

```

rx_file      = /home/bircd/USRP_proj/workspace/bircd_v1/build/Mon_RadarData_2018-05-10T01-38-58_RN1/1.bin
tx_file      = /home/bircd/USRP_proj/workspace/bircd_v1/build/SchFM1_int16_260pad.bin
Npulses     = 143

Doppler bins: 128
Doppler resolution: 56.711 Hz/bin --> 23.556 Km/hr
Number of range samples: 1722
Pulse Width (time between range samples): 0.08 us/bin
Range Resolution (distance between range samples): 12 m/bin
Estimate Noise Floor: 1.6808 dB

PEAK DETECTION
-- 36.932dB at 42us range & -737.242 Hz Doppler
---- SNR: 35.251
-- 36.829dB at 42us range & 850.664 Hz Doppler
---- SNR: 35.148

Processing time: 0 min 0.43814 sec

```

Appendix D Miscellaneous System Details

D.1. Capability Requirements

Table 36 lists branch research interests and corresponding derived capability requirements.

Table 36. *Capability requirements*

Capability Requirements of Research Interests			Sea clutter characterisation	Multi-static adaptive CFAR detection in clutter	Distributed MIMO	Low-bandwidth radar imaging	Requirements for Bistatic Radar Concept Demonstrator	Requirements for future Multi-static Radar Capability (design for, but not with)
CR #	Project	Priority of research objective	1	3	4	2		
1	System	SNR (after Doppler processing and pulse compression)	10dB min. / 20dB des. for a target RCS of -40dB sqm/sqm σ_0 at 10kms range	3dB min. / 10dB desired for a target with RCS of 1sqm at range 1km	'as left'	3dB min. / 10dB desired for a target with RCS of 1sqm at range 1km	10dB min. / 20dB des. for a target RCS of -40dB sqm/sqm σ_0 at 10kms range	'as left'
2	System	Instantaneous bandwidth	10MHz min.	40MHz min. for a PRF of 1KHz	10MHz min. / 40MHz+ desirable for a PRF of 1KHz	1MHz min.	10MHz min. / 40MHz desirable	40MHz min.
3	System	Coherent processing interval (CPI)	20ms min. / 1s desirable	20ms min.	'as left'	20ms min.	20ms min. / 1s desirable	1s desirable
4	System	RTC sync. accuracy (the accuracy between the RTCs of the nodes)	200ns max. error	for phase coherence better than $(2*\pi/\lambda)*0.1 = 2.7$ degrees	'as left'	100ns max. error	100ns max. error	'as left'
5	System	Simultaneous monostatic	one-path desirable	one-path min. / two-path desirable	two-path with simultaneous orthogonal waveforms	one-path min. / two-path desirable	one-path (from remote node)	one-path min. / two-path desirable
6	System	Two-way bistatic operation	desirable	desirable	Req.	Not Req.	Not Req.	desirable
7	Comms. Link	Baseline range	1km min.	100m min. / 1km desirable	'as left'	100m min. / 1km desirable	1km min.	'as left'
8	Comms. Link	Data types	control & config			control & config	control & config	'as left'
9	Remote Node	Number of Remote Nodes	1 min.	2 min. / 3 desirable	2 min. / 3 desirable	1 min. / 3 desirable / 4 ideal	1	2 min. / 3 desirable
10	Remote Node	TX and/or RX	TX min. / TX & RX desirable	either	RX & TX	either (RX more desirable)	TX and RX	'as left'
11	Remote Node	Data storage capacity		1TB min. / more desirable	'as left'	100MB min.	1TB min.	'as left'
12	Remote Node	Location accuracy	+/-15meters	+/-15meters	'as left'	+/-15meters	+/-15meters	'as left'
13	Remote Node	Antenna orientation accuracy (dependent on beam width)	Swaths must overlap	Swaths must overlap	'as left'	Swaths must overlap	Swaths must overlap	'as left'
14	Logistics	Location of possible experiments	coastal (e.g. cliff at Cape Jervis)	coastal (e.g. cliff at Cape Jervis)	'as left'	STF, cliff at Cape Jervis) (3G network available)	STF, coastal (e.g. cliff at Cape Jervis)	'as left'

D.2. XPAR-II System Constraints

Table 37. XPAR-II System constraints

System Constraints	
	<i>XPAR-II (at present)</i>
Operating frequency	1240 - 1400 MHz
Pulse length (τ)	100us max.
Instantaneous bandwidth (BW)	10MHz max
Duty cycle (DC)	5% max.
Coherent processing interval (CPI)	<i>20ms max. (recently changed)</i>
Pulse repetition interval (PRI)	35us min.
Antenna gain (G)	6dBi / column => 24dBi
3dB antenna beamsidith (θ_{3dB})	15° = 0.262 radians
<i>antenna)</i>	70W max. / column => 560W Peak
Antenna polarisation	LH slant linear
Pulse repetition frequency (PRF)	28.6 KHz max.
Antenna noise temperature (T_A)	125° Kelvin
Receiver noise temperature (T_R)	596° Kelvin
Calculated	
Nominal range resolution	$c / 2 * BW = 15m$
Pulse compression ratio (PCR) / fast-time processing gain (<i>ignoring 2-3dB windowing loss</i>)	$PCR = 10 * \log(\tau * BW) = 30dB \text{ max.}$ <i>(Note: mono-static radar will be 'blind' for $3e8 * \tau * 0.5 = 15kms$ here)</i>
System noise temperature (T_S)	$T_S = T_A + T_R = 721° \text{ Kelvin}$
System noise figure (NF)	$NF = 1 + T_s / T_0 = 5dB$

D.3. XPAR-II Search Waveforms

Table 38. XPAR-II search waveform parameters

Waveform	FM1	FM2	FM3	FM4	FM5	FM6	FM7	FM8	
Designator	9M83Q0N	9M62Q0N	9M46Q0N	9M3Q0N	9M18Q0N	8M81Q0N	8M73Q0N	8M67Q0N	
PRF Hz	7259.0	6265.7	5526.1	4734.8	4158.3	2525.3	2210.4	1948.0	
PRI us	137.76	159.6	180.96	211.2	240.48	396	452.4	513.36	
Max PW us	9.27	11.46	13.59	16.62	19.54	35.1	40.74	46.83	
Duty %	6.7	7.2	7.5	7.9	8.1	8.9	9.0	9.1	
PCR	35.875	44.350	52.593	64.319	75.620	135.837	157.664	181.232	
Frequency Deviation MHz	3.87	3.87	3.87	3.87	3.87	3.87	3.87	3.87	
Number of pulses	143	122	106	90	78	47	41	35	
CPI ms	19.69968	19.4712	19.18176	19.008	18.75744	18.612	18.5484	17.9676	
Pulse Rise/Fall Time ns	80	80	80	80	80	80	80	80	At output of compressed transmitter
PW 50% points	9.17	11.36	13.49	16.52	19.44	35	40.64	46.73	At output of compressed transmitter
Necessary BW MHz	9.83	9.62	9.46	9.30	9.18	8.81	8.73	8.67	ITU SM 1541 Annex 8
Reference BW MHz	0.65	0.58	0.53	0.48	0.45	0.33	0.31	0.29	The min reference bandwidth is 1 MHz – para 9 ITU RR 2012 Appendix 3

D.4. System Script File Definition

The script file which defines the exact sequence of radar operations is defined in Table 39. The script file is common to both primary and all remote nodes. While all remote nodes have identical hardware and software, an ID unique to each node is referenced to the script file to direct node specific behaviour. Changes from the original XPAR-II script file definition are outlined in red.

Table 39. Parameter used to define XPAR-II bursts. Changes to the existing definition are shown in red.

Parameter	Parameter Number	Data Type	Units	Range	Description
Burst ID	1	unsigned integer	lines	0 - 1024	The script line that prescribes this burst.
Number of PRIs (NPRI)	2	unsigned short	None	0 - 1024	If set to zero no pulses are transmitted and the PRI is interpreted as the length of an idle dwell.
PRI	3	unsigned long	10 ns clock ticks	<i>If NPRI > 0</i> 3,500,000 to 1,000,000 <i>If NPRI = 0</i> 100,000 to 90,000,000	If NPRI > 0 this sets the pulse repetition interval in the allowed range of 100Hz to If NPRI = 0 sets a wait interval.
Channel	4	unsigned integer	channels	1 - 164	The channel number is described in the Architecture Design Doc appendix 'Frequency Spectrum - Definitions and Control'
Beam Number	5	integer	1, ..., 37		Beam Number The beam numbers correspond to azimuth steering angles in the range -45 to 45 degrees inclusive ; in 2 ½ degree steps. So Beam number 1 is a beam at -45 degrees azimuth. Beam Number 19 is boresight. The azimuth angles of the beams are in the Antenna face coordinate system
IQ pulse data file for TR#1	6	string	NA		This is the IQ pulse data file to be transmitted from transmitter #1
:	:	:	:	:	:
IQ pulse data file for TR#8	13	string	NA		This is the IQ pulse data file to be transmitted from TR#8
IQ pulse data file for RN1	14	string	NA		This is the IQ pulse data file to be transmitted from remote node #1
:	:	:	:	:	:
IQ pulse data file for RN8	21	string	NA		This is the IQ pulse data file to be transmitted from remote node #8

D.4.1. RX Only

An empty IQ pulse data file field indicates that the device is to receive only. An exception exists where if a pulse data file is identified in the first TRm column (Pls1) while the following TRm columns are empty, then all TRms are to play out this same file. This exception does not apply to the remote nodes.

D.5. Modifications Required to the XPAR-II System

1. Deterministic timing between bursts
 - a. During script execution, there are arbitrary delays between successive bursts equal to the burst length plus approximately 15ms.
2. Functionality to begin script execution at a given absolute time.
 - a. It is necessary to begin script execution at an absolute time, which would allow for the complete physical separation of XPAR-II (Protected) and the remote node (Unclassified), simplifying security implications.
3. Changes required to the script file definition to accommodate remote node functionality and receive only functionality
 - a. Refer D.4.
4. Record information necessary for bistatic configuration
 - a. Info such as GPS coordinates are to be recorded along with the receiver data for offline processing.

The changes to allow deterministic timing and a set start time are required before any bistatic configuration is possible with the XPAR-II system, while the other changes can be made at a later date.

D.5.1. Synchronisation of Clocks

Unambiguous and absolute time accuracy is required between the nodes. However, XPAR-II does not have a true real time clock (RTC) functionality; rather, a sequencer clock which rolls over every second. A solution is proposed as follows:

1. lock the XPAR-II master oscillator to a GPS derived source, so that the sequencer clock (the fine clock) runs at the same rate as the GPS clock;
2. synchronise the sequencer clock to the GPS derived PPS signal, so that the sequencer clock rolls over when a PPS signal occurs; and
3. use a counter to register each PPS pulse, as to provide a non-ambiguous clock with a one second resolution.

This solution provides two GPS synchronised clocks: a sequencer clock with a 10ns resolution and a counter with a one second resolution; the combination provide GPS derived unambiguous time.

This page is intentionally blank.

Appendix E Remote Node Assembly Schematics Diagram

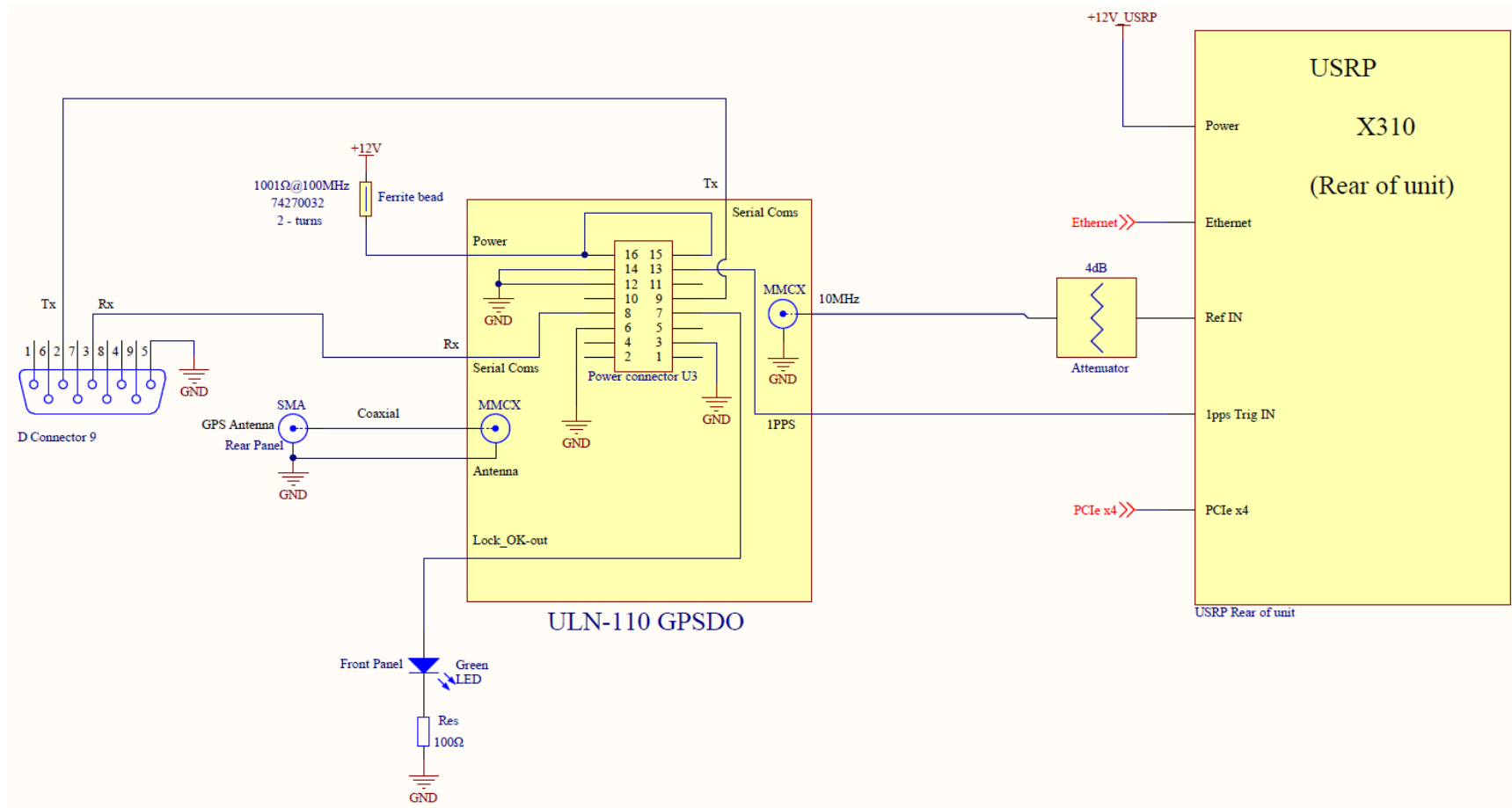


Figure 36. BiRCD - RN GSPDO schematic diagram

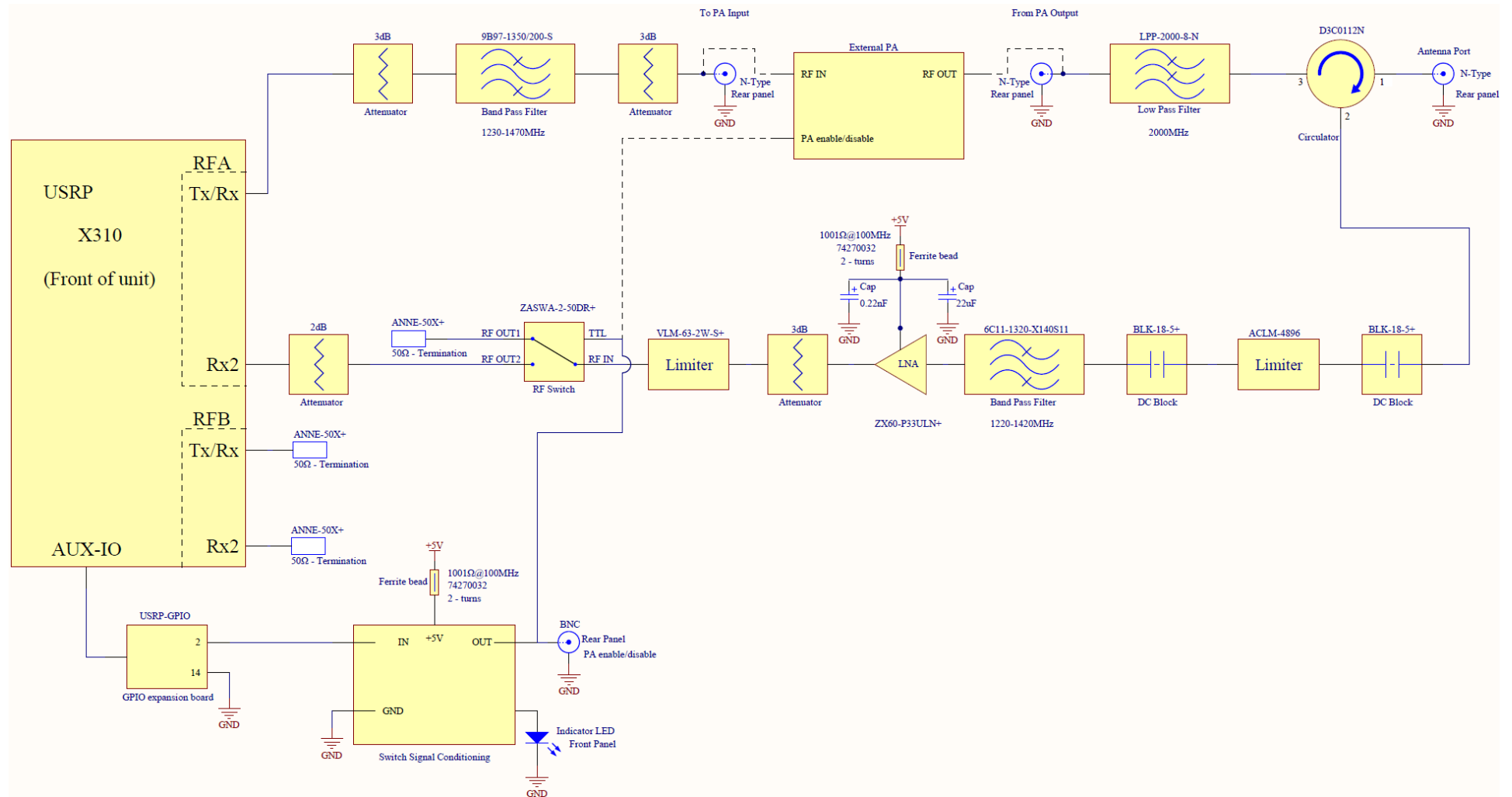


Figure 37. BiRCD - RN RF Front End schematic diagram

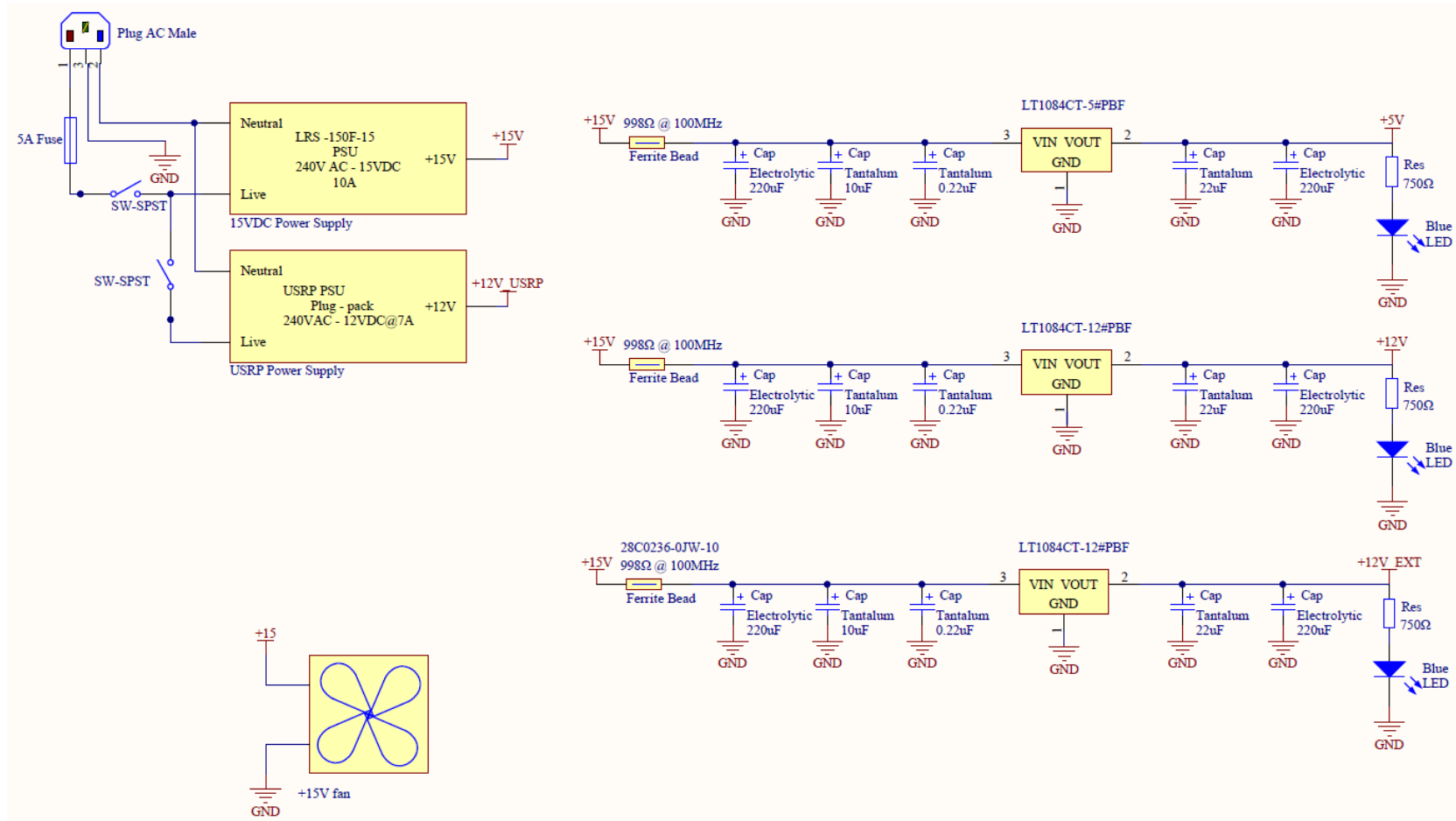


Figure 38. BiRCD - RN PSU schematic diagram

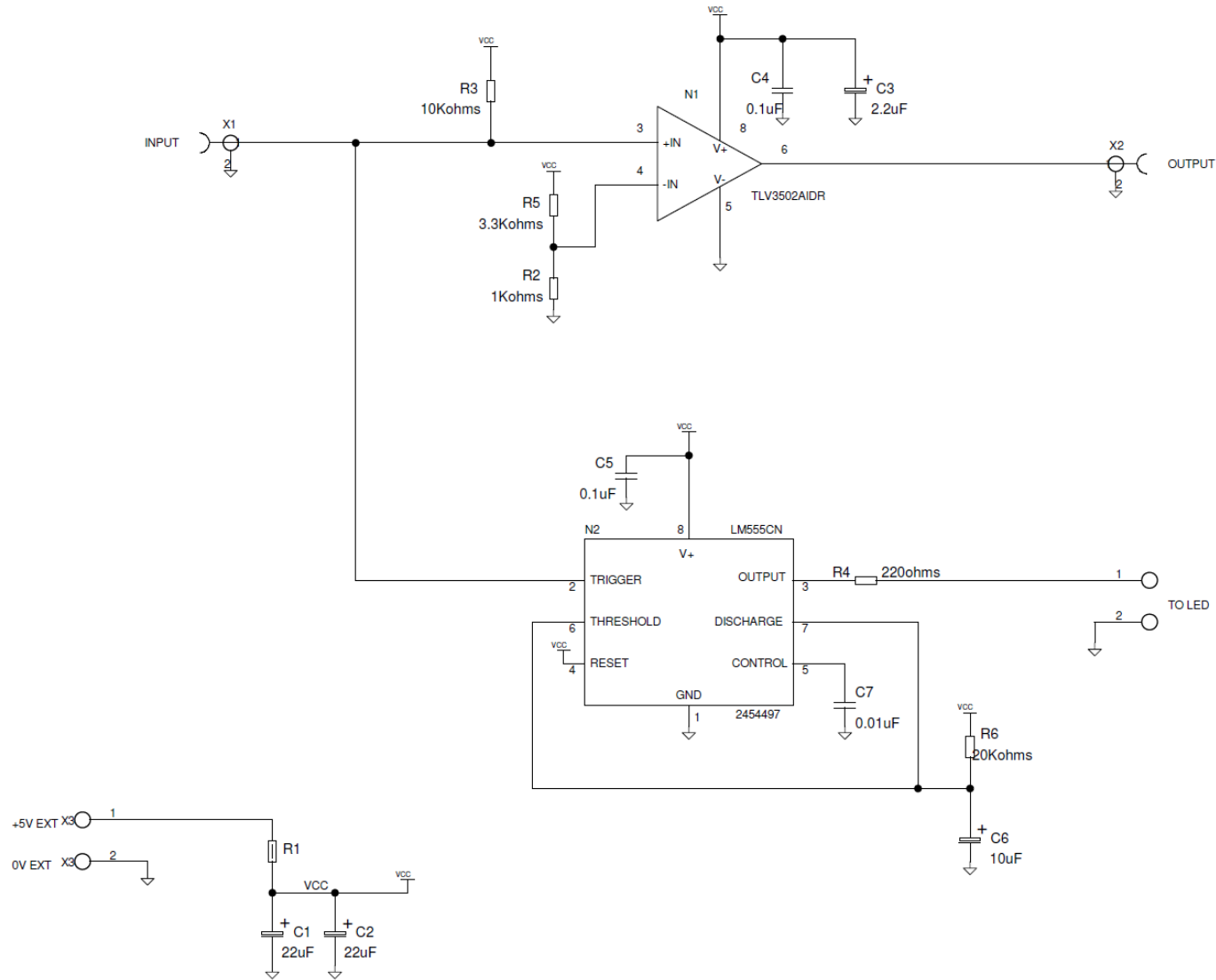


Figure 39. BiRCD - RN PA Enable Conditioner schematic diagram

UNCLASSIFIED

DEFENCE SCIENCE AND TECHNOLOGY GROUP DOCUMENT CONTROL DATA		1. DLM/CAVEAT (OF DOCUMENT)
2. TITLE Bistatic Radar Concept Demonstrator (BiRCD) System Development and Verification		3. SECURITY CLASSIFICATION (FOR UNCLASSIFIED LIMITED RELEASE USE (U/L) NEXT TO DOCUMENT CLASSIFICATION) Document (U) Title (U) Abstract (U)
4. AUTHOR(S) Timothy Chiknaikin		5. CORPORATE AUTHOR Defence Science and Technology Group PO Box 1500 Edinburgh, South Australia 5111, Australia
6a. DST GROUP NUMBER DST-Group-TN-1856	6b. TYPE OF REPORT Technical Note	7. DOCUMENT DATE March 2019
8. TASK NUMBER N/A	9. TASK SPONSOR Dr Joe Fabrizio	10. RESEARCH DIVISION NSID
11. MSTC Surveillance and Reconnaissance Systems		12. STC Microwave Radar Systems
13. SECONDARY RELEASE STATEMENT OF THIS DOCUMENT <i>Approved for public release</i> OVERSEAS ENQUIRIES OUTSIDE STATED LIMITATIONS SHOULD BE REFERRED THROUGH DOCUMENT EXCHANGE, PO BOX 1500, EDINBURGH, SA 5111		
14. DELIBERATE ANNOUNCEMENT No limitations		
15. CITATION IN OTHER DOCUMENTS No limitations		
16. RESEARCH LIBRARY THESAURUS Bistatic radar, microwave radar, passive detection, radar,		
17. ABSTRACT In this document we describe the development and verification of an experimental bistatic radar system. Project objectives are defined followed by the capture and definition of system requirements. A software defined radio (SDR) based hardware platform is outlined, along with a non-real-time radar controller with offline processing of radar data. Analysis of experimental data from a field trial provides validation of system performance. The conclusion considers project outcomes and insights, and discusses possible future work. Technical details and analysis are left to the appendixes.		

UNCLASSIFIED